Fatigue strength of composite wind turbine blade structures

Castro, Oscar

Link to article, DOI:
10.11581/00000037

Publication date:
2018

Document Version
Publisher's PDF, also known as Version of record

DTU Wind Energy
Department of Wind Energy

Ph.D. Thesis

Fatigue strength of composite wind turbine blade structures

Oscar Gerardo Castro Ardila

Risø Campus, Roskilde, 2018

DTU

Technical University of Denmark
DTU Wind Energy
Department of Wind Energy

DTU Risø Campus
Frederiksborgvej 399 Building 125
4000 Roskilde, Denmark
Phone +45 12345678
RogerFederer@dtu.dk
www.vindenergi.dtu.dk

Abstract

Wind turbines are normally designed to withstand 20-30 years of life. During this period, the blades, which are the main rotating structures of a wind turbine, are subjected to high fluctuating load conditions as a result of a combination of gravity, inertia, and aeroelastic forces. For this reason, fatigue is one of the foremost concerns during the design of these structures. However, current standard fatigue methods used for designing wind turbine blades seem not to be completely appropriate for these structures because they are still based on methods developed for metals and not for composite materials from which the blades are made. In this sense, the aim of this work is to develop more accurate and reliable fatigue-life prediction models for composite wind turbine blades.

In this project, two types of fatigue models are implemented: fatigue-life models and damage mechanics models. In the first part of the project, a probabilistic multiaxial fatigue-life model for composite materials, which takes the variability in the material properties into account, is proposed. In this model, novel probabilistic constant life diagrams are developed, which can efficiently estimate probabilistic ε-N curves at any load level and stress ratio. However, due to the low accuracy level of current multiaxial macroscopic fatigue failure criteria and damage accumulation theories for predicting the fatigue-life of composite materials under multiaxial and variable cycle load conditions, the proposed probabilistic fatigue-life model seems unsuitable for wind turbine blades.

Based on this limitation, in the second part of the project, a damage mechanics-based multiscale approach using a 2D finite-element-based cross-section model for analyzing wind turbine blades under fatigue is proposed. By using this approach, reliable predictions about the effect of off-axis matrix cracks on the structural response of the blades are obtained. These results establish a basis for the development of an extended model that allows predicting the off-axis crack evolution in the blades and includes other types of damage, such as delaminations, fiber-related damage, etc. Furthermore, and following the framework of the proposed multiscale approach, a microscale fiber-related damage evolution study for on-axis UD glass/epoxy laminates under fatigue loading conditions is also presented. This study provides significant information for developing future fatigue models that allow predicting the catastrophic failure of multidirectional composite laminates and, therefore, possible failures in wind turbine blades.

Resume

Vindmøller er normalt designet til at holde i 20-30 år. I løbet af denne periode udsættes vingerne, som er de vigtigste roterende strukturer på en vindmølle, for stærkt fluktuerende belastninger som følge af en kombination af tyngdekraften, inerti og aeroelastiske kræfter. Derfor er udmattelse en af de største udfordringer ved konstruktionen af disse strukturer. De nuværende standardmetoder, der anvendes til beregning af udmattelse i vindmøllevinger, synes imidlertid ikke at være helt egnede til disse strukturer, da de stadig er baseret på metoder udviklet til metaller og ikke kompositmaterialer, som vingerne fremstilles af. Derfor er formålet med dette arbejde at udvikle mere præcise og pålidelige modeller til forudsigelse af udmattelse i kompositvindmøllevinger.

I dette projekt implementeres to typer udmattelse modeller: udmattelse levetidsmodeller og skademekaniske modeller. I den første del af projektet foreslås en probabilistisk flerakset udmattelse levetidsmodel for kompositmaterialer, der tager højde for variabiliteten i materialegenskaberne. I denne model udvikles nye probabilistiske diagrammer for konstant levetid, der effektivt kan estimere sandsynlige ε-N-kurver på ethvert belastningsniveau og spændingsforhold. På grund af den lave nøjagtighed for de nuværende flerakset makroskopiske udmattelse svigtkriterier og skadesakkumuleringsteorier der bruges til at forudsige levetiden for kompositmaterialer under flerakset og variable cykliske belastninger, synes den foreslåede probabilistiske udmattelses levetidsmodel ikke at være egnet til vindmøllevinger.

På baggrund af denne begrænsning foreslås i den anden del af projektet en multiskala tilgang baseret på skadesmekanik ved hjælp af 2D finite element tværsnitmodeller til analyse af vindmøllevinger under udmattelse. Ved at anvende denne fremgangsmåde opnås pålidelige forudsigelser af effekten af tværgående resinrevner på vingernes strukturelle respons. Disse resultater skaber grundlag for udviklingen af en udvidet model, der gør det muligt at beregne tværgående revneudviklingen i vingerne og omfatter andre typer skader, såsom delaminering, fiberrelaterede skader osv. Desuden, og i henhold til rammen af den foreslåede multiskala tilgang, er der også fremlagt en mikroskala fiberrelateret metode til undersøgelse af skadesudvikling i UD-glas/epoxy-laminater under udmattelse belastninger. Denne undersøgelse giver væsentlig information til udvikling af fremtidige udmattelse modeller, der muliggør forudsigelse af katastrofale svigt i kompositlaminer og dermed mulige fejl i vindmøllevinger.

Preface

This thesis was prepared in the Department of Wind Energy of the Technical University of Denmark, DTU Wind Energy, in fulfillment of the requirements for acquiring a Ph.D. degree. The Ph.D. project was carried out from January 2015 to February 2018 with the Wind Turbine Structures and Component Design section at DTU Wind Energy.

The project has been supervised by Kim Branner and Povl Brøndsted from DTU Wind Energy. The Ph.D. was founded by the Danish Centre for Composite Structures and Materials for Wind Turbines (DCCSM), grant no. 09-067212 from the Danish Strategic Research Council. The financial support is greatly appreciated.

This dissertation is organized as a collection of papers. The first part of the document provides an overview of the background needed for the investigation and some studies that were not published in journal papers. Part I contains Chapters 2 to 5. In Chapter 2, a brief description of different concepts related to fatigue in wind turbine blades is given. In Chapter 3, a probabilistic multiaxial fatigue model for composite materials is proposed, and an evaluation of its applicability in full wind turbine blades is presented. In Chapter 4, a multiscale approach for fatigue design of wind turbine blades based on damage mechanics models is proposed as well as its implementation in a real wind turbine blade. In Chapter 5, the main conclusions and contributions of the present work are presented.

In Part II, the following three papers are attached, which were written during the Ph.D. study:

- *Paper 1* entitled *Assessment and propagation of mechanical property uncertainties in fatigue life prediction of composite laminates.*
- *Paper 2* entitled *Damage mechanics-based multiscale model for wind turbine blades under fatigue: Part 1. Effect of off-axis cracks on the blade stiffness degradation.*
- *Paper 3* entitled *Fatigue damage evolution in unidirectional glass/epoxy composites under a cyclic load.*

During the Ph.D. studies, part of the work was presented at the 20th International Conference on Composite Materials (ICCM20) Copenhagen, Denmark, 2015; the Danish Center for Composite Structures and Materials for Wind Turbines (DCCSM) Workshop, Middelfart, Denmark, 2015; the 15th International Symposium of the Danish Center for Applied Mathematics and Mechanics (DCAMM), Horsens, Denmark, 2015; the 4th Durability and Fatigue Advances in Wind, Wave and Tidal Energy, Bristol, UK, 2016; the Danish Center for Composite Structures and Materials for Wind Turbines (DCCSM) Workshop, Aalborg, Denmark, 2016; the Damage Workshop, Sevilla, Spain, 2017; and the 2nd International Symposium on Multiscale Experimental Mechanics: Multiscale

Fatigue (ISMEM 2017), Lyngby, Denmark, 2017.

From February to July 2017, an external research stay at University of Padova (Vicenza, Italy) was carried out under the supervision of Professor Marino Quaresimin.

A list of attended conferences and publications is presented below:

List of publications

- Oscar Castro, Kim Branner, and Nikolay Dimitrov, *Assessment and propagation of mechanical property uncertainties in fatigue life prediction of composite laminates*, Journal of Composites Materials (2017). Accepted for publication.
- Oscar Castro and Kim Branner, *Damage mechanics-based multiscale model for wind turbine blades under fatigue: Part 1. Effect of off-axis cracks on the blade stiffness degradation*, (2018). In manuscript.
- Oscar Castro, Paolo Andrea Carraro, Lucio Maragoni and Marino Quaresimin. *Fatigue damage evolution in unidirectional glass/epoxy composites under a cyclic load*, Polymer Testing (2018). Submitted.

List of conferences

- Oscar Castro, Mathew Lennie, Kim Branner, George Pechlivanoglou, Povl Brϕndsted and Christian Nayeri, *Comparing fatigue life estimations of composite wind turbines blades using different fatigue analysis tools*, in 20th International Conference on Composite Materials (ICCM20), Copenhagen, Denmark, 2015. Oral presentation and paper.
- Oscar Castro, *Fatigue strength of composite wind turbine blade structures* in Danish Center for Composite Structures and Materials for Wind Turbines (DCCSM) Workshop, Middelfart, Denmark, 2015. Oral presentation.
- Oscar Castro. *Fatigue strength of composite wind turbine blade structures* in Danish Center for Applied Mathematics and Mechanics (DCAMM), 15th International Symposioum, Horsens, Denmark, 2015. Oral presentation.
- Oscar Castro, Kim Branner, Povl Brϕndsted, Nikolay Dimitrov and Philipp Haselbach, *Fatigue Modeling of Large Composite Wind Turbine Blades*, in 4th Durability and Fatigue Advances in Wind, Wave and Tidal Energy, Bristol, UK, 2016. Oral presentation.
- Oscar Castro, *Preliminary results on reliability analysis of the rotor blade fatigue under multiaxial loading*, in Danish Center for Composite Structures and Materials for Wind Turbines (DCCSM) Workshop, Aalborg, Denmark, 2016. Oral presentation.
- Paolo Carraro, Marino Quaresimin and Oscar Castro, *Micro-scale observations of the fibre failure process in UD laminates under cyclic loading*, in Damage Workshop,

Sevilla, Spain, 2017. Oral presentation.

- Oscar Castro, Paolo Carraro, Lucio Maragoni and Marino Quaresimin, *Fatigue damage evolution of unidirectional glass/epoxy composites*, in 2nd International Symposium on Multiscale Experimental Mechanics: Multiscale Fatigue (ISMEM 2017), Lyngby, Denmark, 2017. Oral presentation and paper.

Oscar Gerardo Castro Ardila

Risø Campus, Roskilde
February 28, 2018

Acknowledgements

There have been many years in which I dreamed of living this moment of my life. And here I am, only one step away from reaching the final goal. They have been years of constant work and sacrifices, but also of joys and great experiences. Years in which I met great people from whom I learned and shared what I needed to be here. And now it is time to thank them.

First, I want to thank the Danish Center for Composite Structures and Materials for Wind Turbines (DCCSM) and the Technical University of Denmark (DTU) for having provided me everything necessary to carry out my Ph.D. studies.

I would like to thank my main supervisor, Kim Branner, for giving me the opportunity to work in this research field so full of challenges. Thank you very much for your constant support.

I would also like to thank my supervisor, Povl Brøndsted, for his wise and timely advice, which gave me confidence in myself in moments when I needed it.

I also want to acknowledge Nikolay Dimitrov, for having taught me to see engineering from another point of view, in which reality is full of uncertainty.

Thanks to my office colleagues, Susana Rojas, Juan Gallego, Philipp U. Haselbach and Ali Sarhadi, because together we built a nice working place in which there was always place and time for a coffee, a conversation outside the workplace, a dance, a chocolate and even a Christmas tree. It was a great time with you guys.

I also want to thank Professor Marino Quaresimin from the University of Padova, Italy, who gave me the opportunity to carry out my external stay with his research group. With him and his group I learned, among others, what teamwork means.

I want to especially thank Paolo Carraro and Lucio Maragoni from the University of Padova, Italy, for having shared with me all their knowledge and experience about fatigue in composite materials. Thanks to you guys I discovered the path I should follow.

I also want to thank all my office colleagues at the University of Padova, Francesco Panozzo, *Il Mod*, Amir Ghorbani, Elisa Novello, and, of course, Lucio Maragoni, for making my stay there an unforgettable experience. Siete grandi ragazzi!

Gracias a mis parceras, Maria Puig, Gina Castiblanco, Alkistis Papetta y Susana Rojas, por su compañía y apoyo especialmente en la última etapa de este proceso. Sin ustedes muchachas, ésto no hubiese sido posible.

Gracias inmensas a mi familia a quienes debo mi esencia de ser. A mi madre por su apoyo incondicional, a mi padre por hacer brotar siempre una sonrisa de mi, a mi hermana por abrirme siempre aquella *ventana azul*, a mi hermano por su apoyo, especialmente con la elaboración de varias figuras de este documento, y a mi pequeño sobrino, por habernos traido luz con su llegada. Ustedes son y seguirán siendo un motivo para seguir soñando

y trabajando.

Y finalmente, a Ingrid M. Padilla, con quien empecé este viaje. Gracias porque, aunque nuestros pasos tomaron caminos diferentes, nunca dejaste de ser mi compañera de viaje.

Contents

CHAPTER 1

Introduction

1.1 Problem statement and motivation

The importance of energy in modern society is enormous, and how energy technology, supply and demand, and policy change every day seems even greater. In fact, one the greatest challenges for mankind nowadays is maintaining the worldwide energy supply while, at the same time, drastically reducing CO_2 emissions and continuing to lower the cost of energy, CoE.

One way to continue supplying energy with a percentage of CO_2 emissions lower than that produced by conventional energy sources is the use of renewable sources such as wind.

Wind energy offers a sustainable option in the pursuit of renewable energy, which can be reflected in its rapid growth in recent decades, see Fig. 1.1. As seen in Fig. 1.1, in 2016, the global cumulative installed wind capacity grew nearby 1937% compared with 2001 and is expected to continue growing by 40% by 2021 [25].

Despite this rapid growth, which has made wind energy one of the fastest-growing sources of electrical power in the world and one of the lowest-priced renewable energy technologies available today, [25], it remains necessary to decrease the CoE produced by wind turbines to make the wind source more competitive, with respect to conventional energy sources.

The CoE produced by a wind turbine during its lifetime can be defined as [33]:

$$CoE = \frac{CoT + CoI + CoM}{PP} \tag{1.1}$$

where CoT is the cost of the turbine (i.e., total cost of foundation, tower, machinery, nacelle, and blades), CoI is the cost of installation and transportation, CoM is the cost of operation and maintenance, and PP is the power produced during the turbine lifetime. Then, if the aim is to decrease CoE, a decrease of CoT, CoI, or CoM or an increment of PP has to be reached.

One way to decrease CoT is making designs closer to the limit of the materials, which would result in a decrease in the amount of materials to be used. In the case of the blades, this decrease in the amount of materials would allow obtaining lighter structures and, therefore, the possibility of designing blades with longer lengths. Considering that the power output of a wind turbine is proportional to the blade length squared (swept area of the rotor), increasing the blade length would produce an increase of PP and therefore an even greater decrease of CoE.

Because wind turbines are conventionally designed for a lifetime expectancy of 20 to 30 years, the blades must be designed to withstand the high degree of fatigue loads

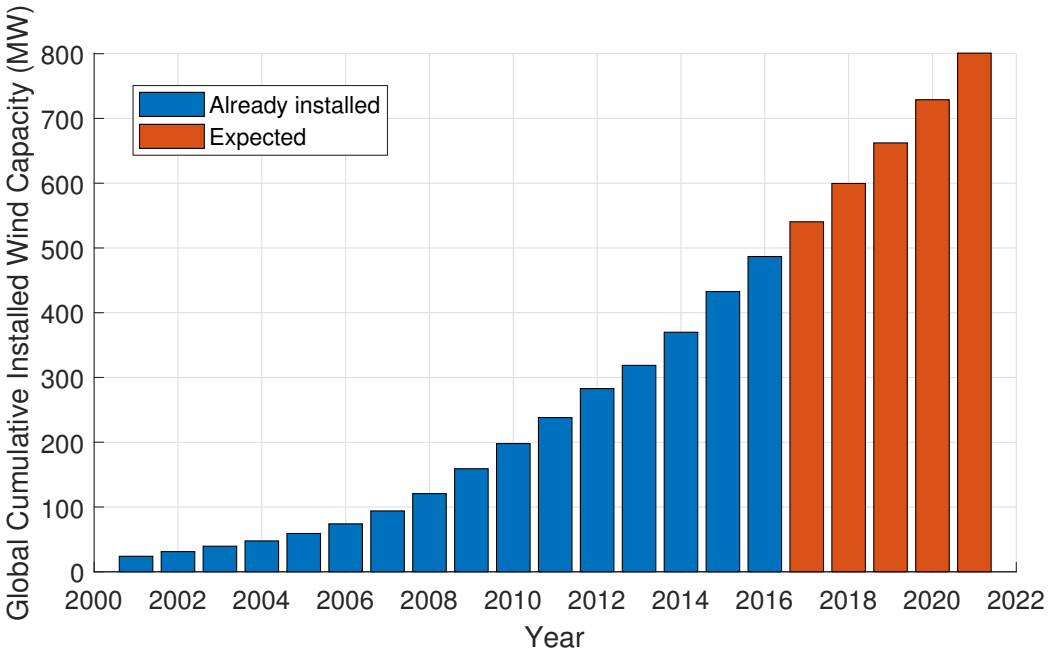

Figure 1.1: Global cumulative installed wind capacity 2001-2016 and expected global cumulative installed wind capacity 2017-2021 [25]

to which they are subjected during this period. In this sense, accurate and reliable fatigue-life prediction methods are needed to improve the structural design of the blades and, therefore, decrease the CoE of the wind turbines.

Wind turbine blades are mainly made of composite materials; however, current prediction methods suggested by the IEC 61400-1 international standard [80] and certification guidelines [60] for designing these structures against fatigue are still based on those methods suggested for metals. This assumption could make the current standard fatigue-life prediction methods for wind turbine blades inaccurate and unreliable, as the fatigue damage mechanisms developed in metals are completely different than those developed in composite materials. This possible inaccuracy and unreliability of the actual fatigue-life methods can be reflected in the conservative design of current wind turbine blades.

In addition to the actual fatigue behavior of composite materials, there are other factors that are not considered in the current standard fatigue-life prediction methods for wind turbine blades, e.g., multiaxial stress states, effects of manufacturing defects, and the stochastic nature of the loads, material properties, and the geometry. All these omissions could make the current methods even more inaccurate and unreliable.

To start considering the above-mentioned factors in the fatigue-life prediction process of wind turbine blades and, therefore, contributing to decrease the CoE of the wind turbines, the development of fatigue-life prediction methods for designing the composite wind turbine blade structures has been chosen as the research subject of this Ph.D. project.

1.2 Scientific objectives and achievements

The purpose of this Ph.D. project is to develop more accurate and reliable fatigue-life prediction models for composite wind turbine blades. The developed models should consider the fatigue behavior of composite materials. In addition, the multiaxial stress states due to the intrinsic anisotropy of the composite materials and the stochastic nature of the fatigue phenomenon should be also taken into account.

The final achievement of this project is to better understand how the fatigue damage initiates, propagates, and affects a typical wind turbine blade.

The present work is part of the Danish Centre for Composite Structures and Materials for Wind Turbines (DCCSM). The vision of the center is to develop a coherent, multiscale-based understanding of the mechanical behavior of composite materials and structures for wind turbine blades. The length scale goes from a nano- and micro-length scale (material) to structural length scale (full blade). The work package related to the present work deals with the structural scale, and the testing and modeling for predicting the structural response and failure of wind turbine blades.

1.3 Thesis overview

The thesis is divided in two parts. The **Part I** of the thesis provides context and background for the research carried out during the Ph.D. studies. This part is organized as follows:

- *Chapter 2* contains a brief description of different concepts related to fatigue in wind turbine blades. In this chapter, the type of fatigue models to be applied in this project along with the fatigue factors to be considered during the analysis are defined.
- *Chapter 3* presents a probabilistic multiaxial fatigue-life model proposed for composite materials. An evaluation of the applicability of this model in full wind turbine blades is also given. This evaluation demonstrates that some limitations found in the proposed model affect its applicability in the fatigue analysis of wind turbine blades.
- As an alternative to the model proposed in Chapter 3, *Chapter 4* presents a multiscale approach for fatigue design of wind turbine blades based on damage mechanics models. The implementation of this model in a real wind turbine blade considering the effect of off-axis matrix cracks is also presented. In addition, a microscale fiber-related damage evolution study for on-axis UD glass/epoxy laminates is provided as a first step toward the development of future models that allow predicting possible catastrophic failures of wind turbine blades under cyclic loading.
- *Chapter 5* provides the contributions and conclusions of this project, evaluates the main contributions and impact of the thesis, and proposes topics for future research.

The **Part II** of the thesis includes all the scientific papers related to this thesis. This part is organized according to the following chapters, each corresponding to a different paper.

- *Paper 1.* Oscar Castro, Kim Branner, and Nikolay Dimitrov, *Assessment and propagation of mechanical property uncertainties in fatigue-life prediction of composite laminates*, Journal of Composites Materials (2017). Accepted for publication.
- *Paper 2.* Oscar Castro and Kim Branner, *Damage mechanics-based multiscale model for wind turbine blades under fatigue: Part 1. Effect of off-axis cracks on the blade stiffness degradation* (2018). In manuscript.
- *Paper 3.* Oscar Castro, Paolo Andrea Carraro, Lucio Maragoni and Marino Quaresimin. *Fatigue damage evolution in unidirectional glass/epoxy composites under a cyclic load*, Polymer Testing (2018). Submitted.

Part I

Background

CHAPTER 2
Fatigue in wind turbine blades

Fatigue lifetime prediction of wind turbine blades is a challenging task because it requires not only the identification of the different factors that are involved in it but also how they interact with each other. Some of these factors are, among others, the intrinsic fatigue behavior of composite materials, presence of adhesive joints and sandwich components, multiaxial stress states, high number of load cases and possible load combinations, effects of manufacturing defects, stochastic nature of the loads, material properties, and the geometry. However, most of these factors are not considered in commonly used fatigue-life prediction methods, as suggested by IEC 61400-1 international standard [80] and DNV GL certification and design guidelines [60]. In this chapter, a brief description of these factors is given in order to identify how they relate to each other and how they are leading to new design trends of wind turbine blades against fatigue.

2.1 What is fatigue in materials?

Before discussing fatigue in composite wind turbine blades, the meaning of fatigue in materials and the basic terminology used to analyze this phenomenon are described in this section.

In materials science, fatigue is a structural damage caused when a material is subjected to external cyclic loading. This damage is characterized by being localized and progressive, which initiates when the state in a point in the material (for the case of metals), or points (for the case of composites), reaches a certain threshold. This state can be described by different variables such as stress, strain, or energy dissipation. In that critical point, the damage initiates with a microscopic crack that grows until a macroscopic crack is formed. The macroscopic crack grows for each cycle, causing deterioration of the mechanical response of the material. Finally, the material fails when the macroscopic crack reaches a critical size and the damage propagates suddenly causing the material to no longer continue to carry loads or perform its design function (e.g., vibration characteristics and deflection limits).

In order to study this type of damage and its effect on the material response, a basic terminology of fatigue can be defined by analyzing a constant amplitude cycle load and assuming the state of the material in terms of stresses, see Fig. 2.1. As shown in Fig. 2.1, the load is composed by N cycles. During each cycle, the stress varies between a maximum stress, σ_{max}, and a minimum stress, σ_{min}. Based on these two parameters, the variation of the stress over time is often defined by two of the following variables: the stress amplitude, σ_{amp}, the mean stress, σ_{mean}, the stress range, σ_{range}, or the R-value, which are defined as follows:

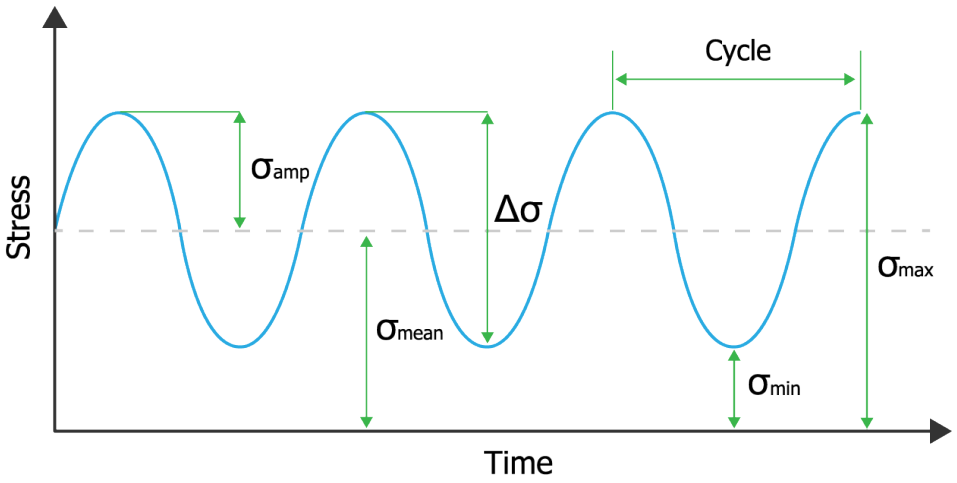

Figure 2.1: Basic fatigue terminology

$$\sigma_{amp} = \frac{\sigma_{max} - \sigma_{min}}{2} \tag{2.1}$$

$$\sigma_{mean} = \frac{\sigma_{max} + \sigma_{min}}{2} \tag{2.2}$$

$$\sigma_{range} = \sigma_{max} - \sigma_{min} \tag{2.3}$$

$$R = \frac{\sigma_{min}}{\sigma_{max}} \tag{2.4}$$

Having defined these basic concepts, the following sections will analyze how fatigue is developed in the wind turbine blades, how fatigue is currently analyzed, and what are the design trends against fatigue in this type of structure.

2.2 Fatigue loading sources in wind turbine blades

Wind turbine blades are exposed to static and dynamic loads during their operational lifetime, which is expected to last 20 to 30 years. The main sources of these loads are the wind and the effect of the gravity on the moving rotor, which fluctuates over time and introduces fatigue loads on the blades.

The fatigue loading of the blades originated from the wind (also called aeroelastic loads) comes from the natural variation in the wind speed, the vertical wind shear, see Fig 2.2, and the wake effects. The natural variation of the wind speed includes short- and long-term variations. The short-term variations, such as gusts, are a sudden and brief increase in wind speed followed by a lull, whereas long-term variations are daily/annual changes in the wind speed caused mainly by pressure gradients and terrain conditions. The loads on the blades also vary during the rotation of the rotor due to the increase of average wind speed with increasing height over the terrain, commonly known as vertical

wind shear. Moreover, in a wind farm, the wind blowing toward a wind turbine can be also affected by the wake effect, which is a loss of momentum (or speed) and extra turbulence due to an upstream wind turbine.

The blades are also exposed to gravity, which produces fatigue loading due to the rotation of the blades, see Fig 2.2. These loads are becoming increasingly important in the design process due to the progressive increase in the blade length, which can reach values nowadays up to 90 m. This is relevant considering the fact that the design lifetime of modern wind turbines corresponds normally to a number of rotations in the order of 10^8 to 10^9.

Furthermore, the blades are also exposed to centrifugal forces during rotation of the rotor. However, the effect of these loads on the fatigue life is not normally considered during the design process due to the low rotational speed of the blades, which are typically from 10 to 15 rpm for large rotor blades.

These loading conditions lead to establishing structural requirements of the blades in terms of stiffness, specific weight, and fatigue lifetime, to guaranty the integrity of the structure, as described below.

2.3 Blade structure, components and materials

Blade structural requirements are directly related with the external loads acting upon them. Each type of external load generates internal loads, which have to be accommodated structurally in order to guarantee the integrity of the blades during their operational lifetime. This has been done by designing several load-bearing components, such as shear web, spar caps, connections, and trailing-edge reinforcement, as shown in Fig. 2.3. From

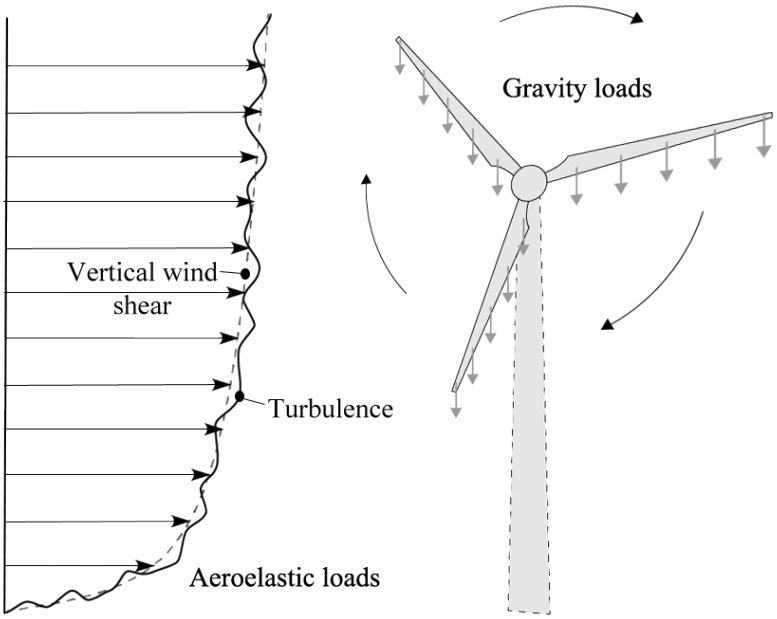

Figure 2.2: Aeroelastic and gravity loads on the wind turbine blades

a structural and an economic point of view, these components make the wind turbine rotor blade an integral structure with a complex and multifaceted design.

The aeroelastic loads, for example, produce a flap-wise bending moment on the blade due to the difference of pressure between the suction and the pressure sides. The flap-wise bending moment is carried by beam-like structures, which consist of two spar caps separated by one or two shear webs. The spar caps are mainly responsible for carrying the flap-wise moment and, therefore, are made mainly of unidirectional (UD) material, which has high axial strength. The pressure-side spar cap material is subjected to predominantly tensile loads, whereas the suction-side spar cap is subjected to predominantly compression loads. The two of them are under high fatigue loading conditions due to the variation of wind speed, wind shear, and gusts. The gravity loads, however, produce an edge-wise bending moment that is normally accommodated by axial reinforcements (i.e., UD material) near the leading and trailing edges.

The UD materials used in wind turbines can be either UD prepreg laminates or/and UD non-crimp fabric (NCF). The prepreg laminates are UD fibers pre-impregnated in a matrix by the manufacturer without a completed cured process, see Fig. 2.4-a. These materials have usually high fiber content and good mechanical properties; however, they are expensive due to their production and manufacturing methods. To address this economic limitation, the wind energy industry is increasingly using more UD NCF composites (see Fig. 2.4-b). These materials are made of normal UD fiber bundles reinforced with backing fiber bundles, which are oriented in a different angle with respect to the UD fiber bundles. In this sense, these materials have a lower fiber content ($\approx 90\%$ of fiber) compared with the pure UD materials (e.g. UD prepreg laminates). However, the backing material provides higher strength, ease of handling, and lower manufacturing costs to the UD fibers compared with the prepreg laminates.

Furthermore, the combination of the aeroelastic and gravity forces leads to torsion and shear loads that are carried mainly by the shear webs but also by aerodynamic shells. The shear webs and the aerodynamic shells are made of sandwich materials with biax and triax skin layers (i.e., $\pm 45°$ and $0/\pm 45°$ laminates, respectively) normally made of woven

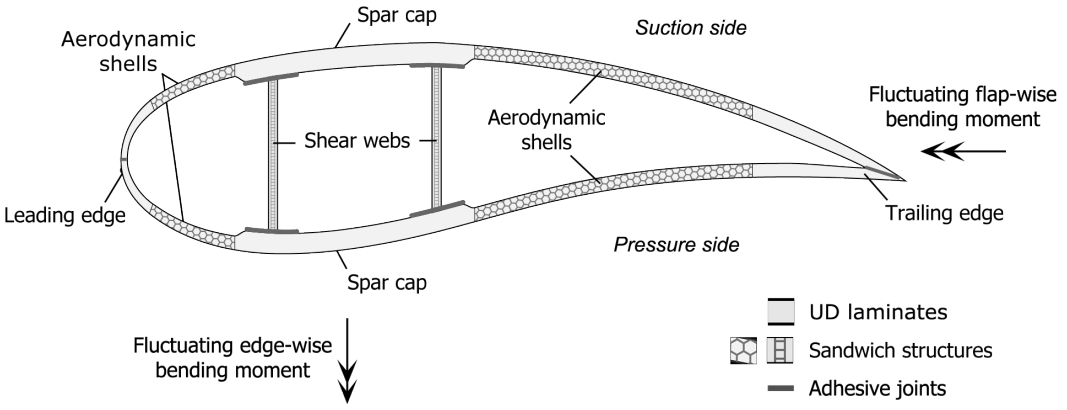

Figure 2.3: Internal loads and structure of the blades

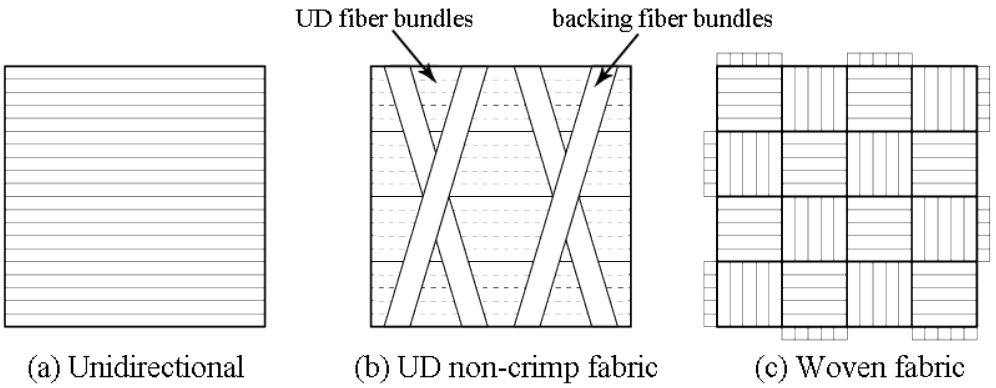

Figure 2.4: Normal composite materials used in wind turbine blades

fabric materials (see 2.4-c) and cores made from balsa wood, honeycomb structures, and polyvinyl chloride (PVC), among other materials.

Besides this, the load bearing components are usually molded and then glued together in an assembly process. This makes the adhesive joints a critical part of the blades because they are responsible for transferring all the internal loads along the load-bearing components.

2.4 Fatigue in composite wind turbine blades

2.4.1 Fatigue damage mechanisms of fiber composites

As shown in the previous section, the wind turbine blades are made of different composite materials, such as woven fabrics and UD prepreg laminates and/or UD noncrimp fabric. The UD prepreg laminates and the UD noncrimp fabric composites can also become multidirectional (MD) by orientating the UD plies in different directions. All these materials are used in different locations along the cross sections depending on the internal load type they must carry. And each of them exhibits different fatigue behaviors due to their internal configurations.

In the following sections, a brief description of the fatigue behavior of both UD and MD prepreg laminates and the UD noncrimp fabric composites is presented. However, no description of woven fabric will be given because, on the one hand, it is not normally used for the design of the blades, and, on the other hand, damage mechanisms presented in these materials are still not clear.

It is important to note that the damage mechanisms described in following sections have been identified during the last 40 years considering only tension-tension loading conditions. Even though a lot work remains, these identified damage mechanisms are an initial step toward a full understanding of the damage mechanisms involved in the other loading conditions.

2.4.1.1 Fatigue damage mechanisms in UD and MD laminates

The development of damage in MD laminates, such as MD prepreg laminates, is illustrated schematically in Fig. 2.5, which is based on observations reported by Reifsnider in [58]. As shown, the damage evolution can be divided into three stages. In the first stage, several off-axis cracks in the matrix initiate and propagate along the fibers in plies that are not aligned with the principal tensile-loading direction. The off-axis crack density increases with the number of cycles until a saturation condition is reached. During this stage, a high drop of the stiffness is presented due to the fast increase of the damage. The second stage initiates when the saturation condition is reached, which is characterized for the initiation and propagation of delaminations. During this stage, the damage increases almost linearly, thus leading to more stable stiffness degradation. Even though the off-axis cracks and delaminations are not critical for the final failure, they do contribute to the property degradation of the material and can trigger the fiber breaks. In the third stage, fiber breaks in the 0° plies initiate due to the high longitudinal stress. During this stage, the damage propagates rapidly until a critical condition is reached, which leads to the laminate separation. A deeper description of the MD laminates will be given in Chapter 4.

In the case of UD laminates, such UD prepeg laminates, the final failure is reached suddenly without any indication of stiffness degradation due to the absence of off-axis cracks and delaminations. So far, the different damage mechanisms involved in this type of laminate (i.e., fiber breaks, fragmentation, fiber/matrix debonding, and coalescence of

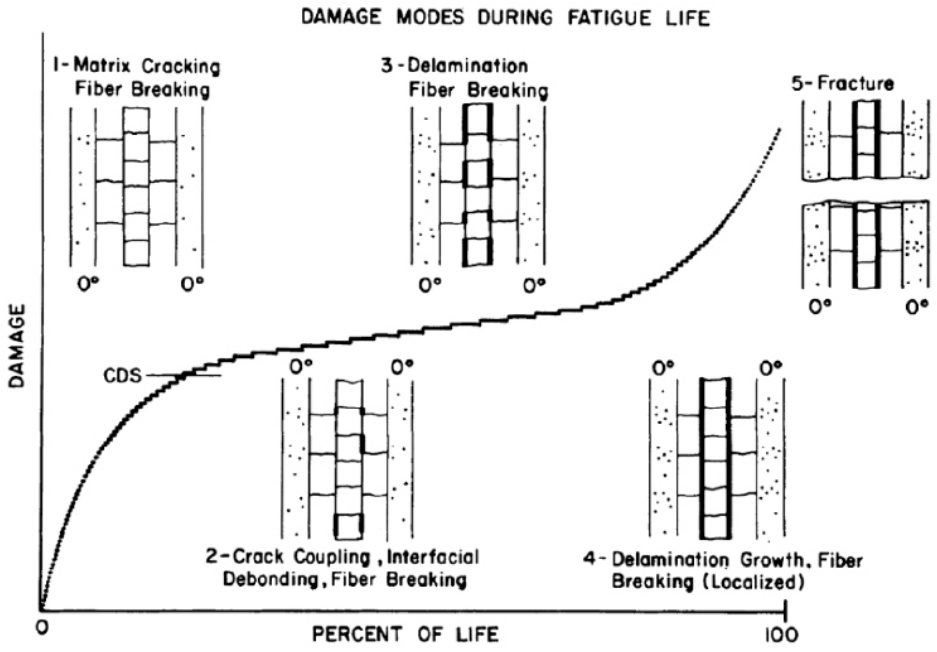

Figure 2.5: Damage progression scheme for composite materials proposed by Reifsnider [58]

isolated fiber breaks) have been identified qualitatively; however, it is still not clear how they interact with each other and how the final failure is reached. A better analysis of the fatigue behavior of UD laminates will be given in Chapters 4 and 8.

2.4.1.2 Fatigue damage mechanisms in UD non-crimp fabric

The development of damage in UD non-crimp fabric exhibits some differences than the one in prepreg laminates. Zangenberg et al. [81] established a damage progression scheme for this type of materials (see Fig. 2.6), which was recently expanded by Jespersen [37] based on a 3D x-ray computed tomography analysis.

As shown in Fig 2.6, the damage evolution of UD noncrimp fabrics is also divided into three stages. In the first stage, some off-axis cracks initiate and propagate in single backing fiber bundles together with UD fiber breaks located in those regions where the backing fiber bundles touch the UD bundle. The amount of off-axis cracks and fiber breaks depends on the local variation in the bundle structure in the composite. As in the prepreg laminates, a high drop of the stiffness is presented during this stage due to the fast increase of the damage. The second stage starts when the saturation condition of the off-axis cracks is close to be reached. The saturation condition seems to depend on the bundle thickness, the local bundle, and fiber architecture. The saturation process of the off-axis cracks is accompanied by UD fiber breaks that continue progressing into the thickness direction of the UD fiber bundle, even after the saturation point at the end of the third stage. During this stage, the property degradation is slower than the one in the first stage due to the saturation process. The damage progression in the last stage is still not clear. During this stage, the fiber breaks continue to spread farther away from the backing fiber bundles. This fiber breaking seems to be connected also with intralaminar splitting that grows until the remaining fibers cannot carry more load and the final failure takes place.

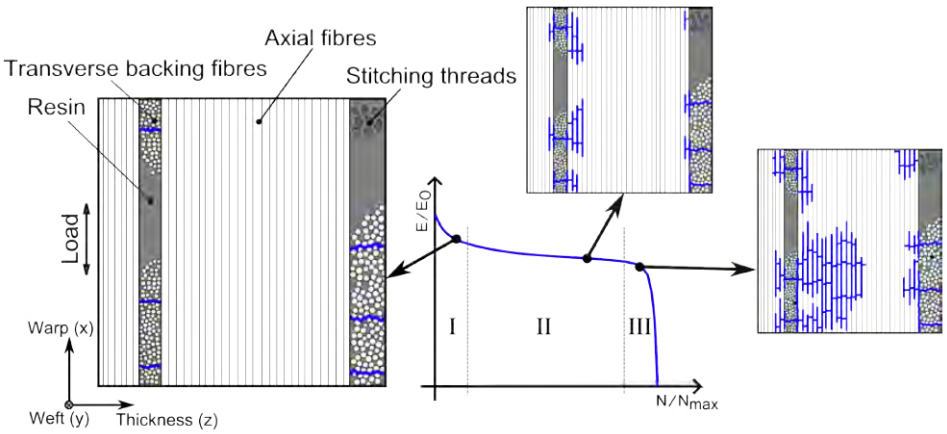

Figure 2.6: Simplified version of the damage progression scheme for UD non-crimp fabric composite materials proposed by Zangenberg et al [81], which was presented in [36]

2.4.2 Multiaxial loading conditions

The wind turbine blades are often treated as typical beam-like structures under separate loads in the edge-wise and/or flap-wise direction(s). However, in reality, the wind turbine blades are always under multiaxial stress states caused either by global multiaxiality or local multiaxiality. The global multiaxiality refers to the combination of gravity and aeroelastic forces, which results in a load component different than the traditional flap-wise and edge-wise load components. This real load component also induces torsion on the blades, which contributes greatly to the cross-sectional shear distortion. Moreover, because the wind turbine blades are made of composite multidirectional laminates, especially the shear webs and the aerodynamic shells, they are always under local multiaxiality due to the intrinsic material anisotropy (even if they are under uniaxial loading).

Both types of multiaxilities produce local stress states that are responsible for generating the damage mechanisms that lead to the global property degradation of the blades and their final failure. Unfortunately, so far, the damage mechanisms developed in composite materials under complex load conditions (e.g., tension-torsion, compression-torsion, nonproportionality bi-axial loads, etc.) are not yet known, which makes the development of precise methodologies to predict the fatigue response of the blades under real load conditions difficult.

Some experimental studies have shown that the multiaxial loading conditions could negatively affect the fatigue response of the composite materials compared with uni-axial loading conditions. For example, in [2, 65, 55], a considerable decrease of the fatigue strength was found in specimens under combined tension and shear loading conditions compared with specimens under only tension-loading conditions. In this sense, it is also expected that a combination of compression and shear loading leads to a detrimental response of the material. However, so far, there is no data related to this type of load due to the difficulty of applying compression on specimens without causing buckling.

Under this view, a decrease of the fatigue strength of the blades could be expected because a shear component may be present during the operation, as previously explained.

In order to evaluate the response of the wind turbine blades under multiaxial stress states, a description and analysis of the most accurate approaches and criteria available for life prediction of composite laminates under multiaxial fatigue will be given in Chapter 3.

2.4.3 Variability and stochastic behavior of loads

As previously explained, wind turbine blades are subjected to fluctuating gravity and aeroelastic loads that produce internal loads that fluctuate cyclically. The cyclic behavior of the internal loads mainly depends on the rotation of the rotor and the variation of the wind speed, see Fig. 2.7. The rotation of the rotor produces internal loads with high-amplitude cycles, which can be assumed deterministic and are easily calculated, whereas the variation of the wind speed produces internal loads with low-amplitude cycles, which cannot be assumed deterministic due to the stochastic behavior of the wind

and, therefore, are difficult to predict. For this reason, stochastic load predictions should be carried out during the design of the blades considering the variation of the wind speed and the turbulence intensity for each type of wind turbine.

The variation of the internal loads in the wind turbine blades may have a detrimental effect on the global properties of the composite materials and, therefore, accelerate the final failure of the structure. In [23], for example, it was shown that load sequences from high to low amplitude levels result in shorter lifetimes of cross-ply laminate than under load sequences from low to high amplitude levels. However, and despite its importance in the design of structural components, the effect of the variable amplitude loading conditions on the fatigue response of composite materials is, thus far, not well understood. In fact, most of the existing analyses that aimed to identify the fatigue damage mechanisms of composite materials have been carried out under constant amplitude loading conditions, and few of them under specific variable loading conditions.

Moreover, the damage accumulation theories applied in composite materials are still based on those created for metals, even knowing that the fatigue damage mechanisms are completely different in both materials. One of the main reasons for this lack of knowledge is the need for a high number of experiments in order to validate all possible combinations of load sequences, which demand longer times and high costs in terms of human resources and raw material.

For wind turbine blades, only a limited number of standardized variable amplitude load sequences are available. They are mainly the WISPER (WInd turbine reference SPEctRum) [31], WISPERX (shortened version of WISPER) [31] and NEW WISPER [47] load sequences, which will be described and analyzed further in Chapter 3.

2.4.4 Stochastic behavior of material properties

The fatigue behavior of the wind turbine blades is normally estimated assuming the material properties as deterministic. However, the composite materials exhibit high

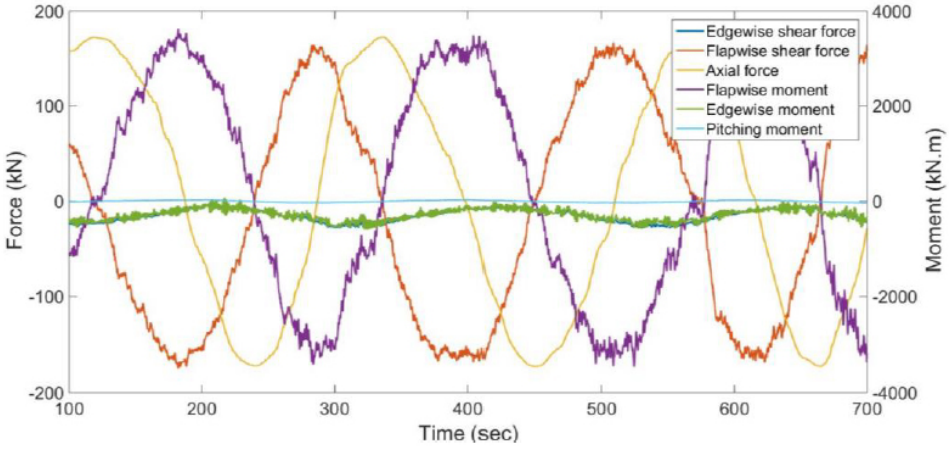

Figure 2.7: Cyclic behavior of internal loads of the blades

variability in their properties due to the inhomogeneous nature of their constituent materials (fiber and matrix) and to the manufacturing process, which can significantly affect the fatigue strength and the property degradation of the blades.

The variability of the material properties due to the manufacturing process can be related to cycle curing, bonding defects, fiber volume fraction, and imperfections, such as voids. The random scatter in these factors can affect the fatigue response of the materials at different levels. For example, in [43], it was shown that the detrimental effect of the presence of voids on the fatigue performances in composite laminates significantly varies with the void area fraction. For $[0/90_2]_s$ laminates, for example, the life to crack initiation was reduced by 80% for void area fractions only of 0.34% and by 98% for void area fractions of 6.7%.

This significant variability of the material fatigue response suggests that the stochastic behavior of the material properties should also be considered during the structural design of the wind turbine blades. For this reason, the effect of the variability of the material properties on the fatigue response of composite materials will be analyzed in the following chapters.

2.5 Current design methods against fatigue in wind turbine blades

Different models have been proposed to analyze the fatigue behavior of composite wind turbine blades based on fatigue models suggested for composite materials. These models can be grouped into three types of models: fatigue-life models, phenomenological models and damage mechanics models. Each of these models has advantages and disadvantages that make them more suitable, or less suitable, for better fatigue analysis of wind turbine blades.

In the following, a brief description of these models is provided.

2.5.1 Fatigue-life models

The fatigue-life models are simple and straightforward models based on empirical relations that can be easily implemented for the fatigue analysis of wind turbine blades. In fact, most of the analysis presented in the literature about fatigue of wind turbine blades are based on this type of models [48, 39, 79, 70, 35, 15], including the current standard lifetime prediction methods suggested by the IEC 61400-1 international standard [80] and the DNV GL certification and design guidelines [60], see Fig 2.8.

The IEC61400-1 standard suggests the evaluation of different design load cases related with normal power production, transitional, and parked conditions, such as power production (DLC 1.2), power production plus occurrence of fault (DLC 2.4), start-up (DLC 3.1), normal shutdown (DLC 4.1) and parked (DLC 6.4). These loads are normally calculated from aeroelastic simulations according to the wind speed and turbulence parameters of the wind turbines.

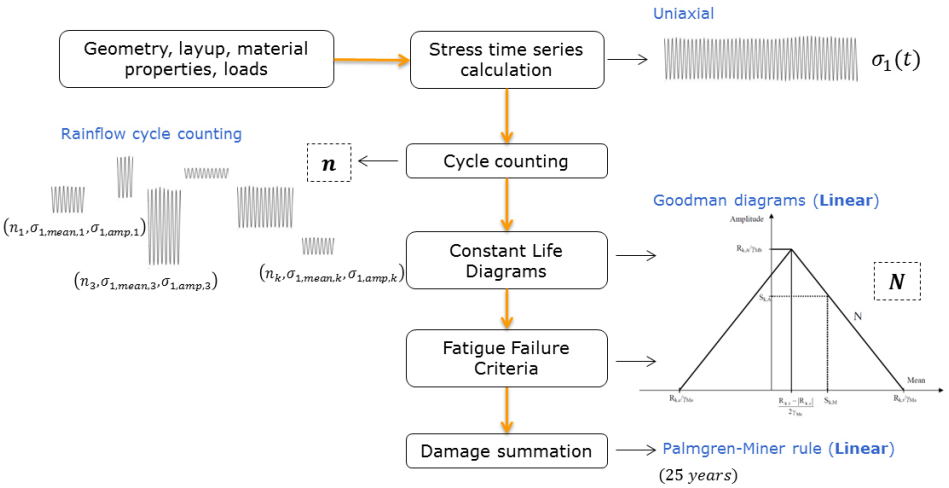

Figure 2.8: Current standard fatigue method for wind turbine blades

Based on the aeroelastic loads, flap-wise and edge-wise moments may be applied independently along the blade in order to obtain, for each of them, normal stress (or strain) time series in different points along desired blade cross sections. Using the rain-flow-cycle counting method, these normal stress (strain) time series are then converted into blocks of a certain numbers of cycles, n_i, with equal amplitude and mean values. Based on the load conditions of each block of cycles, the number of allowable cycles, N_i, is obtained via the Goodman diagram, which suggests a linear relationship between the mean and the amplitude stresses (strains). The number of allowable cycles can then be found as follows:

$$N_i = \left(\frac{R_{k,amp} - \mid \gamma_{m,shorttem} . S_{k,mean} - \left(\frac{R_{k,t} - |R_{k,c}|}{2} \right) \mid}{\gamma_{m,fatigue} . S_{k,amp}} \right)^m \tag{2.5}$$

assuming $R_{k,amp} = R_{k,t} + \mid R_{k,c} \mid /2$, where $R_{k,amp}$ is the amplitude of characteristic structural member resistance for $N = 1$, $R_{k,t}$ is the characteristic short-term structural member resistance in tension, $R_{k,c}$ is the characteristic short-term structural member resistance in compression, m is the slope parameter of the S-N curve, $\gamma_{m,shorttem}$ is the reduction factor γ_m for short-term verification, $\gamma_{m,fatigue}$ is the reduction factor γ_m for fatigue verification, $S_{k,mean}$ is the mean value of the load and $S_{k,amp}$ is the amplitude value of the load.

The last step in the lifetime prediction is the calculation of the damage accumulation, which is based on the linear Palmgren-Miner rule:

$$D = \sum_i \frac{n_i}{N_i} \leqslant 1 \tag{2.6}$$

where D is the total damage, n_i is the number of load cycles in the fatigue load block i, and N_i is the allowable number of cycles for the load amplitude $S_{k,amp}$ and mean $S_{k,mean}$ in block i.

By applying this standard model, the cumulative damage and lifetime prediction of each ply from a given blade's cross-section can be easily obtained; however, this model does not provide detail about stiffness degradation of the structure and does not consider either any physical failure mechanisms of the material. In addition, the fact that linear, uni-axial, phenomenological, and mainly deterministic approaches are used in this model lead to the conservative designs of the current wind turbine blades.

To provide better solutions for composite materials, and thereby for wind turbine blades, some modifications to the described standard fatigue-life model have been proposed in the last years, such as new constant life diagrams and multiaxial macroscopic fatigue failure criteria. A more detailed description of the fatigue-life models and their modifications will be given in Chapter 3.

2.5.2 Phenomenological fatigue models

The phenomenological models are also based on empirical relations, but they do predict the material property degradation in terms of stiffness and/or strength. However, the evolution laws used for the property degradation predictions are not directly related to the physical damage mechanisms developed inside the material.

In [62], the fatigue lifetime of a wind turbine blade under operating and external loading conditions was estimated by using this type of model. In this study, the estimation of the fatigue lifetime was based on a stiffness degradation technique developed in [61], which used the Hashin's criterion to predict the failure of the plies. Even though the Hashin's fatigue failure criterion was proposed based on different damage modes found during the failure of composite materials [30], it does not really consider the evolution of any damage mechanism developed in the material. Moreover, even though the model proposed in [62] was based on the stiffness degradation of the material, the stiffness degradation of the entire blade was not estimated.

Perhaps the most critical limitation of the phenomenological models is related to their applicability, which is restricted only to the laminates that were tested to develop the model. This would entail a non-viable experimental effort for applications on wind turbine blades since these structures are made of several types of laminates, which thickness and layup change continuously along the blade. In this sense, based on the opinion of the author, the phenomenological fatigue models are unfeasible for wind turbines blades and, therefore, will not be analyzed in this study.

2.5.3 Damage mechanics models

In contrast with previous models, the damage mechanics models predict the fatigue lifetime and the material property degradation of composite materials (and by implication, of structures made of these materials) based on their actual physical damage mechanisms, such as off-axis matrix cracks, delaminations, and fiber breakages.

A recent study [46] proposed an interesting multiscale approach based on damage mechanics models for predicting the fatigue response of wind turbine blades. By combining computational micromechanics and continuum damage mechanics in a 3D finite element

model, the evolution of off-axis matrix cracks in different regions of a blade was predicted in this study. In addition, the effect of the off-axis matrix cracks on the structural response of the blade in terms of tip displacement was also predicted through its fatigue lifetime.

As shown in [46], the damage mechanics models along with multiscale models are a potential approach for developing more accurate and reliable models for wind turbine blades. However, these models are much more computationally intensive than the fatigue-life and phenomenological models, which makes their implementation in wind turbine blades more difficult in terms of computational resources. A more detailed description of these models and their applicability on wind turbine blades will be given in Chapter 4.

2.6 Design trends against fatigue in wind turbine blades

In the last years, multiscale approaches have attracted significant attention in the wind energy sector as a strategy for the structural design of the blades. With the multiscale approach, different analysis models at different scales, such as the microscale (material), macroscale (test specimen), subcomponent scale (blade sections, spars, shell, etc.), and full scale (wind turbine rotor blade) are sequentially coupled (see Fig 2.9), thus giving a better description of structural response of the blades [64].

This coupling process demands some challenges in terms of developing high-fidelity models in all scales, which must be validated against experimental testing, along with developing consistent and computationally efficient interfaces between the different scales. These challenges are based on current limitations presented in the different scales, which should be addressed simultaneously.

In the micro- and macroscale level, for example, more accurate fatigue models of composite materials under multiaxial and variable load conditions are still needed. Development of these models at these scales (micro and macro) is a challenging problem that has to be solved in order to make a better fatigue characterization of the blades at higher scales. Thus far, the fatigue behavior of composites has been studied by using fatigue-life and phenomenological and damage mechanics models; however, none of them adequately address the above limitations. In addition, as discussed in the previous section, each of these fatigue models has other limitations that constrain their application for the fatigue analysis of wind turbine blades.

Besides the fact that the fatigue models must consider the effects of multiaxial and variable load conditions, they must also be applicable to composite materials under different fatigue loading conditions (i.e., tension-tension, tension-compression, compression-tension, compression-compression), which are presented in wind turbine blades during their lifetime. Moreover, the stochastic behavior of the material properties in terms of nature variability of the constituent materials (fiber and matrix) and the imperfections generated during the manufacturing process (e.g., voids) must be also considered.

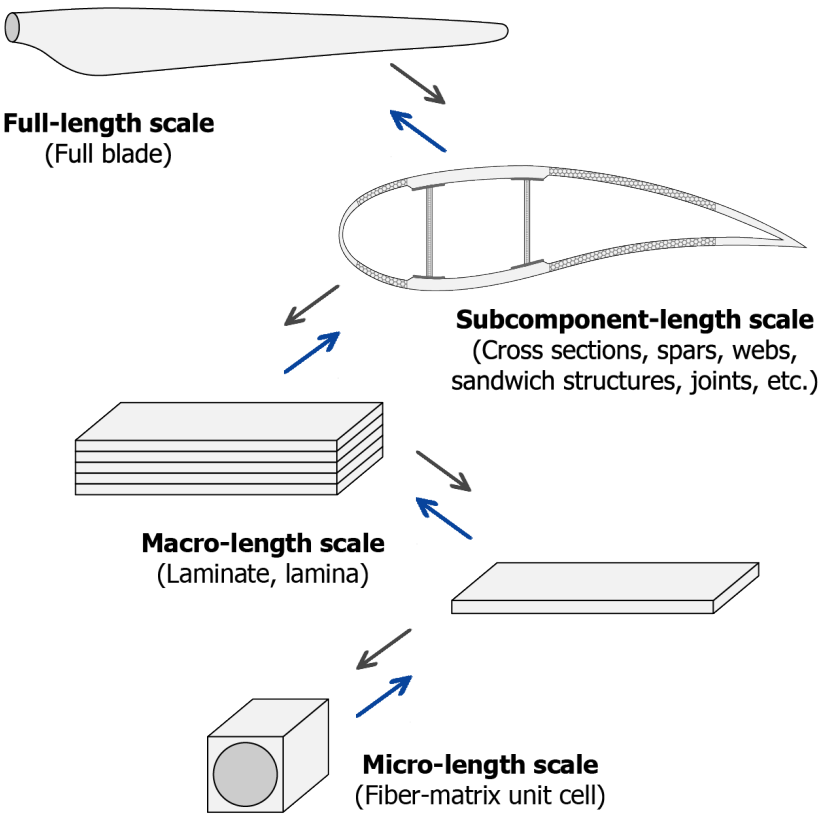

Figure 2.9: Multiscale approach for designing wind turbine blades

In the subcomponent scale level, one of the current limitations is the lack of more generic analytical models that can predict the initiation and propagation of cracks in the different joints located in wind turbine blades. The development of these models is extremely challenging but, at the same time, necessary because the structural integrity of the blades depends largely on the joints, which are the most likely locations for failure initiation. Another important limitation in this scale level is the complexity of replicating the load conditions and mechanical behavior of the blade substructures at the laboratory, which makes the experimental validation difficult for the analytical models.

In the full-scale level, the fact that the fatigue models in lower scale levels are still not accurate is a limitation itself because they determine the fatigue model of the full structure. Furthermore, the scaling laws are currently unknown or poorly understood. Besides, there is also a big challenge for the wind energy industry, which needs to develop fast and efficient fatigue test methods that better match the variability, multiaxiality, and stochastic behavior of the loads to which the blades are exposed to in real operational conditions. This challenge is currently being addressed by DTU Wind Energy in cooperation with different industrial partners in the wind energy field, and DNV GL through the BLATIGUE (fast and efficient fatigue test of large wind turbine blades) project, which is supported by the EUDP (Energy Technology Development and Demonstration Program). The BLATIGUE project is primarily focused on developing

advanced multiaxis fatigue-testing methods and multiaxis fatigue exciters for large blades.

2.7 Fatigue factors considered in current project

Since the aim of this project is to develop accurate and reliable models for designing wind turbine blades against fatigue, the fatigue factors described above, or some of them must be considered in the models proposed in this study.

As a first step towards the development of models that allow predicting the completed fatigue response of the wind turbine blades, in this project special attention will be given to the effects of the stochastic behavior of the material properties and the implicit multiaxial stress state of the composite materials on the fatigue response of these structures. This will be done by using both fatigue-life models and damage mechanics models.

In the next chapter, a probabilistic multiaxial fatigue model for composite materials considering the uncertainties in the material properties is proposed; whereas in Chapter 4, a multiscale approach for fatigue design of wind turbine blades based on damage mechanics models is suggested, in which the multiaxiality state and the property variability of the composite materials can be also considered.

CHAPTER 3
Probabilistic multiaxial fatigue-life models

As described in the previous chapter, a better design of wind turbine blades against fatigue could be obtained if the stochastic behavior of the loads, the material properties, and the multiaxial stress states to which the blades are exposed to during their operational lifetime are considered during the design process.

In this chapter, a probabilistic multiaxial fatigue model for composite materials is proposed. This model is based on fatigue-life methods and takes uncertainties in the material properties into account. Fatigue-life predictions of different glass/epoxy laminates are carried out to validate the proposed model against experimental data. Based on the obtained results, an evaluation of the applicability of the proposed model in full wind turbine blades is performed at the end of the chapter. This evaluation demonstrates that the low accuracy level of current fatigue-life criteria and damage accumulation theories for predicting the fatigue lifetime of composite materials affects the applicability of the proposed probabilistic multiaxial fatigue model in wind turbine blades.

3.1 Probabilistic multiaxial fatigue-life model approach

As described in section 2.6, three types of models can be used to analyze fatigue behavior of composite materials: fatigue-life models, phenomenological models, and damage mechanics models. Compared with the phenomenological and damage mechanics models, the fatigue-life models have been used extensively to model fatigue behavior of composite materials (see summary in [55]) due to their simplicity and capabilities of considering variable amplitude loading conditions, different load conditions (e.g., tension-tension, tension-compression, etc.) and complex stress states (i.e., multiaxiality). Moreover, they can be applied to any type of laminate configuration if the mechanical properties of the constitutive plies are known.

The fatigue-life models for composites were originally inspired by deterministic fatigue-life models developed for metals, which assume a symmetric and linear fatigue behavior of the material from tension to compression, see Goodman diagram in Fig. 2.8. These assumptions perform well for metals due to their natural homogeneity; however, they lead to inaccurate estimations for composite materials whose fatigue response is different under tension and compression loading conditions. Furthermore, these original models only consider uniaxial stress states, which further limits their application in composite

materials because they are, in most cases, under multiaxial stress states, as described in section 2.4.2.

Despite these limitations, the fatigue-life models for composites have been used extensively for the standard design of wind turbines blades, as described in section 2.5, which has resulted in conservative designs.

To provide better solutions for composite materials, some modifications to the original fatigue-life models have been proposed in the last 40 years, which are illustrated in Fig. 3.1. One of these modifications has been the development of more sophisticated constant life diagrams (CLDs) as opposed to the classical Goodman diagram shown in Fig. 2.8. The CLDs provide a graphical representation of given fatigue lives and their corresponding safe regime of constant amplitude loading at any R-ratio. All the proposed CLDs aim to consider the differences in the fatigue response of the composite materials under the different loading conditions by means of an interpolation process between known S-N curves and static strength data, see summary in [76, 77].

Another modification to the original fatigue-life models is the development of deterministic multiaxial macroscopic fatigue failure criteria (MMFF), which take the effect of the transverse and shear stress components into account for the estimation of the material fatigue lifetime, see Fig. 3.1. Most of these criteria are adaptations of static criteria, in which the failure tensor components are substituted by the corresponding S-N curves, see summary in [55]. A more detailed description of MMFF criteria will be given in section 3.3.2.

Based on the described original and modified deterministic fatigue-life models, probabilistic fatigue models have been proposed in order to consider the stochastic behavior of different parameters, such as loads and materials properties. These models have been proposed mainly for the design of wind turbine blades (see, e.g., [69, 78, 71, 44, 3, 20]), in

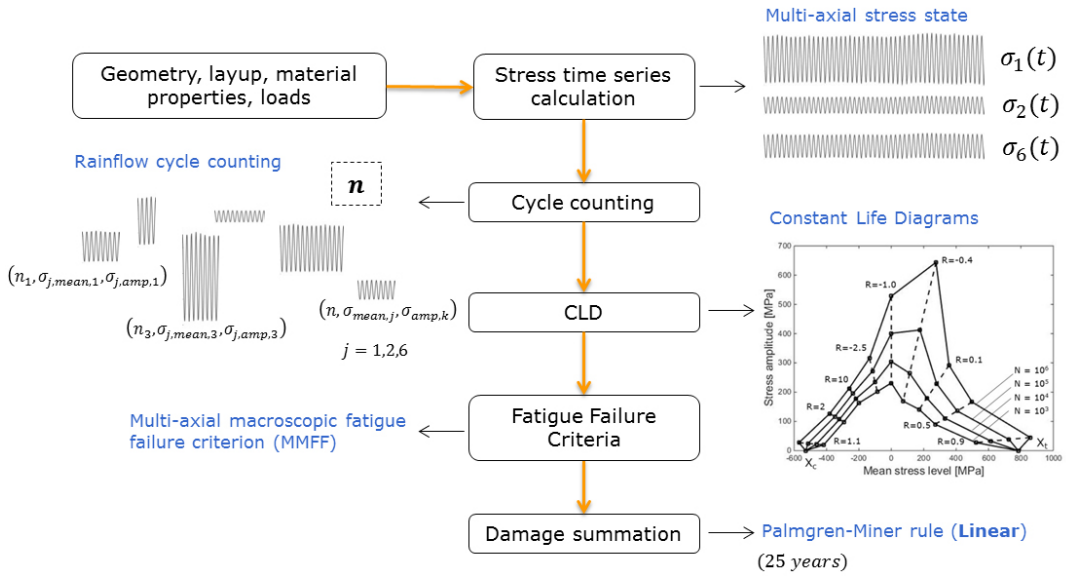

Figure 3.1: Deterministic multiaxial fatigue-life approach

which the materials properties are assumed as stochastic variables, X_{mat}, and the loads are assumed as model uncertainties, X_L, see Fig 3.2. These models also take into account additional uncertainties related to the different steps along the fatigue calculation process, such as uncertainties in calculated stresses, X_{st}, rain-flow counting method, X_{RFC}, and cumulative damage model, X_{CDM}.

The probabilistic fatigue-life models are based on reliability analysis that relates the uncertain demand S and the uncertain capacity C by considering the following $C - S$ limit state equation:

$$g(X) = C(X; X_{capacity}) - S(X; X_{demand}) \tag{3.1}$$

where the demand and the capacity are functions of the stochastic variables X (i.e., X_{mat}), and the variables X_{demand} and $X_{capacity}$, which are related to the other uncertainties (i.e., X_L, X_{st}, X_{RFC}, X_{CDM}, etc.).

In most of these models, [69, 78, 71, 44, 3, 20], the reliability is estimated assuming uniaxial stress states and, only in [20], a probabilistic fatigue-life model for multiaxial stress states was developed. In addition, all of them consider the stochastic behavior of the material properties through probabilistic S-N curves obtained from experimental coupon tests under specific loading conditions, i.e., only under $R = 0.1$ or under $R = -1$. This means that the applicability of these approaches is limited to the loading conditions that were tested to develop the models and no variable amplitude loading conditions with different R-ratios can be taken into account.

Considering the fact that the wind turbine blades are subjected to several loading conditions and complex stress states during their lifetime, a probabilistic fatigue-life model that takes into account variable amplitude loading conditions and multiaxial stress states is proposed in the following sections.

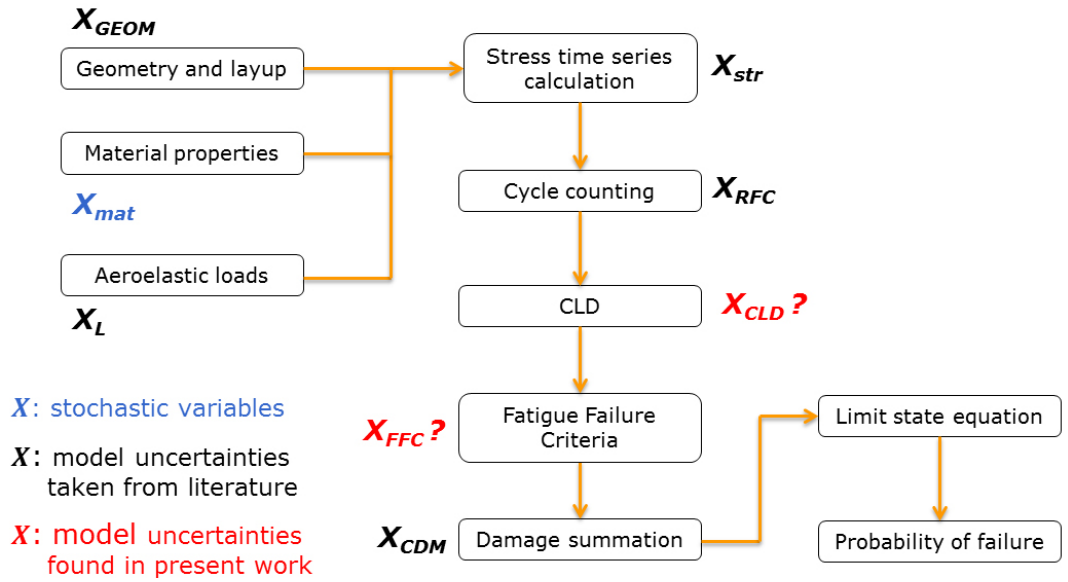

Figure 3.2: Probabilistic multiaxial fatigue-life approach

In the next section, probabilistic constant life diagrams (P-CLDs) built based on the uncertainty in the fatigue properties of the materials are developed. The model uncertainty in the P-CLDs, X_{CLD}, is then used in a reliability analysis for fatigue-limit state of composite laminates under variable amplitude loading cycles and under uniaxial stress states. In section 3.3, the X_{CLD} uncertainty is also propagated through multiaxial fatigue-life criteria to quantify the probability of failure of composite laminates under multiaxial stress states, X_{FFC}.

All this process is carried out analyzing not only the level of accuracy of the estimated model uncertainties along the fatigue calculation process but also the level of accuracy of the methods in themselves (i.e., CLDs, fatigue failure criteria, and cumulative damage model). Based on this analysis, an evaluation of the applicability of the proposed probabilistic multiaxial fatigue-life model for the design against fatigue of full wind turbine blades is carried out in section 3.4.

3.2 Assessment and propagation of mechanical property uncertainties in uniaxial fatigue-life models of composite laminates

Paper 1. Oscar Castro, Kim Branner, and Nikolay Dimitrov (2017). Assessment and propagation of mechanical property uncertainties in fatigue life prediction of composite laminates. Journal of Composites Materials. Accepted for publication.

With the aim of evaluating the advantages of considering the variability in the material properties during the fatigue lifetime estimation, *Paper 1* (see Chapter 6) presented a probabilistic uniaxial fatigue-life model developed for composite materials under constant and variable amplitude loading conditions.

The variability in the fatigue properties (i.e., ε-N curves) of the materials was determined from fatigue coupon tests. ε-N curves (where ε is the normalized stress respect to the static stiffness, $\varepsilon = \sigma/E_0$) were used instead of S-N curves. A log-log ε-N curve based on the Basquin equation was assumed to fit experimental data and model the fatigue behaviour of the material, as follows:

$$\log \varepsilon_{amp} = \log K - m \log N + \epsilon \tag{3.2}$$

where N is the number of cycles to failure, ϵ is the fitting error, which was assumed normally distributed with standard deviation s_ϵ, and $\log K$ and m are the intercept and the slope of the curve, respectively. Note that Eq. 3.2 considers the applied stress level as a function of the number of cycle to failure (i.e., $\log \varepsilon_{amp} = f(\log N)$), which is the opposite of what is proposed by Basquin equation. The form of Eq. 3.2 was assumed in this way in order to facilitate the propagation of the ε-N curve uncertainty in constant life diagrams (CLDs), see more details in section 2.1 of *Paper 1* (Chapter 6).

The parameters $\log K$ and m, and the parameter s_ϵ, were estimated by the maximum likelihood method by maximizing the LogLikelihood function $L(\log K, m, s_\epsilon^2) = \sum_{j=1}^{n} \log(p(\log \hat{\varepsilon_{amp}}_j | \log \hat{N}_j; \log K, m, s_\epsilon^2))$. The slope m was assumed deterministic and

the parameters $\log K$ and s_ϵ were assumed uncorrelated. The parameters $s_{\log K}$ and s_{s_ϵ} were estimated using the following covariance matrix $\mathbf{C}$, see, e.g., [41]:

$$\mathbf{C} = [-\mathbf{H}]^{-1} \tag{3.3}$$

where $\mathbf{H}$ is the Hessian matrix of second order derivatives of the log-likelihood function. Then, the variability in the parameter $\log \varepsilon_{amp}$, $s_{\log \varepsilon_{amp}}$, was expressed as

$$s_{\log \varepsilon_{amp}} = \sqrt{s_{\log K}^2 + s_\epsilon^2} \tag{3.4}$$

and the variability in the normalized stress amplitude, $s_{\varepsilon_{amp}}$, of an ε-N curve was approximated to the following expression:

$$s_{\varepsilon_{amp}} \approx |\varepsilon_{amp}(\ln(10) s_{\log \varepsilon_{amp}})| \tag{3.5}$$

Moreover, the variability in the number of cycles to failure, s_N, for a given normalized stress amplitude ε_{amp} was expressed as

$$s_N = \frac{1}{m} \frac{(K)^{\frac{1-m}{m}}}{\varepsilon_{amp}^{1/m}} s_{\varepsilon_{amp}} \tag{3.6}$$

Based on this, probabilistic fatigue-life diagrams (P-CLDs) were developed by propagating the determined variability in the ε-N curves in existing constant lifetime diagrams, see Fig. 3.3. The uncertainty propagation was carried out using the first-order Taylor series, in which the quantity $z = f(x_1, x_2, ..., x_{N_x})$ depending on N_x stochastic variables is linearized as follows:

$$z - \mu_z = \sum_{i=1}^{N_x} \frac{\partial f}{\partial x_i}(x_i - \mu_{x_i}) \tag{3.7}$$

where all higher-order terms were assumed to be negligible and $\mu_z = f(\mu_1, \mu_2, ..., \mu_{N_x})$. By using this method, the variance of z is estimated by the expectation of the squared deviation $(z - \mu_z)^2$, i.e. $E[(z - \mu_z)^2] = s_z^2$, which can be expressed as

$$s_z^2 = \sum_{i=1}^{N_x} \Big(\frac{\partial f}{\partial x_i}\Big)^2 s_i^2 + 2 \sum_{i=1}^{N_x - 1} \sum_{j=i+1}^{N_x} \frac{\partial}{\partial x_i} \frac{\partial}{\partial x_j} s_i s_j \rho_{ij} \tag{3.8}$$

where $s_i^2 = E[(x_i - \mu_{x_i})^2]$ is the variance of x_i and ρ_{ij} is the correlation coefficient of x_i and x_j.

For the construction of the P-CLDs, the normalized stress amplitude of an unknown ε-N curve, ε'_{amp}, was assumed as the quantity z in Eqs. (3.7) and (3.8). The function f and the parameters x_i depended on the interpolation method used by deterministic CLDs in each of the tension-tension (T-T), tension-compression (T-C), compression-tension (C-T), and compression-compression (C-C) loading conditions. Assuming deterministic the stress ratio R' of the desired ε-N curve and the stress ratios R_i of the known ε-N curves, it was demonstrated that the normalized stress amplitude ε'_{amp} of the desired

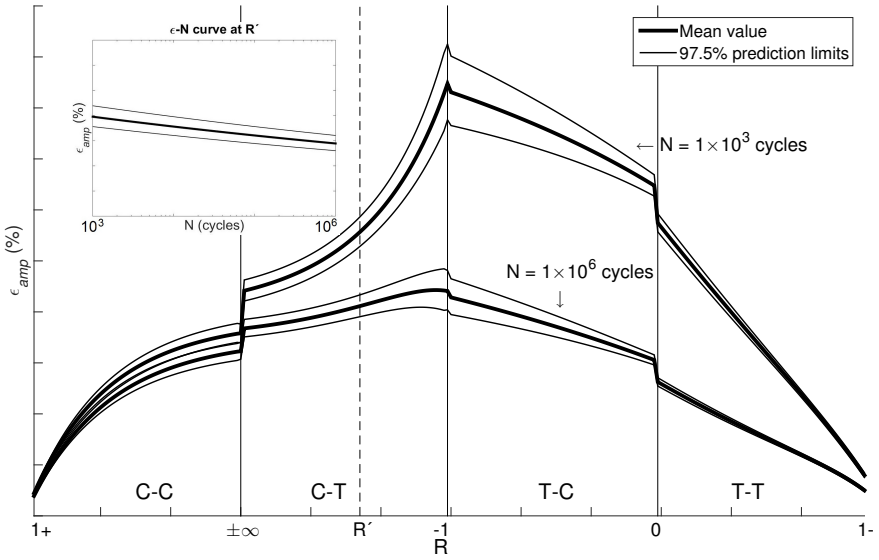

Figure 3.3: Probabilistic constant life diagram (P-CLD). Thick lines represent mean $\varepsilon - N$ curve, thin lines represent ± 1 standard deviations from the mean.

ε-N curve can be estimated as a function only of the normalized stress amplitude ε_{ampi} of the known ε-N curves; see more details in *Paper 1* (Chapter 6).

In this way, the parameter ε_{ampi} was considered as the stochastic variable x_i in Eq. 3.7, leading to the following equation, which was used to estimate the model uncertainty $s_{\varepsilon'_{amp}}$ in each region (i.e., at T-T, T-C, C-T, C-C) of the deterministic CLD:

$$s^2_{\varepsilon'_{amp}} = \sum_{i=1}^{2} \Big(\frac{\partial f}{\partial \varepsilon_{ampi}}\Big)^2 s^2_{\varepsilon_{ampi}} \tag{3.9}$$

where $\partial f / \partial \varepsilon_{ampi}$ is the partial derivative of the interpolation function used by the deterministic CLD with respect to the known normalized stress amplitude ε_{ampi} and $s_{\varepsilon_{ampi}}$ is the variability in the ε-N curves defined in Eq 3.5. In addition, the variability in the number of cycles to failure, s_N, for a given normalized stress amplitude ε'_{amp} from an interpolated ε-N curve was estimated by Eq. 3.6.

By using these P-CLDs, any probabilistic ε-N curves at any load level and R-ratio were efficiently calculated by interpolation process between known ε-N curves. In this work, unidirectional (UD) and multidirectional (MD) $[[\pm 45/0]_4/\pm 45]$ E-glass/epoxy laminate were analyzed. Based on obtained results, it was shown that the variability in the ε-N curves estimated by the P-CLDs was comparable with that estimated from the experimental data.

In addition, a reliability analysis was also carried out to estimate the probability of failure of composite laminates under variable amplitude loading cycles, considering the variability in the ε-N curves obtained from the developed P-CLDs. The reliability was

estimated assuming a limit state equation based on the Palmgren-Miner's rule through the Monte Carlo simulation method.

The reliability analysis was evaluated for repeated block tests and spectrum fatigue data using WISPER (WInd turbine reference SPEctRum) [31], WISPERX (shortened version of WISPER) [31] and NEW WISPER [47] standardized load spectra for wind turbine blades. Comparison with the experimental data shows that reliable fatigue-life predictions of composite materials under variable amplitude loading cycles can be efficiently obtained by using the proposed reliability analysis.

However, it was also shown that the low level of accuracy of the Palmgren-Miner's rule for predicting the fatigue lifetime of composite materials affects the applicability of the proposed reliability model. This is due to the fact that the Palmgren-Miner's rule does not consider possible nonlinearities during the progressive damage of composite materials under different fatigue loading conditions; therefore, the estimated fatigue limit can take either higher or lower values than the one at failure.

3.3 Propagation of the uncertainties in multiaxial fatigue-life criteria

3.3.1 Preliminary definitions on multiaxial stress states

As explained in Quaresimin et al. [55], when composite materials are subjected to external cyclic loads, an internal plane stress state acting in each point O of the material is caused, see Fig. 3.4. This stress state can be analyzed from a global point of view by using a reference coordinate system xyz related to the entire laminate or from a local point of view through a reference coordinate system 123 related to each ply of the laminate.

In order to define the basic concepts of multiaxial stress states, assume that the material is subjected to the following global synchronous sinusoidal stress state, which is a simplification of the stress states in real structures:

$$\begin{aligned} \sigma_x(t) &= \sigma_{x,mean} + \sigma_{x,amp}\sin(\omega \cdot t) \\ \sigma_y(t) &= \sigma_{y,mean} + \sigma_{y,amp}\sin(\omega \cdot t - \delta_{y,x}) \\ \tau_{xy}(t) &= \tau_{xy,mean} + \tau_{xy,amp}\sin(\omega \cdot t - \delta_{xy,x}) \end{aligned} \tag{3.10}$$

In this global synchronous sinusoidal stress state, all global time series $\sigma_x(t)$, $\sigma_y(t)$ and $\tau_{xy}(t)$ (i.e., global axial, transverse, and shear stresses, respectively) have the same angular velocity, ω, but phase shifts $\delta_{y,x}$ and $\delta_{xy,x}$, which are defined as the phase shifts between $\sigma_y(t)$ and $\sigma_x(t)$ and between $\tau_{xy}(t)$ and $\sigma_x(t)$, respectively. Based on this, and as described in [55], the level of global multiaxiality can be determined by using the following global biaxility ratios:

$$\lambda_C = \frac{\sigma_{y,amp}}{\sigma_{x,amp}} \tag{3.11}$$

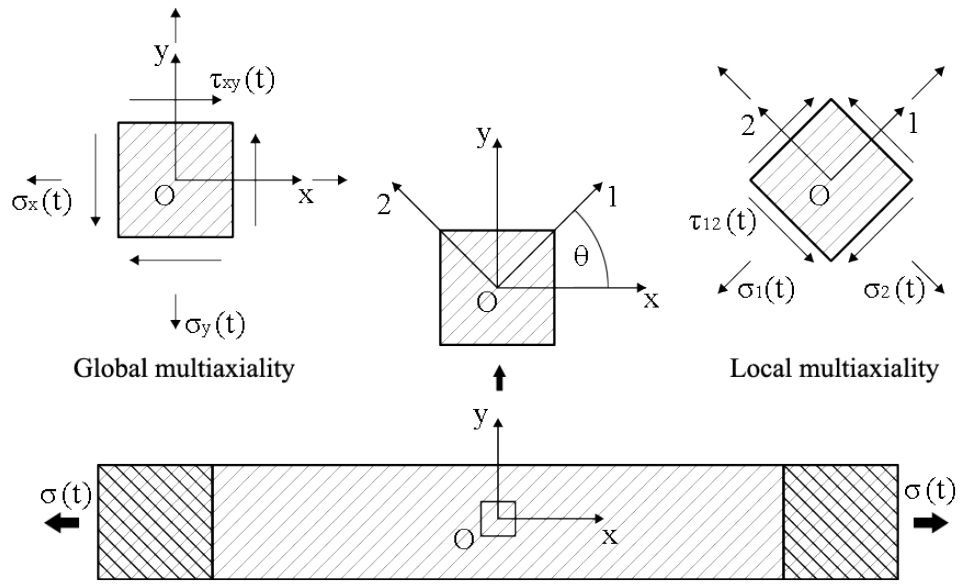

Figure 3.4: Multiaxial stress states in composite materials

$$\lambda_T = \frac{\tau_{xy,amp}}{\sigma_{x,amp}} \tag{3.12}$$

where $\sigma_{x,amp}$, $\sigma_{y,amp}$ and $\tau_{xy,amp}$ are the global axial, transverse, and shear amplitude stresses, respectively.

However, because fatigue is a localized structural damage, the actual stress states that lead to the local damage mechanisms in each ply can be hidden if the global stress states are used. Hence, it is more convenient to use the local stress states in each ply, which can be defined as a function of the global stress states, as follows:

$$\begin{Bmatrix} \sigma_1(t) \\ \sigma_2(t) \\ \sigma_6(t) \end{Bmatrix} = \begin{bmatrix} \cos^2(\theta) & \sin^2(\theta) & 2\cos(\theta)\sin(\theta) \\ \sin^2(\theta) & \cos^2(\theta) & -2\cos(\theta)\sin(\theta) \\ -\cos(\theta)\sin(\theta) & \cos(\theta)\sin(\theta) & (\cos^2(\theta) - \sin^2(\theta)) \end{bmatrix} \begin{Bmatrix} \sigma_x(t) \\ \sigma_y(t) \\ \sigma_{xy}(t) \end{Bmatrix} \tag{3.13}$$

where $\sigma_1(t)$, $\sigma_2(t)$ and $\sigma_6(t)$ are the local axial, transverse, and shear stresses, respectively, and θ is the angle between the local reference coordinate system 123 with respect to the global reference coordinate system xyz. Based on Eq.3.10 and Eq.3.13, the local stress states can be also assumed as a synchronous sinusoidal stress state, as follows:

$$\begin{aligned} \sigma_1(t) &= \sigma_{1,mean} + \sigma_{1,amp}\sin(\omega \cdot t) \\ \sigma_2(t) &= \sigma_{2,mean} + \sigma_{2,amp}\sin(\omega \cdot t - \delta_{2,1}) \\ \sigma_6(t) &= \sigma_{6,mean} + \sigma_{6,amp}\sin(\omega \cdot t - \delta_{6,1}) \end{aligned} \tag{3.14}$$

where $\delta_{2,1}$ and $\delta_{6,1}$ are, in this case, the phase shifts between $\sigma_2(t)$ and $\sigma_1(t)$ and between $\sigma_6(t)$ and $\sigma_1(t)$, respectively. Then, the level of local multiaxiality can be determined by using the following local biaxility ratios:

$$\lambda_1 = \frac{\sigma_{2,amp}}{\sigma_{1,amp}} \tag{3.15}$$

$$\lambda_2 = \frac{\sigma_{6,amp}}{\sigma_{1,amp}} \tag{3.16}$$

where $\sigma_{1,amp}$, $\sigma_{2,amp}$ and $\sigma_{6,amp}$ are the local axial, transverse, and shear amplitude stresses, respectively.

The complexity of the local multiaxial stress state is related to the similarities of the different stress time series (i.e., $\sigma_j(t)$ where $j = 1, 2, 6$), which can vary depending on the global multiaxial loading conditions, the mechanical properties of the entire laminate, and the orientation of each ply with respect to the applied loads. Assuming the synchronous sinusoidal stress state presented in Eq. 3.14, this complexity in the local multiaxial stress state can be evaluated by analyzing if the stress time series are in phase or out of phase with each other through $\delta_{2,1}$ and $\delta_{6,1}$.

However, it is also possible that the stress time series do not follow a synchronous sinusoidal behavior and that they are completely different from each other. In this case, the degree of similarity can be evaluated using the following correlation coefficients between the stress time series:

$$\rho_{1,2} = \frac{cov(\sigma_1(t), \sigma_2(t))}{s_{\sigma_1(t)}, s_{\sigma_2(t)}} \tag{3.17}$$

$$\rho_{1,6} = \frac{cov(\sigma_1(t), \sigma_6(t))}{s_{\sigma_1(t)}, s_{\sigma_6(t)}} \tag{3.18}$$

where $\rho_{1,2}$ and $\rho_{1,6}$ are the correlation coefficients between $\sigma_1(t)$ and $\sigma_2(t)$ and between $\sigma_1(t)$ and $\sigma_6(t)$, respectively, *cov* mean co-variance, and $s_{\sigma_1(t)}$, $s_{\sigma_2(t)}$ and $s_{\sigma_6(t)}$ are the standard deviations of $\sigma_1(t)$, $\sigma_2(t)$ and $\sigma_6(t)$, respectively. These correlation coefficients can vary from 0 to ± 1, where the closer the coefficient is to either -1 or 1, the stronger the correlation between the variables, whereas the closer the coefficient is to 0, the less correlation between the variables.

3.3.2 Theoretical considerations of the proposed probabilistic multiaxial fatigue model

Having defined the basic concepts on the multiaxial stress state, a probabilistic multiaxial fatigue-life model is proposed in this section. In this model, the model uncertainty in the P-CLD diagrams developed in section 3.2 are propagated in existing multiaxial macroscopic fatigue failure criteria (MMFF) in order to estimate their model uncertainties, X_{FFC}.

As mentioned in section 3.1, different MMFF criteria have been suggested in the literature since the 1970s, see summary in [55, 75]. All these MMFF criteria predict the number of cycles to failure of fiber-reinforced composites under multiaxial stress states by using known S-N curves as input data. In this study, three of these MMFF criteria are analyzed: Hashin-Rotem (HR) [30]; failure tensor polynomial in fatigue (FTPF) [52,

51]; and Kawai-Teranuma (KT) [38]. The FTPF and KT criteria were developed based on adaptations of known static failure theories for fatigue by replacing the principal static strengths with the principal fatigue strengths. The FTPF criterion is based on the Tsai-Hahn tensor polynomial (see Eq. 3.19), and the KT criterion is based on the Tsai-Hill static criterion, see Eq. 3.20, whereas the HR criterion was developed based on two failure modes presented in unidirectional fiber laminates: the fiber mode and the matrix mode, see Eq. 3.21.

$$\left(\frac{\sigma_{1,amp}}{\sigma'_{1,amp}(N)}\right)^2+\left(\frac{\sigma_{2,amp}}{\sigma'_{2,amp}(N)}\right)^2-\frac{\sigma_{1,amp}\sigma_{2,amp}}{\sigma'_{1,amp}(N)\sigma'_{2,amp}(N)}+\left(\frac{\sigma_{6,amp}}{\sigma'_{6,amp}(N)}\right)^2=1 \tag{3.19}$$

(tension dominated)

$$\left(\frac{\sigma_{1,amp}}{\sigma'_{1,amp}(N)}\right)^2+\left(\frac{\sigma_{2,amp}}{\sigma'_{2,amp}(N)}\right)^2-\frac{\sigma_{1,amp}\sigma_{2,amp}}{(\sigma'_{1,amp}(N))^2}+\left(\frac{\sigma_{6,amp}}{\sigma'_{6,amp}(N)}\right)^2=1$$

(compression dominated)

$$\left(\frac{\sigma_{1,amp}}{\sigma'_{1,amp}(N)}\right)^2+\left(\frac{\sigma_{2,amp}}{\sigma'_{2,amp}(N)}\right)^2-\frac{\sigma_{1,amp}\sigma_{2,amp}}{(\sigma'_{1,amp}(N))^2}+\frac{\sigma^2_{6,amp}}{(\sigma'_{6,amp}(N)-\mu_L\sigma'_{2,amp}(N))^2}=1 \tag{3.20}$$

$$\begin{aligned}\left(\frac{\sigma_{1,amp}}{\sigma'_{1,amp}(N)}\right)^2+\left(\frac{\sigma_{6,amp}}{\sigma'_{6,amp}(N)}\right)^2=1 \quad \text{(fiber mode)}\\ \left(\frac{\sigma_{2,amp}}{\sigma'_{2,amp}(N)}\right)^2+\left(\frac{\sigma_{6,amp}}{\sigma'_{6,amp}(N)}\right)^2=1 \quad \text{(matrix mode)}\end{aligned} \tag{3.21}$$

where $\sigma'_{1,amp}(N)$, $\sigma'_{2,amp}(N)$ and $\sigma'_{6,amp}(N)$ denote the corresponding S-N curves derived for the same loading conditions, R-ratio, than those of the actual stress state $\sigma_{1,amp}$, $\sigma_{2,amp}$ and $\sigma_{6,amp}$, respectively. These S-N curves are assumed to follow the next log-log form, which considers the applied stress level as a function of the number of cycle to failure (i.e., $\log\sigma'_{j,amp}=f(\log N)$) in order to facilitate the propagation of the fatigue material uncertainty, as explain in section 3.2:

$$\log\sigma'_{j,amp}=\log Ko_j-m_j\log N+\epsilon_j \quad (j=1,2,6) \tag{3.22}$$

where ϵ_j is the fitting error, which is assumed normally distributed with standard deviation s_{ϵ_j}.

It is worth nothing that, in order to apply the different MMFF criteria (see Eq. 3.19-3.21) and obtain a unique value of the number of cycles to failure N, a proportionality between the stress time series $\sigma_j(t)\quad(j=1,2,6)$ has to be assumed. Otherwise, for each stress time series $\sigma_j(t)\quad(j=1,2,6)$, a different value of N would have to be calculated and the system would become indeterminate. The proportionality between the stress time series can be done by assuming the synchronous sinusoidal stress state defined in Eq. 3.14.

The propagation of the P-CLD uncertainty in the MMFF is carried out by using the first-order Taylor series defined in Eq. 3.7 and 3.8. In this case, the number of cycles to failure N is assumed as the quantity z in Eq. 3.7. The function f refers to each MMFF criterion (see Eq. 3.19-3.21) and the S-N curves $\sigma'_{j,amp}(t) \quad (j = 1, 2, 6)$ are assumed as the stochastic variables x_i. The actual stress state $\sigma_{j,amp} \quad (j = 1, 2, 6)$ in the local coordinate system of the laminate is assumed deterministic for all MMFF criteria as well as the material constant μ_L used in the KT criterion.

As described above, S-N curves are needed to apply the different MMFF. Because ε-N curves were used instead of S-N curves for the construction of the P-CLDs, a scaling process between the ε-N curves and the S-N curves is needed. The scaling process can be done by using Hooke's law for unidirectional stress state (i.e., $\sigma'_{1,amp} = E_1\varepsilon'_{1,amp}$, $\sigma'_{2,amp} = E_2\varepsilon'_{2,amp}$ and $\sigma'_{6,amp} = G_{12}\varepsilon'_{6,amp}$). Then, assuming E_1, E_2, G_{12} and m_j as deterministic values, it can be shown that the uncertainties in the S-N curves, $s_{\sigma'_{j,amp}}$, and the uncertainty in the ε-N curves, $s_{\varepsilon'_{amp}}$, are the same:

$$s_{\sigma'_{j,amp}} = s_{\varepsilon'_{j,amp}} \tag{3.23}$$

and that the intercept in the different S-N curves, $\log Ko_j$, and the intercept in the different ε-N curves, $\log K_j$, are related to each other as follows:

$$\log Ko_1 = E_1 \log K_1; \quad \log Ko_2 = E_2 \log K_2; \quad \log Ko_6 = G_{12} \log K_6 \tag{3.24}$$

Based on this and assuming no correlation between variables, Eq. 3.8 leads to following equation, which can be used to estimate the model uncertainty in the different MMFF criteria:

$$s_N^2 = \Big(\frac{\partial f}{\partial \sigma'_{j,amp}}\Big)^2 s^2_{\sigma'_{j,amp}} \tag{3.25}$$

where s_N is the model uncertainty in the analyzed MMFF criterion denoted as X_{FFC} in Fig. 3.2. Note that Eq. 3.25 can be written in terms of $s_{\sigma'_{amp}}$, as follows:

$$s_{\sigma'_{amp}} = m' \frac{{\sigma'}^{1/m'}_{amp}}{(K')^{\frac{1-m'}{m'}}} s_N \tag{3.26}$$

where m' and $\log K'$ (which is related to K' in Eq. 3.26) are the slope and the intercept of the S-N curve obtained from the applied MMFF criterion.

In addition, if a variable amplitude loading condition is analyzed, the model uncertainty s_N has to be calculated for each bin of cycles obtained from the rain-flow cycle counting. Then, these uncertainties can be propagated in cumulative damage models by using the reliability analysis proposed in section 2.3 of *Paper 1* (see Chapter 6).

3.3.3 Experimental data

The test data used in this study were taken from [50]. In that study, an extensive experimental characterization of a multidirectional (MD) $[0/(\pm 45)_2/0]_T$ glass/polyester

laminate was analyzed, in which the number of cycles to failure of coupons cut at 0°, 15°, 30°, 45°, 60°, 75° and 90° under stress ratio $R = 10, -1$ and 0.1 and various maximum normalized stresses were obtained. In the present work, the test data from 0°, 45° and 90° coupons were used to build the P-CLDs in the axial, transverse, and shear directions of the laminate, respectively, whereas the data obtained from the rest of the orientations were used to validate the proposed probabilistic multiaxial fatigue-life model.

The specimens were tested under cyclic uniaxial loading conditions, which always leads to synchronous sinusoidal stress states if the entire laminate is assumed as a unified material. It can be shown that, for any θ and any R-ratio loading condition, $\sigma_1(t)$ and $\sigma_2(t)$ are in-phase and $\delta_{6,1}$ is equal to 180.

3.3.4 Results and discussion

The parameters and the variability of the experimental ε-N curves needed to build P-CLDs in the axial, transverse, and in-plane shear directions are presented in Table 3.1. As shown in Table 3.1, for both axial and in-plane shear directions, the highest $s_{\log \varepsilon_{amp}}$ variability was reported at T-T loading cases (i.e., $R = 0.1$), whereas for the transverse direction the highest $s_{\log \varepsilon_{amp}}$ variability was reported at T-C loading cases (i.e., $R = -1$).

Table 3.1: Physical and statistical uncertainties on S-N curves in longitudinal, transverse and in-plane shear directions at different stress ratios

	R	m (-)	$\log K$ (-)	s_ϵ (-)	$s_{\log K}$ (-)	$\mathrm{CoV}_{(s_\epsilon)}$ (%)	$\mathrm{CoV}_{(\log K)}$ (%)	$s_{\log \varepsilon_{amp}}$ (-)	Test n
Axial	10.0	0.05	-2.48	0.0169	0.0269	20.00	-1.09	0.0175	14
	-1.0	0.05	-2.37	0.0117	0.0308	27.74	-1.30	0.0124	8
	0.1	0.07	-2.35	0.0360	0.0782	21.82	-3.33	0.0374	12
Transverse	10.0	0.04	-3.12	0.0145	0.0247	21.82	-0.79	0.0151	12
	-1.0	0.07	-2.65	0.0397	0.0696	18.57	-2.63	0.0409	16
	0.1	0.08	-3.14	0.0169	0.0247	20.85	-0.79	0.0175	13
In-plane shear	10.0	0.06	-2.61	0.0273	0.0568	22,94	-2.18	0.0285	11
	-1.0	0.05	-2.59	0.0324	0.0471	21.82	-1.81	0.0337	12
	0.1	0.08	-2.76	0.0362	0.0545	21.82	-1.97	0.0377	12

Based on these probabilistic ε-N curves, the P-CLDs in the different directions can be built by propagating the uncertainty in existing CLDs, as described in section 3.2. However, in the present work, no P-CLDs are needed because all analyzed $R-$ratios match with those of the probabilistic ε-N curves obtained experimentally, i.e., $R = 0.1$, $R = -1$ and $R = 10$. By using Eq. 3.24-3.25, these experimental probabilistic ε-N curves can be used to estimate the probabilistic S-N curves $\sigma'_{j,amp}(N) \quad (j = 1, 2, 6)$ needed for applying the different MMFF criteria in Eq. 3.19-3.21.

The model uncertainties in the evaluated MMFF criteria for different $R-$ratio and multiaxiality levels λ_1 and λ_2 are presented in Table 3.2. As shown in Table 3.2, the estimated variability in the different MMFF criteria is similar but much lower than the variability obtained from the experimental data, which was estimated by using the Maximum Likelihood method. The reliability level of these predictions seems to vary with the multiaxility levels λ_1 and λ_2. For example, for multiaxiality levels higher than one (i.e., λ_1 and $\lambda_2 > 1$), the estimated uncertainties are much lower than the ones fitted

from the experimental data; whereas, for multiaxility levels lower than one (i.e., λ_1 and $\lambda_2 < 1$), the estimated uncertainties are still low but closer to the fitted ones, especially for the specimens tested in the transverse direction at $\theta = 15°$. These results can be also analyzed graphically from Fig. 3.5-3.7 as $\varepsilon - N$ curves, in which it is easier to observe the difference between the experimental variability and the variability estimated from the different MMFF criteria.

Table 3.2: Comparison between uncertainties propagated on the different MMFF criteria and uncertainties fitted from experimental data for $[0/(\pm 45)_2/0]_T$ laminate

					$s'_{\varepsilon_{amp}}(-)$			
R	$\theta(°)$	$\lambda_1(-)$	$\lambda_2(-)$	Test n	Exp.	FTPF	HR	KT
10	30	0.33	0.58	14	0.0172	0.0104	0.0097	0.0081
	60	3.00	1.73	15	0.0175	0.0086	0.0081	0.0079
0.1	15	0.07	0.27	13	0.0211	0.0140	0.0174	0.0120
	75	13.93	3.73	11	0.0182	0.0085	0.0084	0.0085
-1	30	0.33	0.58	14	0.0297	0.0170	0.0185	0.0148
	60	3.00	1.73	11	0.0319	0.0121	0.0114	0.0112

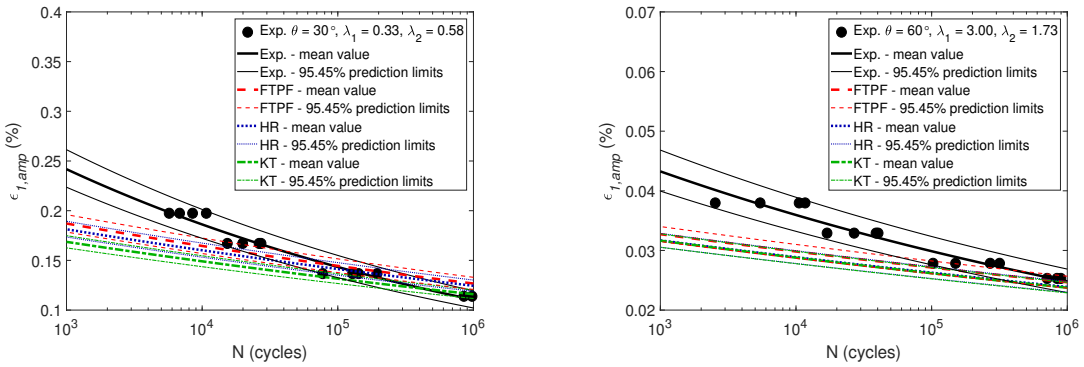

(a) $\theta = 30°$ (b) $\theta = 60°$

Figure 3.5: Comparison of propagated uncertainties in different MMFF criteria (i.e. FTPF, HR and KT) and experimental data for $[0/(\pm 45)_2/0]_T$ laminate under $R = 10$. Thick lines represent the mean, thin lines represent ± 2 standard deviations from the mean.

Moreover, the accuracy level of all MMFF criteria can be also analyzed from Fig. 3.5-3.7. As shown, the accuracy level of all MMFF criteria are similar each other but with some small differences. For example, better predictions are obtained by the FTPF criterion for coupons under $R = 10$ with 30° and 60° off-axis and under $R = -1$ with 60° off-axis, whereas better predictions are obtained by the KT criterion for coupons under $R = 0.1$ with 15° off-axis and under $R = -1$ with 30° off-axis. However, in general, the level of accuracy of the different MMFF criteria is acceptable but not high enough to always guarantee the safety of the material. For example, nonconservative predictions are obtained for those coupons under $R = 0.1$ with 15°, see Fig. 3.6a.

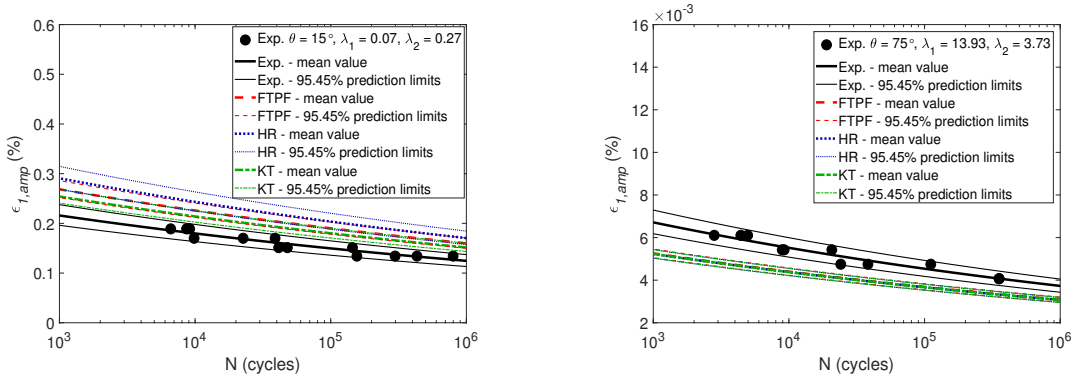

(a) $\theta = 15°$ (b) $\theta = 75°$

Figure 3.6: Comparison of propagated uncertainties in different MMFF criteria (i.e. FTPF, HR and KT) and experimental data for $[0/(\pm 45)_2/0]_T$ laminate under $R = 0.1$. Thick lines represent the mean, thin lines represent ± 2 standard deviations from the mean.

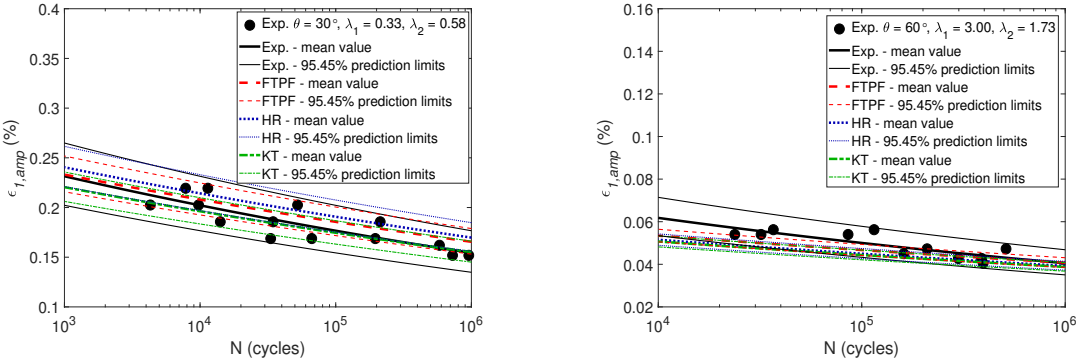

(a) $\theta = 30°$ (b) $\theta = 60°$

Figure 3.7: Comparison of propagated uncertainties in different MMFF criteria (i.e. FTPF, HR and KT) and experimental data for $[0/(\pm 45)_2/0]_T$ laminate under $R = -1$. Thick lines represent the mean, thin lines represent ± 2 standard deviations from the mean.

Based on these results, an evaluation of the different advantages and disadvantages of the proposed probabilistic multiaxial fatigue-life model is presented in the next section in order to define how suitable the proposed model could be for designing wind turbine blades against fatigue.

3.4 Applicability of probabilistic multiaxial fatigue-life models in wind turbine blades

In this section, an evaluation of the applicability of the proposed probabilistic multiaxial fatigue-life model for the design against fatigue of wind turbine blades is given based on the results obtained in previous sections. Before continuing, it is suggested to first read the *Paper 1* (see Chapter 6) in order to have more clarity with what is discussed in this section.

The proposed probabilistic fatigue model was developed by propagating the variability of the fatigue properties of the materials along deterministic multiaxial fatigue-life models. This propagation was carried out specifically in existing constant life diagrams, existing multiaxial fatigue failure criteria, and the Palmgren-Miner's rule.

By propagating the variability in the material properties in existing constant life diagrams, probabilistic fatigue life diagrams, P-CLDs, were developed; which can efficiently, accurate and reliably estimate probabilistic ε-N curves at any load level and R-ratio without using any iterative process (see example in section 4.2 of *Paper 1*, Chapter 6). The developed P-CLDs themselves are useful tools for applications of composite structures under constant amplitude cycle loading and uniaxial stress states because probabilistic ε-N curves of materials under these loading conditions can be estimated; however, they cannot be used directly for the design of wind turbine blades because these structures are subjected to variable amplitude cycle loading conditions and multiaxial stress states during their lifetime.

Based on this, it was shown that reliable fatigue-life predictions of composite materials under variable amplitude loading cycles and uniaxial stress states can be efficiently obtained with the proposed probabilistic fatigue model when the model uncertainty in the developed P-CLDs are propagated in cumulative damage rules through a reliability analysis. This could be observed from the study presented in sections 4.3 and 5.2 of *Paper 1* (see Chapter 6) on the estimation of the probability of failure of UD and MD laminates under both repeated block tests and spectrum tests. The results from this study showed good agreement between the probability of failure estimated from the proposed probabilistic fatigue model and the one obtained from experimental data. However, it was also shown that the applicability of the proposed reliability model depends on the level of accuracy of the implemented cumulative damage rule. In this sense, because the level of accuracy of the implemented Palmgren-Miner's rule for predicting the fatigue lifetime of composite materials can vary depending on the loading condition (as discussed in section 5.2.1 in *Paper 1*, see Chapter 6), it is clear that new cumulative damage rules for composite materials are still needed for better implementation of the proposed reliability model in wind turbine blades.

Additionally, this study also showed that neither reliable nor accurate fatigue-life predictions of composite materials under multiaxial loading conditions can be obtained by propagating the model uncertainty in the developed P-CLDs in existing MMFF criteria, see section 3.3.4. On the one hand, the first-order Taylor series seems not to be suitable for propagating the P-CLD uncertainty in the MMFF criteria; therefore,

another uncertainty propagation method should be used for this purpose in order to obtain reliable fatigue predictions. On the other hand, the current MMFF criteria are not accurate enough to predict the fatigue lifetime of composite materials because they do not consider the actual physical failure mechanisms.

Moreover, as described in section 3.3.2, the application of the MMFF criteria can be carried out if the different stress time series, $\sigma_j(t) \quad (j = 1, 2, 6)$, are proportional to each other or follow a synchronous sinusoidal behavior. However, in reality, the wind turbine blades are under complex loading conditions that create complex local stress states, which are not proportional to each other. For example, Fig. 3.8 shows the correlation coefficients $\rho_{1,2}$ and $\rho_{1,6}$ for a cross-section of a wind turbine blade under simulated aeroelastic loading conditions. As shown, the correlation coefficients $\rho_{1,2}$ are high all around the cross-section. However, the correlation coefficients $\rho_{1,6}$ are low in most of the cross-section meaning that nonproportionality between $\sigma_1(t)$ and $\sigma_6(t)$ exists; therefore, none of the MMFF criteria in Eq. 3.19-3.21 can be directly applied. This is because different values of N would have to be calculated for each cycle bin of $\sigma_1(t)$ and $\sigma_6(t)$, which would make each of the MMFF criteria in Eq. 3.19-3.21 indeterminate.

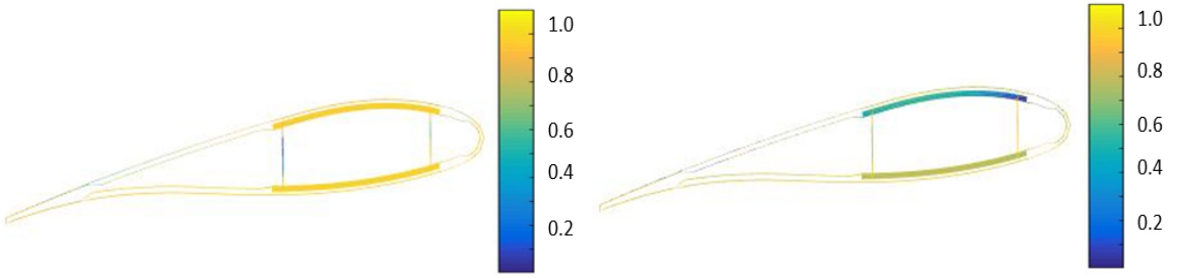

(a) $\rho_{1,2}$ (b) $\rho_{1,6}$

Figure 3.8: Correlation coefficients $\rho_{1,2}$ and $\rho_{1,6}$ in the SSP34 wind turbine blade at 30m blade span and wind speed of 16 m/s. The stress time series were calculated from BECAS (BEam Cross section Analysis Software) [6]

In this sense, the stress time series could be re-estimated to make them proportional to each other by using the following correlation variables, see Fig. 3.9:

$$\sigma_{j,amp} = \rho_{1,j}\Big(\frac{\sigma_{1,amp}}{s_{\sigma_1(t)}}\Big)s_{\sigma_j(t)} \quad j = 2, 6 \tag{3.27}$$

where $\rho_{1,j}$ is the correlation coefficient between $\sigma_1(t)$ and $\sigma_j(t)$, $j = 2, 6$, whereas $s_{\sigma_1(t)}$ is the standard deviation of axial stress time series $\sigma_1(t)$ and $s_{\sigma_j(t)}$ is the standard deviation of the stress time series $\sigma_j(t)$.

However, if the correlation coefficient $\rho_{1,j}$ is lower than 1 (see Fig. 3.9-b), the high amplitude cycles are eliminated. This can lead to even more inaccurate fatigue load predictions, especially if $\rho_{1,6} < 1$ considering the fact that the presence of shear stress components significantly affect the fatigue properties of the material [55].

Even though the simplicity of the proposed probabilistic multiaxial fatigue-life model makes it attractive for easy implementation in numerical codes, it can be concluded that

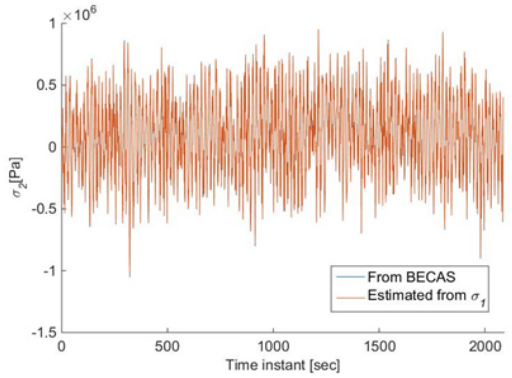

(a) Re-estimated $\sigma_2(t)$, $\rho_{1,2} = -1.0$

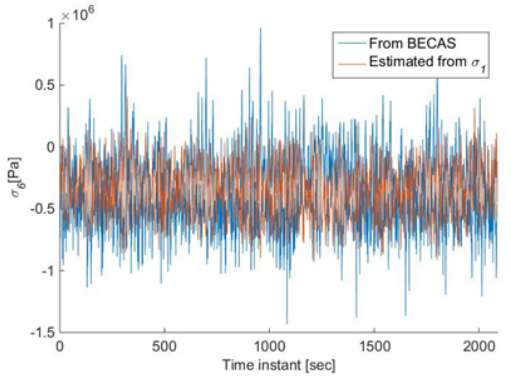

(b) Re-estimated $\sigma_6(t)$, $\rho_{1,6} = -0.6$

Figure 3.9: Comparison between stress time series obtained from BECAS and those calculated from Eq. 3.19. These stress time series correspond to a point located in the suction-side spar cap of the blade section shown in Fig 3.8.

its applicability for the design of wind turbine blades is currently not suitable due to the existing limitations in the current cumulative damage theories and MMFF criteria. In this sense, better cumulative damage theories and MMFF criteria that consider the actual damage modes of composite materials during failure and better uncertainty propagation methods in MMFF criteria could make the proposed probabilistic multiaxial fatigue-life model applicable for these structures. In addition, the proposed model does not allow one to predict the gradual property degradation of the structure, which is an important design parameter for wind turbine blades because they must remain stiff to avoid, among others, collision with the tower under extreme loading conditions and structural instabilities, such as local or global buckling [60].

In this sense, the fatigue analysis of wind turbine blades must be carried out by following another approach. One option is to implement phenomenological models which do allow one to predict the stiffness and/or strength degradation of the material. However, based on the author's perspective, these models are also not suitable for wind turbine blades because the property degradation is also predicted based on empirical relations and not on the actual physical damage mechanisms developed in the material. In addition, a nonfeasible experimental work must be done to characterize all possible laminates in the wind turbine blades because the applicability of this approach is limited to the laminates that were tested to develop the model.

Another option is to apply damage mechanics models. These models seem to be suitable for the blade designing against fatigue because they allow one to predict the fatigue lifetime and the property degradation of the material according to the actual physical damage mechanisms. Hence, in the next chapter, a damage mechanics-based multiscale approach is proposed for analyzing and designing these structures under fatigue. Considering that the main limitation of the damage mechanics models is their computationally cost, the proposed multiscale approach is suggested to be implemented using a 2D finite-element-based cross-section analysis, thus simplifying the model complexity.

CHAPTER 4
Damage mechanics models

As discussed in the previous chapter, a potential approach for designing wind turbine blades against fatigue is the implementation of damage mechanics models. These models would allow predicting not only the catastrophic failure of the materials but also their progressive property degradation. In this way, more realistic and accurate fatigue predictions of wind turbine blades can be obtained compared with those estimated from other fatigue models, such as the fatigue-life models discussed in Chapter 3.

In the first part of the present chapter, a multiscale approach for fatigue design of wind turbine blades based on damage mechanics models is proposed. The proposed multiscale approach is then implemented for a real wind turbine blade, in which the effect of off-axis matrix cracks on the structural response of the blade is analyzed. In the last part of the chapter, a micro-scale fiber-related damage initiation and progression study for on-axis UD glass/epoxy laminates is presented, which is the first step toward the development of future models that allow predicting possible failures in wind turbine blades under cyclic loading.

4.1 Multiscale approach for fatigue design of wind turbine blades

As explained in [68], the fatigue behavior of composite materials is characterized by irreversible changes caused by different fractures, or breakage, of the material, such as fiber breaks, fiber/matrix debonding, delaminations, and matrix cracks. The distribution of these changes in the material is commonly known as *damage*. Some examples of damage are multiple off-axis matrix cracks in multidirectional laminates or multiple fiber breaks in unidirectional laminates.

In composite materials, the length scale in which the damage initiates and propagates is not unique. In fact, as discussed in [68], the damage evolution is a multiscale process whose length scales are defined by the microstructural configuration of the material (i.e., matrix, reinforcements, etc.) and by the driving forces to which the material is subjected. For example, in UD materials, which are made of long fibers orientated in the same direction and embedded in a matrix, the damage initiates from breaks in the fibers and propagates as interfacial fiber/matrix debonding that coalescence, thus creating macro-cracks that further seem to lead to the final failure. Hence, the damage initiates from a micro-length scale, related to the fiber diameter, and passes through a macroscale length scale, related to the length of the macro-cracks.

These considerations suggest that the multiscale nature of damage and its effect on the material degradation should be taken in account during the fatigue modeling of

composite materials and, by implication, during the fatigue modeling of structures made of this type of materials, such as wind turbine blades.

A common multiscale approach applied for composite wind turbine blades is schematically shown in Fig. 2.9. As shown in that figure, composite materials are often defined as laminates made of several plies stacked with different fibers orientations. The plies and the laminates are macro-scale entities with a thickness of order of magnitude of millimeters. These macroscale entities can be assumed as an assembling of several smaller structural elements, being the smallest one a fiber-matrix unit cell of order of magnitude of micrometres, see Fig. 2.9. However, it is often more convenient to use as a structural element a representative volume element (RVE) containing a representative sample of damage [9]. As described above, the length scale in which the damage develops in composite materials depends on the microstructural configuration of the material and on the driving forces; therefore, the length scale of the RVEs can vary from a micro-length scale to a macro-length scale.

Furthermore, the laminates are often bonded together by means of adhesive joints to build subcomponents, such as spars, shells, and blade sections. Then, if any failure takes place in a subcomponent, it is due to either the failure of the laminates, which initiates from the RVE's length scale and propagates toward the ply/laminate length scale (see more details in section 4.2), or by the failure of the bondline, which is also caused by damage accumulation at smaller length scales. Similarly, the subcomponents are bonded together to obtain the final structure, e.g., a full wind turbine blade (see Fig. 2.9). Consequently, if the full structure fails, or its mechanical response degrades, it is due to the propagation of the damage at all the smaller length scales (i.e., subcomponent, macro, and micro).

In this sense, a multiscale approach based on damage mechanics models seem to be suitable for the fatigue modeling of composite wind turbine blades for two reasons. On the one hand, the damage mechanics models allow predicting the initiation and progression of the damage in different length scales as well as its effect on the progressive degradation of the material, which eventually leads to the final failure [63, 27, 42, 73]; understanding as final failure when the material exceeds the design limits for which it is used (e.g., load-bearing limits, deformation limits, etc.). On the other hand, with the multiscale approach, the predicted response of the material can be sequentially coupled from a micro-length scale (i.e., material length scale) to a full-length scale (i.e., blade length scale), thus giving a better description of the structural response of the blades.

The capabilities of the multiscale approach based on damage mechanics models were recently studied by Mortesano et al. in [46], in which an interesting physics-based multiscale progressive damage model was proposed to predict the durability of wind turbine blades. In this study, the evolution of off-axis matrix cracks in different regions of the blade structure was predicted by combining computational micromechanics and continuum damage mechanics in a 3D finite element model.

However, because other damage mechanisms besides the off-axis matrix cracks can develop at different length scales in this type of structures (e.g., delaminations, fiber breaks, etc. [64]), additional damage mechanics models might be needed to fully predict the structural fatigue response of the wind turbine blades. This could increase considerably

the complexity of the model and the computational resource demand, making the implementation of the multiscale progressive damage models in 3D finite element models probably unfeasible.

Based on this, a damage mechanics-based multiscale approach using a 2D finite-element-based cross-section analysis is proposed in the present study to analyze and predict the fatigue behavior of composite wind turbine blades, see Fig. 4.1. By using the 2D finite-element-based cross-section analysis, the entire blade is modeled as a beam composed of several cross-sections [6]. This would allow saving computational time compared with 3D finite element models because 2D models are carried out instead, which simplifies the complexity of the blade in terms of geometry and material distribution [7]. In addition, the accuracy of the 2D finite-element-based cross-section analysis when predicting the stresses/strains is not compromised compared with the 3D finite element models [6, 7], which provides confidence in the implementation of the damage mechanics models regarding the estimation of the damage initiation and propagation, as described later.

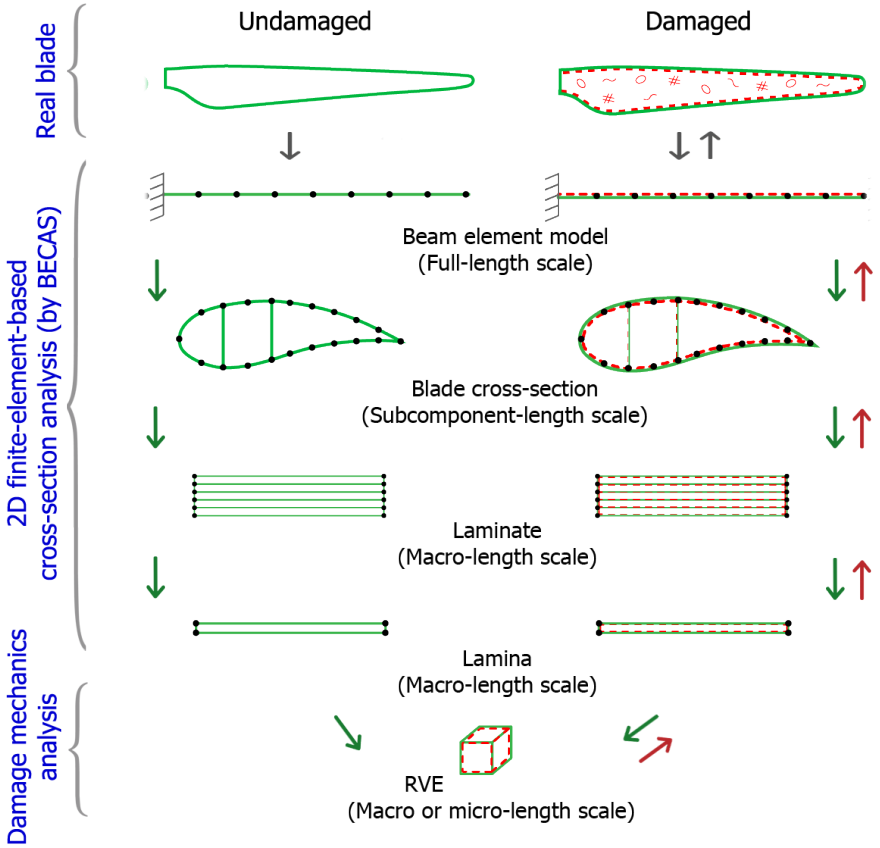

Figure 4.1: Multiscale approach for fatigue design of wind turbine blades based on damage mechanics models.

In the proposed multiscale approach, the damage evolution of the real blade is modeled by using two types of analysis once the geometry, material configuration,

material properties, and loading conditions of the blade are defined (see Fig. 4.1): i) a 2D finite-element-based cross-section analysis; and ii) a damage mechanics analysis. During the 2D finite-element-based cross-section analysis, the state of the blade is estimated using continuum mechanics theories (e.g., classical laminate theory), whereas during the damage mechanics analysis, the evolution of the damage is estimated using damage mechanics models, which can vary depending on the damage type to be analyzed. In the present work, the 2D finite-element-based cross-section analysis is carried out using BECAS (BEam Cross section Analysis Software) tool developed by DTU Wind Energy [6]. BECAS is a general-purpose cross-section analysis tool developed to analyze efficiently and accurately the mechanical response of complex beam-like structures, such as wind turbine blades. The damage mechanics models used in the present work to estimate the damaged state of the blade are described in Chapter 7.

According to the 2D finite-element-based cross-section analysis, the real blade (full-length scale) is modeled as a beam composed of several cross-sections by using a beam finite element model, in which the beam finite element stiffness matrix is constructed based on the different cross-section stiffness matrices (see more details in [6]). In order to define the stiffness of each cross-section (subcomponent-length scale), the geometry, laminate configuration, and material properties of the analyzed cross-section must be first defined. Then, by discretizing the cross-section in finite elements, in which each element represents either a laminate, a ply, a sandwich structure or a joint, the cross-section stiffness is calculated using BECAS (see more details in [6, 24]).

The stress state of the cross-sections can also be estimated from BECAS knowing the loading conditions at each cross-section. This cross-section stress state is used as an input for the damage mechanics analysis, in which the regions where the damage might develop are identified, and the damage initiation and propagation are calculated for each evaluated loading condition (e.g., each applied cycle or block of cycles in case of fatigue). This can be done because each cross-section finite element (macro-length scale) is discretized in RVEs (micro-length scale or macro-length scale depending on the damage type) containing a representative sample of damage. Moreover, because the local stresses change as a result of the damage, a re-calculation of the stresses is carried out and the stiffness properties of the damaged regions are evaluated.

Then, based on the degraded stiffness of the damaged regions, the stiffness of the entire cross-section is updated using BECAS and, therefore, the stress-strain states and possible failure characteristic of the cross-section can be also estimated. Once this analysis is done for all blade cross-sections, the response of the full blade in terms of failure characteristics, critical regions, stress-strain response, deflections and vibration (i.e., natural frequencies) characteristics can be calculated using a beam finite element model. All this process is schematically presented in Fig. 4.2 and explained in more detail in Chapter 7.

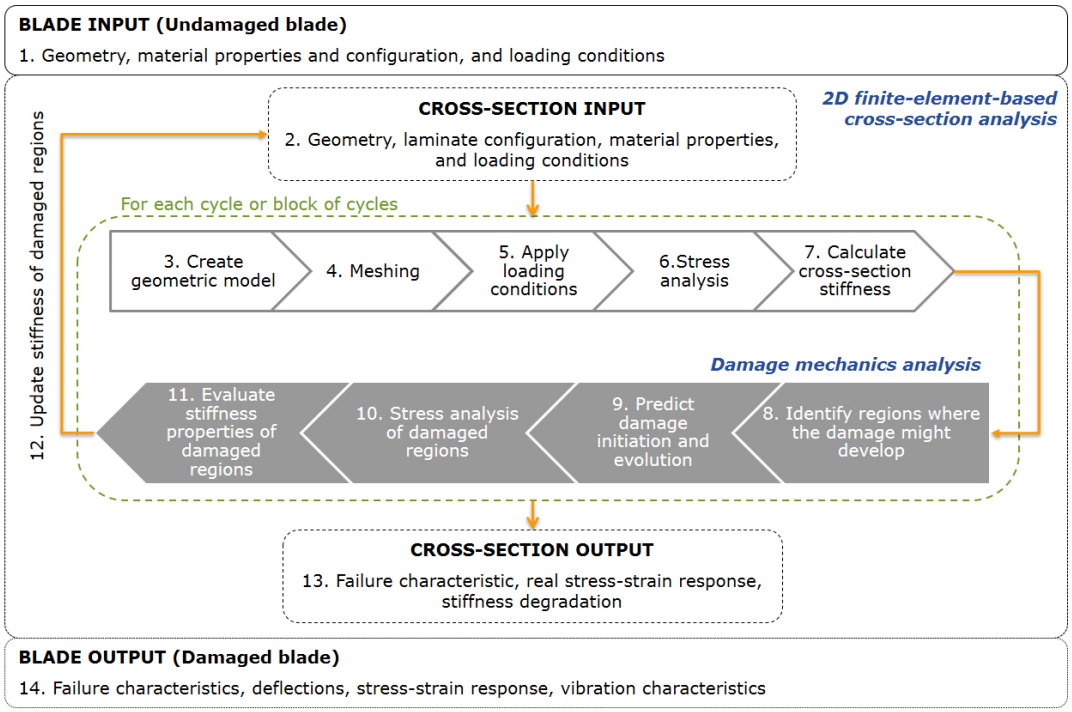

Figure 4.2: Flow chart of the proposed multiscale approach for fatigue design of wind turbine blades based on damage mechanics models

4.1.1 Multiscale fatigue analysis assumptions for current work

In the next sections, an implementation of the proposed multiscale damage-mechanics-based approach for the fatigue analysis of a commercial wind turbine blade is carried out. In this analysis, the following assumptions are made:

- The effect of the backing fiber bundles in the non-crimp UD materials, which was described in section 2.4.1.2, is not considered. This means that only pure UD materials are assumed.
- The effect of material imperfections (e.g., voids, inclusions, etc.) on the structural response of the blade is not considered.
- Adhesive joints are not taken into account as perfect bonding is assumed.

Nevertheless, future models that take these possible additional assumptions into account might be needed for better characterization of the structural response of the blades.

4.2 Damage evolution in multidirectional composite laminates

As described in section 2.3, multidirectional laminates are used in the shear webs and the aerodynamic shells of the wind turbine blades to improve the torsion and shear strength of these structures and to prevent buckling. In fact, the spar caps are also made of multidirectional laminates, even though most of the plies are unidirectional. Because the transverse direction of the unidirectional plies is extremely weak due to the poor matrix properties, few plies in the spar caps are orientated in 90°, 45° and −45° in order to prevent possible failures of the laminate in the transverse and shear directions. Accordingly, because multidirectional laminates are used in most regions of the wind turbine blades, predicting the damage initiation and progression in this type of laminate is relevant in the fatigue analysis of these structures. In this section, a description of the damage progression in multidirectional composite laminates is presented.

Multidirectional composite laminates are composite materials consisting of multiple plies oriented in different directions and bonded together through the matrix, see Fig. 4.3. As exemplified above, this type of composite material is used in most engineering applications because it provides better mechanical properties of the material in different directions than the one provided by unidirectional laminates, whose mechanical properties are high only in one direction.

The plies of a multidirectional laminate can be composed of short fibers, unidirectional continuous fibers or woven fibers. For the case of multidirectional laminates consisting of unidirectional continuous fibers, the laminate can be analyzed using a xyz orthogonal coordinate system, as shown in Fig. 4.3. The orientations of the plies are indicated by the angle θ with respect to the x-axis, which is positive in the counterclockwise direction. The number of plies with the same orientation is denoted by a numerical subscript. For example, the $[0_4/90_3/45_5]$ laminate contains one group of four plies orientated at 0°, another group of three plies orientated at 90° and a last group of five plies orientated

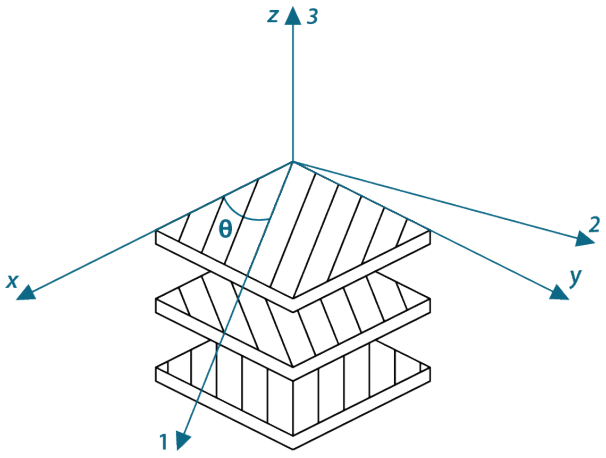

Figure 4.3: Multidirectional laminates

at 45°. If the laminate is symmetric with respect to the midplane, a subscript s is used to indicate the symmetry. For example, the laminate $[0_4/90_4/0_4]$ can be re-written as $[0_4/90_2]_s$.

As explained in section 2.4.1.1, the fatigue damage evolution of the multidirectional laminates made of pure UD fibers can be divided into three stages [58], according to the different damage mechanisms that develop during the fatigue lifetime and their effect on the laminate response, see Fig. 4.4 and 4.5.

In the first stage, a high drop of laminate stiffness is developed due to several matrix cracks that initiate and propagate quickly along the fibers in the off-axis plies, see Fig. 4.4-a and Fig. 4.5. This type of crack is normally known as an off-axis crack. As the number of cycles increases, the off-axis crack density increases until reaching a saturation point in which the mechanical response of the laminate tends to a stable condition. This phenomenon has been analyzed experimentally over many years [58, 72, 4, 54, 56]. Furthermore, different analytical and numerical models have been also proposed since the 1970s in order to predict the degradation of the elastic properties of the material as a function of density of off-axis cracks, e.g., [59, 29, 27, 45, 40, 74, 12]. In [12], for example, an accurate analytical model that allows predicting the elastic property degradation of any multidirectional symmetric laminate with off-cracks in different plies, considering the interaction between all cracks, was proposed. Moreover, analytical models for predicting the off-axis crack density evolution of multidirectional symmetric laminate under fatigue load conditions as a function of the applied load level and the number of cycles have recently been proposed in [11, 26]. With these models, it is now possible to predict the elastic property degradation of multidirectional symmetric laminate with off-axis cracks through the fatigue lifetime.

In the second stage of the damage evolution of multidirectional laminates, delaminations between the different plies initiate when the saturation condition of the off-axis cracks is reached, see Fig. 4.4-b. In this stage, the delaminations propagate almost linearly, generating a stable drop of the stiffness, see Fig. 4.5. Extensive experimental studies have been carried out since the 1980s in order to study the onset of delaminations in different multidirectional laminates under quasi-static [16, 18, 49, 8, 32, 1, 66] and fatigue [49, 32, 1] loading conditions. At the same time, different analytical models based on shear lag [19, 5], variational [29, 57] and fracture mechanism [21, 82, 13] approaches

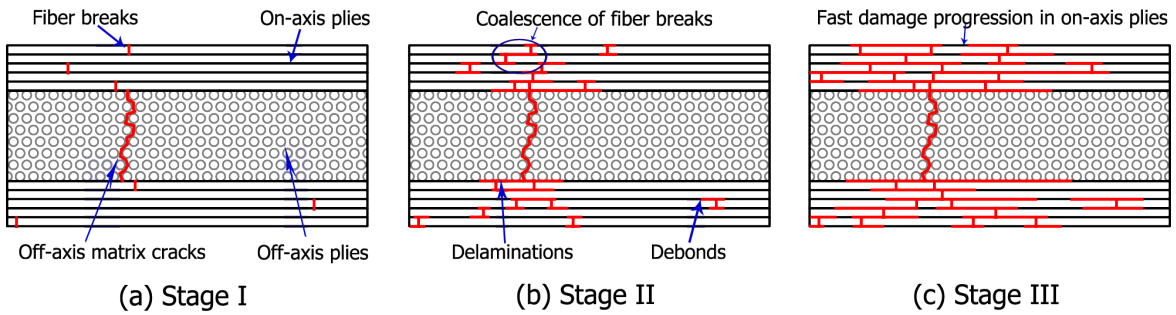

Figure 4.4: Damage progression of multidirectional laminates

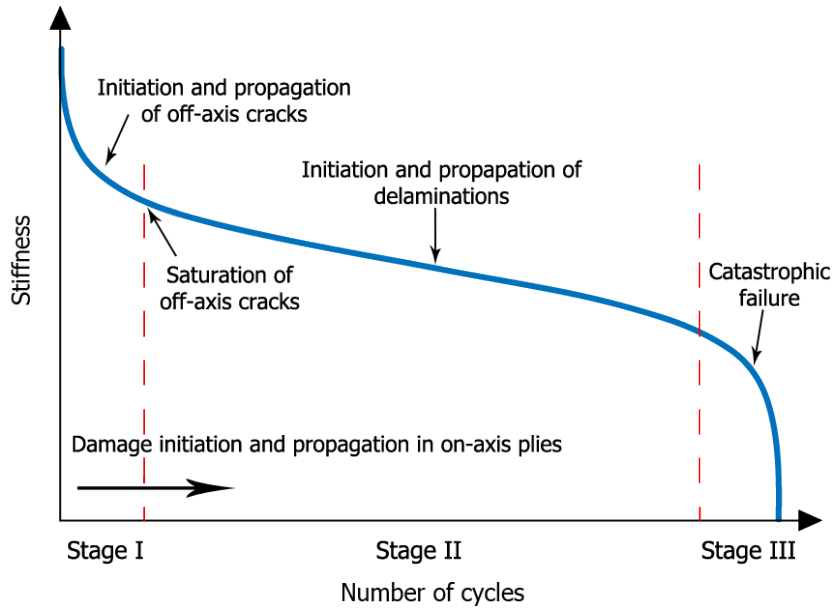

Figure 4.5: Stiffness degradation of multidirectional laminates

have been proposed for predicting the initiation and propagation of this type of damage mechanisms. Recently, numerical models based on the use of cohesive zone models (CZMs) in finite element analyses [10, 34, 17] have also been proposed, as an alternative option to the analytical models.

In the third stage, the catastrophic failure of the material takes place as a result of the rapid evolution of the damage in the 0° plies, see Fig. 4.4-c and 4.5. The damage in the 0° plies begins since the first stage when some fiber fails due to the statistical strength distribution of the fibers and the high-stress concentration at the off-axis crack tips, see Fig. 4.4-a. Then, new fiber breaks occur through the fatigue lifetime as a consequence of stress redistributions caused by matrix/fiber debonds and by the delaminations, see Fig. 4.4-b. This means that, even though the off-axis cracks and the delaminations are not critical for the final failure, they do trigger the fiber breaks [53]. Finally, because the 0° plies provide the structural load-bearing capacity of the laminate, the laminate separation takes place when the damage in the 0° plies evolves rapidly and a critical condition is reached. The damage initiation and propagation in the 0° plies under fatigue loading conditions have been identified qualitatively through experiments since the 1980s [67, 22]. However, there is still not a quantitative method that allows predicting this type of damage along the fatigue lifetime and, therefore, predicting the final failure of multidirectional laminates.

Based on the described fatigue damage evolution, Quaresimin et al. in [53] proposed the following framework for designing composite structures made of multidirectional laminates against fatigue:

1. The initiation and propagation of off-axis cracks (the crack density evolution),
2. The initiation and propagation of delaminations induced by off-axis cracks, and

3. The failure of the fibers of the load-bearing plies.

However, because the multidirectional laminates used in wind turbine blades could also consist of UD non-crimp fabric (NCF) plies orientated in different directions, additional damage mechanisms to the ones mentioned above, and their effects on the laminate response must be also considered. As described in section 2.4.1.2, the UD NCF materials are made of bundles of normal UD fibers reinforced with backing fiber bundles. When a tension-tension fatigue load is applied to this type of material, off-axis cracks in the single backing fiber bundles initiate and propagate during the first loading stage causing an increment of UD fiber breaks near those regions where the backing fiber bundles touch the UD bundle [81, 36]. Consequently, an additional drop of stiffness to the one presented in multidirectional laminates made of pure UD fibers occurs [81, 36].

In this sense, in addition to the framework described above for composite structures made of multidirectional laminates with pure UD fibers, it is necessary to predict, among others, the additional damage mechanisms developed in UD NCF in order to fully predict the stiffness degradation and final failure of wind turbine blades, as follows:

- The initiation and propagation of off-axis matrix cracks (the crack density evolution) in off-axis plies,
- The initiation and propagation of delaminations induced by the off-axis matrix cracks,
- The initiation and propagation off-axis cracks in backing bundles, and
- The fiber-related damage at the load-bearing regions, such as UD bundles and on-axis plies.

Based on this, a damage mechanics-based multiscale model for wind turbine blades under fatigue loads considering the effects of matrix cracks in the off-axis plies is presented in the next section as a contribution to the first step in the afore-described framework for wind turbine blades. Later, in section 4.4, a study on the fiber damage initiation and progression in on-axis pure UD glass/epoxy laminates under fatigue loading conditions is presented according to the last step of this framework. This study is the first step toward future models that allow predicting the failure in multidirectional laminates under cyclic loading and, by implication, of structures made of this type of materials, such as wind turbine blades.

Note that the effect of delaminations on the fatigue response of wind turbines blades is not considered in the current Ph.D. thesis. This will be done in the near future by the structural design and testing team at the DTU wind energy department, as a continuation of this Ph.D. thesis. In addition, the damage mechanism developed in UD NCF, such as off-axis cracks in backing bundles, is not considered in this thesis, either. The understanding and modeling of these damage mechanisms is an ongoing research at the material-length scale, which is being carried out at the composites and materials mechanics section (COM) at the DTU wind energy department. The results of this research are expected to contribute in the future improvement of the proposed multiscale approach.

4.3 Implementation of damage mechanics models in wind turbine blades

Paper 2. Oscar Castro and Kim Branner (2018). Damage mechanics-based multiscale model for wind turbine blades under fatigue: Part 1. Effect of off-axis cracks on the blade stiffness degradation. In manuscript.

As part of the first step in the framework for designing composite wind turbine blades described in section 4.2, *Paper 2* (see Chapter 7) presents an analysis about the effects of off-axis cracks on the structural response of wind turbine blades, which was carried out by implementing the damage mechanics-based multiscale approach proposed in section 4.1.

Following the concept of the proposed multiscale approach, a damage mechanics model developed by Carraro and Quaresimin [12] was implemented in the present model to predict the material property degradation at the macro-length scale of the blade (i.e., laminate length scale) as a consequence of the presence of off-axis cracks. Subsequently, the effects of this material property degradation on the subcomponent and full-length scales of the blade were predicted using a 2D finite-element-based cross-section analysis.

The proposed multiscale model was applied in a 34m long blade designed for a wind turbine with a power capacity of 1.5MW, with which the effects of the off-axis cracks were observed at the macro-, subcomponent and full-length scales. The response of the damaged blade at the full-length scales in term of deflections was also compared with experimental deflections of this blade obtained from full quasi-static tests [28].

The obtained results showed that, by using the proposed multiscale approach, reliable predictions of the structural response of the blade with the presence of off-axis cracks are obtained. Moreover, it was found that the stiffness of the blade decreases as the number of off-axis cracks increases until a saturation condition of the off-axis cracks at the macro-length scale is reached. It was also found that the degradation level of the blade stiffness varies along the blade and in the flap-wise and edge-wise directions. The factors that might affect this stiffness variation in the blade, such as laminate thickness and cross-section geometry, were also analyzed.

One of the advantages of using the proposed multiscale approach compared with 3D finite element models, for example, is its capability of providing high computational efficiency during the processing stage because 2D finite-element-based cross-section analysis is carried out instead. The potential of this computational efficiency will be demonstrated in the second part of this study [14], in which an extended multiscale model is proposed to predict the evolution of off-axis cracks in wind turbine blades under fatigue loading conditions. This second part is an ongoing research, and the corresponding paper is not included in this Ph.D. thesis.

The damage mechanics-based multiscale model proposed in this work for analyzing the effect of off-axis cracks on the structural response of wind turbines blades lays the basis for future extensions of this model in which other damage types developed this type of structure, such as delaminations, fiber-related damage, and off-axis cracks in backing bundles, are also included.

4.4 Fatigue behavior of unidirectional composite laminates

Paper 3. Oscar Castro, Paolo Andrea Carraro, Lucio Maragoni and Marino Quaresimin (2018). Fatigue damage evolution in unidirectional glass/epoxy composites under a cyclic load. Polymer Testing. Submitted.

In *Paper 3* (see Chapter 8), the fiber-related damage initiation and progression in on-axis UD glass/epoxy materials under longitudinal fatigue loading conditions is analyzed. This work is an initial step in developing a model that allows predicting the fatigue damage evolution and final failure of the load-bearing regions of multidirectional laminates, as a contribution to the final step in the framework for designing composite wind turbine blades described in section 4.2.

In this work, UD glass/epoxy specimens were tested under uniaxial tension-tension fatigue loading conditions. The damage evolution of the material was evaluated, both qualitatively and quantitatively, in terms of stiffness degradation and fiber breakage, including initial fiber breaks, evolution of the density of broken fibers, and fragmentation progression.

Qualitatively, it was found that the fiber damage evolution depends on the number of cycles, the applied load level, the presence of imperfections, the number of broken fibers during the first cycle, and the local fiber volume fraction. In fact, it was observed that damage tends to propagate faster in matrix-rich regions, especially those close to the scrim fiber.

Quantitatively, the probability of survival of the fibers (P_{sf}) along the fatigue lifetime was obtained, which was calculated as the sum of the fiber segments without any break, divided by the total number of fiber segments. It was found that, for low load levels, P_{sf} remains almost constant during the fatigue lifetime because the load is too low for promoting debond; therefore, no (or few) new breaks appear after the first cycle, whereas for high load levels, P_{sf} decreases even when most of the fiber breaks seem to take place during the first cycle. In addition, it was also observed that fiber fragmentation occurs, but most broken fibers failed only once. This seems to be the main reason why the material stiffness did not decrease considerably throughout the fatigue lifetime, as most of the fragmentation lengths kept long; thereby, the fibers recovered their nominal load-bearing capacity.

CHAPTER 5
Contributions and conclusions

This thesis contributes to the development of new methods that allow obtaining accurate and reliable fatigue-life predictions of composite wind turbine blades under fatigue load conditions.

As a first step in this process, the different factors that are involved in fatigue of wind turbine blades were identified (see Chapter 2) in order to specify the requirements of the fatigue models to be developed and, consequently, select the types of fatigue models that fit better with those requirements. Some of the identified factors were, for example, the intrinsic fatigue behavior of composite materials, multiaxial stress states, variability of loads, and the stochastic behavior of material properties.

Based on these factors, a probabilistic multiaxial fatigue-life model was proposed in Chapter 3, in which the effects of the variability in the material properties on the fatigue lifetime estimations were analyzed. The fatigue-life models were selected as a first option in this project because of their simplicity and capabilities to be applied to any type of laminate configuration under variable amplitude loading conditions, different load conditions (e.g., tension-tension, tension-compression, etc.), and complex stress states (i.e., multiaxiality), which made them seem suitable for wind turbine blades.

Even though accurate and reliable fatigue-life predictions were obtained using the proposed probabilistic fatigue-life model when composite laminates under uniaxial and constant amplitude loading conditions were analyzed (see Chapter 6), it was also shown that probabilistic multiaxial fatigue-life models that consider the variability in the material properties are still not suitable for wind turbine blades due to the low accuracy level of the existing cumulative damage rules and multiaxial macroscopic fatigue failure criteria (MMFFs), see Chapters 3 and 6. Consequently, we concluded that either improvements to the existing cumulative damage rules and MMFF criteria should be done to make the probabilistic multiaxial fatigue-life models suitable for wind turbine blades, or another type of fatigue model should be used for analyzing the fatigue behavior of these structures.

Based on this, we decided to go further and work on another type of fatigue model that would allow us to obtain accurate and reliable fatigue-life predictions in wind turbine blades considering the aforementioned fatigue factors. In this sense, we decided to apply damage mechanics models, with which not only the catastrophic failure of the composite materials but also their progressive property degradation could be predicted, with the advantage that this is done based on the actual physical damage mechanisms developed in the material.

Hence, a new damage mechanics-based multiscale approach for wind turbine blades under fatigue loading conditions was proposed in Chapter 4. With this multiscale approach, the effects on the natural damage evolution in composite materials (and by implication in composite structures) on the structural response of the blades could be

analyzed. Moreover, the multiscale approach is suggested to be implemented using a 2D finite-element-based cross-section analysis, which could provide a higher computational efficiency than, for example, using 3D finite element models.

Based on the results obtained from a first implementation of the proposed multiscale approach in which the effect of off-axis cracks on the structural response of the blade was analyzed (see Chapter 7), it was shown that reliable predictions in wind turbine blades can be obtained with the proposed multiscale model. Furthermore, parallel to this process, an experimental-based analysis of the damage evolution in UD glass/epoxy materials under fatigue loading conditions was carried out in agreement with the framework proposed in the multiscale approach (see Chapter 8). This experimental study provides relevant information that can be used for the development of future models about the fiber-related damage evolution of multidirectional laminates and, therefore, possible failures in wind turbine blades.

Accordingly, it was concluded that the proposed damage mechanics-based multiscale approach is a potential option for predicting the fatigue response of wind turbine blades because the initiation, propagation and effect of the different types of damage in wind turbine blades could be estimated with this approach. Further efforts should then be done in this direction in order to develop a damage mechanics-based multiscale model that can fully predict the fatigue response of wind turbine blades under fatigue loading conditions.

Probabilistic multiaxial fatigue-life models

In the first part of the project, the benefits of considering the variability in the fatigue properties of composite materials during the fatigue lifetime estimation of wind turbine blades were analyzed. For this, it was first necessary to develop probabilistic models that allow taking this variability in the fatigue properties into account when predicting the fatigue life of composite laminates under both uni-axial and multiaxial loading conditions, and both constant and variable amplitude cyclic loading, in order to evaluate later their applicability in wind turbine blades.

Based on this, it was shown that accurate and reliable fatigue-life predictions can be obtained for composite laminates under uniaxial and constant amplitude loading conditions when considering the variability in the fatigue properties of the material. These predictions can be obtained using the probabilistic fatigue lifetime diagrams, P-CLDs, developed in this project, with which probabilistic ε-N curves at any load level and R-ratio for which no experimental data are available can be efficiently estimated without using an iterative process. The developed P-CLDs can be used for designing composite components and/or structures under uniaxial and constant amplitude loading conditions, providing to the designer the option of evaluating any probability of reaching a certain life at any combination of load level and R-ratio.

Moreover, it was also shown that reliable fatigue-life predictions regarding probability of failure could be obtained for composite laminates under uniaxial and variable amplitude loading conditions, taking the variability in the fatigue properties into account; however, it was found that the accuracy of these predictions highly depended on the accuracy of

the implemented cumulative damage rule. This could be concluded from the reliability analysis for the fatigue-limit state proposed in this project, in which the number of cycles to failure estimated by the developed P-CLDs were assumed as stochastic variables. In this reliability analysis, a limit state equation based on the Palmgren-Miner's rule was used; however, due to the low accuracy level of this rule in composite materials, the resistance in this limit state equation was assumed equal to the limit damage fraction obtained from experiments. This means that, even though reliable estimations can be obtained from the proposed reliability analysis, experimental data for each type of analyzed load is needed to make the model accurate, which makes this analysis unfeasible for wind turbine blades.

Furthermore, it was also shown that neither reliable nor accurate fatigue lifetime predictions of composite materials under multiaxial loading conditions can be obtained when the variability in the fatigue properties obtained from the developed P-CLDs are propagated in existing multiaxial macroscopic fatigue failure criteria (MMFFs). The low reliability in the predictions was found to be related to the implemented uncertainty propagation method (i.e., the first-order Taylor series), which seems not to be suitable for propagating the P-CLD uncertainty in the MMFF criteria. In addition, the low accuracy in the predictions was found to be related to the used MMFF criteria themselves, which are not accurate enough to predict the fatigue life of composite materials because they do not consider the actual physical failure mechanisms in these materials.

In this sense, based on the low accuracy level of the existing cumulative damage rules and MMFF criteria, it can be concluded that the proposed probabilistic multiaxial fatigue-life model is still not suitable for designing and analyzing wind turbine blades.

Damage mechanics-based multiscale model

In the second part of the project, the benefits of considering the effects of the fatigue-related damage in the structural response of wind turbine blades at different length scales were analyzed. For that, a new damage mechanics-based multiscale approach was proposed. This multiscale approach could provide high computational efficiency during the processing stage of the analysis because it is implemented using a 2D finite-element-based cross-section analysis. In this way, the complexity of the blade in terms of geometry and material distribution is simplified, which would make it easier to implement different models (if comparing with 3D finite element models, for example) for predicting the effects of the different damage mechanisms developed in composite materials, such as off-axis cracks in off-axis plies, delaminations, off-axis cracks in backing fiber bundles, and fiber-related damage, on the structural response of the blade.

A first implementation of this multiscale approach was carried out in this project, where the effect of off-axis cracks on the structural response of the blade was analyzed. Based on the obtained results, it was shown that reliable predictions can be made with the proposed multiscale model, which was demonstrated doing a comparison with experimental deflections of a real 34m long blade at full-length scale. In addition, response of the blade at different length scales (i.e., macro, subcomponent, and full-length), as a function of the number of off-axis cracks, was also identified. Concerning this, it was

shown that the degradation level of the blade can be affected by factors related to the macrolength scale, such as the effect of the laminate thickness or the saturation state of off-axis cracks but also by factors related to the subcomponent-length scale as, for example, the cross-section geometry.

Accordingly, this first implementation of the proposed multiscale approach lays the basis for future extensions of the model in which, for example, the evolution of the off-axis cracks in wind turbine blades under fatigue loading conditions can be analyzed, and the effects of other damage types, such as delaminations, off-axis cracks in backing fiber bundles, and fiber-related damage can be included.

Moreover, because the fiber-related damage is one of the damage mechanisms that is still not well understood in composite materials; therefore, there are no models that can fully predict their evolution and effects on the laminates. Further, an experimental-based analysis about the damage evolution in UD glass/epoxy materials under fatigue loading conditions was also carried out in order to better understand the evolution of this type of damage. Based on this analysis, it was qualitatively shown how the fiber-related damage can be affected by different factors, such as the presence of manufacturing imperfections, the local stress state developed due to previous fiber breaks, and especially by the local fiber volume fraction, which makes the damage evolution more critical in regions with high matrix content. In addition, the trend of the probability of survival of the fibers along the fatigue life was obtained quantitatively. From this trend, it was also found that, even though the fiber can fragment twice or more times, most of the damage fiber break only once, which seems to be the main reason why the stiffness of the unidirectional composite materials does not change considerably during the fatigue lifetime.

The results obtained from this fiber-related damage analysis are relevant for the development of future damage mechanics models that can be included in the proposed multiscale approach, with which the effects of the fiber-related damage on the structural response and possible failure of wind turbine blades can be predicted. However, because the results obtained in this study were based on observations on the specimen surfaces, further experimental studies might be needed in order to confirm these findings in which the 3D response of the material under the same evaluated loading conditions can be analyzed.

General contributions and impact of the thesis

From my point of view, the most important contributions of this project are:

- Development of novel probabilistic constant life diagrams, P-CLDs, which take the variability in the fatigue material properties into account.
- The possibility of estimating probabilistic ε-N curves at any load level and R-ratio without carrying out an iterative process by using the proposed P-CLDs.
- Development of a reliability fatigue model that allows predicting the probability of failure of composite laminates under variable amplitude loading cycles and uniaxial loading conditions, considering the variability in the fatigue material properties.

- Extensive analysis concluding that probabilistic multiaxial fatigue-life models are still not suitable for designing and analyzing wind turbine blades.
- Development of a damage mechanics-based multiscale approach for wind turbine blades under fatigue loading conditions.
- An implementation of the proposed damage mechanics-based multiscale approach with which the effects of off-axis cracks on the structural response of wind turbine blades can be predicted.
- Initial experimental studies as a basis for the development of future models that allow predicting the fiber-related damage evolution in multidirectional laminates and, therefore, possible failures in wind turbine blades.

Future work

Regarding fatigue life models (see Chapters 3 and 6), new multiaxial macroscopic fatigue failure criteria (MMFF) based on the actual damage mechanisms developed in composite materials might be useful to improve the applicability of this type of model in wind turbine blades (and other types of composite structures). In addition, these new MMFF criteria must also consider nonproportionality between the different stress time-series (i.e., $\sigma_1(t)$, $\sigma_2(t)$ and $\sigma_6(t)$), which can occur in wind turbine blades during their operational life.

In addition, the development of new cumulative damage rules for composite materials must be carried out to improve the applicability of the fatigue-life models in wind turbine blades because these structures are subjected to variable amplitude loading conditions.

Regarding the proposed damage mechanics-based multiscale approach (see Chapter 7), there is still a lot of work to be done. The next most immediate step is an extension of the multiscale model presented in this work, with which the evolution of off-axis cracks in wind turbine blades under fatigue loading conditions can be evaluated. With this extended model, the critical zones in the different cross-section regions and along the blade, where the off-axis cracks would develop, could be identified as well as the actual response of the blade under this type of damage. All this should be done considering the multiaxiality in the stress states and the variability in the fatigue behavior of composite materials. This extended model is an ongoing study, which is expected to be made public in the near future in [14].

Furthermore, some improvements to the proposed multiscale model must be done at the different length scales of the wind turbine blades. At the micro- and macro-length scales, an extension of the implemented damage mechanics model for predicting the evolution and effects of off-axis cracks on multidirectional laminates must be done in order to allow its application not only in symmetric cracked laminates but also in any type of cracked laminate. In addition, the development of damage mechanics models that allow predicting the evolution and effects of other types of damage, such as delaminations, fiber-related damage, and off-axis crack in backing bundles, on multidirectional laminates should be done. All these models must satisfy some requirements needed to be applied

in wind turbine blades, e.g., multiaxiality in the stress states, variability in the fatigue behavior of composite materials, damage initiation, and propagation under different fatigue loading conditions (e.g., tension-compression, compression-tension, compression-compression), and computational efficiency.

At the subcomponent and full-length scales, one of the current limitations is the lack of experimental data at these length scales that allow validating all proposed fatigue models. In this sense, fatigue tests at the subcomponent and full-length scales must be carried out, in which the different developed damage types and their effects on the structural response of the blade can be identified and quantified. For this, an additional effort should be made in order to replicate in the laboratory the loads to which the blades are exposed to in real operational conditions, in a fast and efficient way. Currently, DTU Wind Energy, in cooperation with different industrial partners in the wind energy field, and DNV GL are working in this direction through the BLATIGUE (fast and efficient fatigue test of large wind turbine blades) project by developing advanced multiaxis fatigue-testing methods and multiaxis fatigue exciters for large blades.

On the other hand, regarding the fiber-related damage in unidirectional composites (see Chapter 6), the results found in this study related to the evolution of fiber breaks along the fatigue life should be confirmed considering a 3D analysis of the bulk material under the same loading conditions. In addition, considering the complexity of the damage evolution in UD composites, it would be interesting to evaluate alternative methods that not necessarily describe the entire damage evolution of the UD composite. An example of this could be by using S-N curves of 0° plies (which already include all the actual phenomena) considering the stress redistribution caused by other damage types, such as delaminations, off-axis cracks in off-axis plies, or off-axis cracks in backing bundles.

Bibliography

[1] J. Andersons, M. Hojo, and S. Ochiai. "Empirical model for stress ratio effect on fatigue delamination growth rate in composite laminates". eng. In: *International Journal of Fatigue* 26.6 (2004), pages 597–604. ISSN: 18793452, 01421123. DOI: 10.1016/j.ijfatigue.2003.10.016.

[2] K. Atcholi et al. "Superposed torsion flexure of composite-materials - experimental-method and example of application". eng. In: *Composites* 23.5 (1992), pages 327–333. ISSN: 18787134, 00104361. DOI: 10.1016/0010-4361(92)90332-O.

[3] *Probabilistic analysis of wind turbine blades considering stiffness, strength and stability under extreme and fatigue loading*. Copenhagen, Denmark: ICCM, 2015.

[4] J. Bartley-Cho et al. "Damage accumulation in quasi-isotropic graphite/epoxy laminates under constant-amplitude fatigue and block loading". eng. In: *Composites Science and Technology* 58.9 (1998), pages 1535–1547. ISSN: 18791050, 02663538. DOI: 10.1016/S0266-3538(97)00214-5.

[5] J.M. Berthelot and J.F. Le Corre. "A model for transverse cracking and delamination in cross-ply laminates". eng. In: *Composites Science and Technology* 60.7 (2000), pages 1055–1066. ISSN: 18791050, 02663538. DOI: 10.1016/S0266-3538(00)00006-3.

[6] J.P.A.A. Blasques and M. Stolpe. "Multi-material topology optimization of laminated composite beam cross sections". eng. In: *Composite Structures* 94.11 (2012), pages 3278–3289. ISSN: 18791085, 02638223.

[7] J.P.A.A. Blasques et al. "Accuracy of an efficient framework for structural analysis of wind turbine blades". eng. In: *Wind Energy* 19.9 (2016), pages 1603–1621. ISSN: 10991824, 10954244. DOI: 10.1002/we.1939.

[8] J.C. Brewer and P.A. Lagace. "Quadratic stress criterion for initiation of delamination". eng. In: *Journal of Composite Materials* 22.12 (1988), pages 1141–1155. ISSN: 1530793x, 00219983. DOI: 10.1177/002199838802201205.

[9] V.N. Bulsara, R. Talreja, and J. Qu. "Damage initiation under transverse loading of unidirectional composites with arbitrarily distributed fibers". eng. In: *Composites Science and Technology* 59.5 (1999), pages 673–682. ISSN: 18791050, 02663538. DOI: 10.1016/S0266-3538(98)00122-5.

[10] P.P. Camanho, C.G Davila, and D.R. Ambur. "Numerical Simulation of Delamination Growth in Composite Materials". eng. In: (2009). DOI: 10.1.1.28.8393.

[11] P.A. Carraro, L. Maragoni, and M. Quaresimin. “Prediction of the crack density evolution in multidirectional laminates under fatigue loadings”. eng. In: *Composites Science and Technology* 145 (2017), pages 24–39. ISSN: 18791050, 02663538. DOI: 10.1016/j.compscitech.2017.03.013.

[12] P.A. Carraro and M. Quaresimin. “A stiffness degradation model for cracked multidirectional laminates with cracks in multiple layers”. eng. In: *International Journal of Solids and Structures* 58 (2015), pages 34–51. ISSN: 18792146, 00207683. DOI: 10.1016/j.ijsolstr.2014.12.016.

[13] P.A. Carraro et al. “Delamination onset in symmetric cross-ply laminates under static loads: Theory, numerics and experiments”. eng. In: *Composite Structures* 176 (2017), pages 420–432. ISSN: 18791085, 02638223. DOI: 10.1016/j.compstruct.2017.05.030.

[14] O.G. Castro and K. Branner. “Damage mechanics-based multiscale model for wind turbine blades under fatigue: Part 2. Prediction of off-axis crack evolution”. In: *In manuscript* ().

[15] O.G. Castro et al. “Comparing fatigue life estimations of composite wind turbine blades using different fatigue analysis tools”. eng. In: *Proceedings of the 20th International Conference on Composite Materials* (2015).

[16] W.S. Chan. “An analytical and experimental investigation of edge delamination in laminates subjected to tension, bending, and torsion”. und. In: (1989).

[17] B.Y. Chen et al. “Modelling the tensile failure of composites with the floating node method”. eng. In: *Computer Methods in Applied Mechanics and Engineering* 308 (2016), pages 414–442. ISSN: 18792138, 00457825. DOI: 10.1016/j.cma.2016.05.027.

[18] F.W. Crossman et al. “Initiation and growth of transverse cracks and edge delamination in composite laminates Part 2. Experimental correlation”. eng. In: *Journal of Composite Materials* 14.1 (1980), pages 88–108. ISSN: 1530793x, 00219983. DOI: 10.1177/002199838001400107.

[19] L.R. Dharani and H. Tang. “Micromechanics characterization of sublaminate damage”. eng. In: *International Journal of Fracture* 46.2 (1990), pages 123–140. ISSN: 15732673, 03769429. DOI: 10.1007/BF00041999.

[20] N.K. Dimitrov, A.D. Kiureghian, and C. Berggreen. “Bayesian inference model for fatigue life of laminated composites”. In: *Journal of Composite Materials* 50.2 (2016), pages 131–143. ISSN: 0021-9983. DOI: 10.1177/0021998315571772.

[21] A. Farrokhabadi, H. Hosseini-Toudeshky, and B. Mohammadi. “A generalized micromechanical approach for the analysis of transverse crack and induced delamination in composite laminates”. eng. In: *Composite Structures* 93.2 (2011), pages 443–455. ISSN: 18791085, 02638223. DOI: 10.1016/j.compstruct.2010.08.036.

[22] E.K. Gamstedt, L.A. Berglund, and T. Peijs. “Fatigue mechanisms in unidirectional glass-fibre-reinforced polypropylene”. eng. In: *Composites Science and Technology* 59.5 (1999), pages 759–768. ISSN: 18791050, 02663538. DOI: 10.1016/S0266-3538(98)00119-5.

[23] E.K. Gamstedt and B.A. Sjogren. “An experimental investigation of the sequence effect in block amplitude loading of cross-ply composite laminates”. eng. In: *International Journal of Fatigue* 24.2-4 (2002), pages 437–446. ISSN: 18793452, 01421123. DOI: 10.1016/S0142-1123(01)00099-8.

[24] V. Giavotto et al. “Anisotropic beam theory and applications”. eng. In: *Computers and Structures* 16.1-4 (1983), pages 403–413. ISSN: 18792243, 00457949. DOI: 10.1016/0045-7949(83)90179-7.

[25] GWEC Global Wind Energy Council. *Global Wind Report, Annual Market Update 2016*. eng. 2016. URL: http://www.gwec.net/wp-content/uploads/vip/GWEC_PRstats2016_EN_WEB.pdf.

[26] J. Glud et al. “A stochastic multiaxial fatigue model for off-axis cracking in FRP laminates”. mul. In: (2017).

[27] P. Gudmundson and W.L. Zang. “An analytic model for thermoelastic properties of composite laminates containing transverse matrix cracks”. eng. In: *International Journal of Solids and Structures* 30.23 (1993), pages 3211–3231. ISSN: 18792146, 00207683. DOI: 10.1016/0020-7683(93)90110-S.

[28] P.U. Haselbach and K. Branner. “Effect of trailing edge damage on full-scale wind turbine blade failure”. In: *Proceedings of the 20th International Conference on Composite Materials*. ICCM20 Secretariat, 2015.

[29] Z. Hashin. “Analysis of cracked laminates - a variational approach”. eng. In: *Mechanics of Materials* 4.2 (1985), pages 121–136. ISSN: 18727743, 01676636. DOI: 10.1016/0167-6636(85)90011-0.

[30] Z. Hashin and A. Rotem. “A fatigue failure criterion for fiber reinforced materials”. In: *Journal of Composite Materials* 7.4 (1973), pages 448 –464.

[31] A.A. ten Have. *WISPER and WISPERX final definition of two standardised fatigue loading sequences for wind turbine blades*. Technical report. National Aerospace Laboratory NRL, 1988.

[32] M. Hojo et al. “Effect of stress ratio on near-threshold propagation of delamination fatigue cracks in unidirectional CFRP”. eng. In: *Composites Science and Technology* 29.4 (1987), pages 273–292. ISSN: 18791050, 02663538.

[33] T.K. Jacobsen. “Materials technology for large wind turbine rotor blades - limits and challenges”. eng. In: *Proceedings of the ... Riso International Symposium on Materials Science* (2011), pages 35–43. ISSN: 09070079.

[34] M. Jalalvand, H. Hosseini-Toudeshky, and B. Mohammadi. "Numerical modeling of diffuse transverse cracks and induced delamination using cohesive elements". eng. In: *Proceedings of the Institution of Mechanical Engineers Part C-journal of Mechanical Engineering Science* 227.7 (2013), pages 1392–1405. ISSN: 20412983, 09544062. DOI: 10.1177/0954406212460974.

[35] Y.J. Jang et al. "Development of fatigue life prediction method and effect of 10-minute mean wind speed distribution on fatigue life of small wind turbine composite blade". eng. In: *Renewable Energy* 79.1 (2015), pages 187–198. ISSN: 18790682, 09601481. DOI: 10.1016/j.renene.2014.10.006.

[36] K.M. Jespersen et al. "Fatigue damage assessment of uni-directional non-crimp fabric reinforced polyester composite using X-ray computed tomography". In: *Composites Science and Technology* 136 (2016). CC BY-NC-ND 3.0, pages 94–103. ISSN: 0266-3538. DOI: 10.1016/j.compscitech.2016.10.006.

[37] K.M. Jespersen et al. "Fatigue damage evolution in fibre composites for wind turbine blades". PhD thesis. Denmark, 2017.

[38] M. Kawai and T. Teranuma. "A multiaxial fatigue failure criterion based on the principal constant life diagrams for unidirectional carbon/epoxy laminates". In: *Composites Part A: Applied Science and Manufacturing* 43.8 (2012), pages 1252–1266. ISSN: 1359-835X. DOI: http://dx.doi.org/10.1016/j.compositesa.2012.03.003. URL: http://www.sciencedirect.com/science/article/pii/S1359835X12000966.

[39] C. Kong et al. "Investigation of fatigue life for a medium scale composite wind turbine blade". eng. In: *International Journal of Fatigue* 28.10 (2006), pages 1382–1388. ISSN: 18793452, 01421123. DOI: 10.1016/j.ijfatigue.2006.02.034.

[40] S. Li, C.V. Singh, and R. Talreja. "A representative volume element based on translational symmetries for FE analysis of cracked laminates with two arrays of cracks". eng. In: *International Journal of Solids and Structures* 46.7-8 (2009), pages 1793–1804. ISSN: 18792146, 00207683. DOI: 10.1016/j.ijsolstr.2009.01.009.

[41] D.V. Lindley. *Introduction to probability and statistics from a Bayesian viewpoint:* Cambridge: Cambridge University Press, January 1965. ISBN: 9780511662973. DOI: 10.1017/CBO9780511662973. URL: https://www.cambridge.org/core/books/introduction-to-probability-and-statistics-from-a-bayesian-viewpoint/996804FA37EAA4213B93F5EEF523D809.

[42] P. Lundmark and J. Varna. "Constitutive relationships for laminates with ply cracks in in-plane loading". eng. In: *International Journal of Damage Mechanics* 14.3 (2005), pages 235–259. ISSN: 15307921, 10567895. DOI: 10.1177/1056789505050355.

[43] L. Maragoni et al. "Fatigue behaviour of glass/epoxy laminates in the presence of voids". eng. In: *International Journal of Fatigue* 95 (2017), pages 18–28. ISSN: 18793452, 01421123. DOI: 10.1016/j.ijfatigue.2016.10.004.

[44] S. Marquez-Dominguez and John D. Sørensen. “Fatigue Reliability and Calibration of Fatigue Design Factors for Offshore Wind Turbines”. In: *Energies* 5.6 (2012), pages 1816–1834. ISSN: 1996-1073. DOI: 10.3390/en5061816. URL: http://www.mdpi.com/1996-1073/5/6/1816.

[45] L.N. McCartney. “Theory of stress transfer in a $0° - 90° - 0°$ cross-ply laminate containing a parallel array of transverse cracks”. eng. In: *Journal of the Mechanics and Physics of Solids* 40.1 (1992), pages 27–68, 27–68. ISSN: 18734782, 00225096. DOI: 10.1016/0022-5096(92)90226-R.

[46] J. Montesano, H. Chu, and C. V. Singh. “Development of a physics-based multi-scale progressive damage model for assessing the durability of wind turbine blades”. eng. In: *Composite Structures* 141 (2016), pages 50–62. ISSN: 18791085, 02638223. DOI: 10.1016/j.compstruct.2016.01.011.

[47] R. Nijssen. *(NEW) WISPER(X) test results and analysis*. Technical report 10313. 2005.

[48] R.P.L. Nijssen and D.R.V. Van Delft. “Alternative fatigue formulations for variable amplitude loading of fibre composites for wind turbine rotor blades”. eng. In: *Esis Publication* 32 (2003), pages 563–574. ISSN: 15661369.

[49] T.K. Obrien. “Characterization of delamination onset and growth in a composite laminate”. und. In: (1981).

[50] T.P. Philippidis and A.P. Vassilopoulos. “Complex stress state effect on fatigue life of GRP laminates.: part I, experimental”. In: *International Journal of Fatigue* 24.8 (2002), pages 813 –823. ISSN: 0142-1123. DOI: https://doi.org/10.1016/S0142-1123(02)00003-8. URL: http://www.sciencedirect.com/science/article/pii/S0142112302000038.

[51] T.P. Philippidis and A.P. Vassilopoulos. “Complex stress state effect on fatigue life of {GRP} laminates. Part II, Theoretical formulation”. In: *International Journal of Fatigue* 24.8 (2002), pages 825 –830. ISSN: 0142-1123. DOI: http://dx.doi.org/10.1016/S0142-1123(02)00004-X. URL: http://www.sciencedirect.com/science/article/pii/S014211230200004X.

[52] T.P. Philippidis and A.P. Vassilopoulos. “Fatigue strength prediction under multiaxial stress”. In: *Journal of Composite Materials* 33.17 (1999), pages 1578 – 1599.

[53] M. Quaresimin. “A damage-based approach for the fatigue design of composite structures”. eng. In: *Iop Conference Series: Materials Science and Engineering* 139.1 (2016), page 012006. ISSN: 1757899x, 17578981. DOI: 10.1088/1757-899X/139/1/012006.

[54] M. Quaresimin and P.A. Carraro. “Damage initiation and evolution in glass/epoxy tubes subjected to combined tension-torsion fatigue loading”. eng. In: *International Journal of Fatigue* 63 (2014), pages 25–35. ISSN: 18793452, 01421123. DOI: 10.1016/j.ijfatigue.2014.01.002.

[55] M. Quaresimin, L. Susmel, and R. Talreja. "Fatigue behaviour and life assessment of composite laminates under multiaxial loadings". eng. In: *International Journal of Fatigue* 32.1 (2010), pages 2–16. ISSN: 18793452, 01421123. DOI: 10.1016/j.ijfatigue.2009.02.012.

[56] M. Quaresimin et al. "Damage evolution under cyclic multiaxial stress state: A comparative analysis between glass/epoxy laminates and tubes". eng. In: *Composites Part B: Engineering* 61 (2014), pages 282–290. ISSN: 18791069, 13598368. DOI: 10.1016/j.compositesb.2014.01.056.

[57] J.L. Rebiere and D. Gamby. "A criterion for modelling initiation and propagation of matrix cracking and delamination in cross-ply laminates". eng. In: *Composites Science and Technology* 64.13-14 (2004), pages 2239–2250. ISSN: 18791050, 02663538. DOI: 10.1016/j.compscitech.2004.03.008.

[58] K.L. Reifsnider. *Fatigue of composite materials*. eng. Volume 4. Elsevier, 1991, 12+519 s. ISBN: 0444705074, 044442525x.

[59] K.L. Reifsnider. "Some fundamental aspects of the fatigue and fracture response of composite materials". und. In: (1977).

[60] *Rotor blades for wind turbines*. Standard. DNV GL, 2015.

[61] M.M. Shokrieh and L.B. Lessard. "Progressive fatigue damage modeling of composite materials, Part I: Modeling". eng. In: *Journal of Composite Materials* 34.13 (2000), pages 1056–1080. ISSN: 1530793x, 00219983. DOI: 10.1177/002199830003401301.

[62] M.M. Shokrieh and R. Rafiee. "Simulation of fatigue failure in a full composite wind turbine blade". eng. In: *Composite Structures* 74.3 (2006), pages 332–342. ISSN: 18791085, 02638223. DOI: 10.1016/j.compstruct.2005.04.027.

[63] C.V. Singh and R. Talreja. "A synergistic damage mechanics approach for composite laminates with matrix cracks in multiple orientations". eng. In: *Mechanics of Materials* 41.8 (2009), pages 954–968. ISSN: 18727743, 01676636. DOI: 10.1016/j.mechmat.2009.02.008.

[64] B.F. Sørensen et al. *Improved design of large wind turbine blade of fibre composites based on studies of scale effects (Phase 1). Summary report*. eng. 2004.

[65] I. Susuki. "Fatigue damage of composite laminate under biaxial loads". eng. In: *Int S Stren* (1992), B543–B548.

[66] N. Takeda and S. Ogihara. "Initiation and growth of delamination from the tips of transverse cracks in CFRP cross-ply laminates". eng. In: *Composites Science and Technology* 52.3 (1994), pages 309–318. ISSN: 18791050, 02663538. DOI: 10.1016/0266-3538(94)90166-X.

[67] R. Talreja. “Fatigue of composite materials: Damage mechanisms and fatigue-Life diagrams”. In: *Proceedings of the Royal Society of London A: Mathematical, Physical and Engineering Sciences* 378.1775 (1981), pages 461–475. ISSN: 0080-4630. DOI: 10.1098/rspa.1981.0163. eprint: http://rspa.royalsocietypublishing.org/content/378/1775/461.full.pdf. URL: http://rspa.royalsocietypublishing.org/content/378/1775/461.

[68] R. Talreja. “Multi-scale modeling in damage mechanics of composite materials”. In: *Journal of Materials Science* 41.20 (2006), pages 6800–6812. ISSN: 1573-4803. DOI: 10.1007/s10853-006-0210-9. URL: https://doi.org/10.1007/s10853-006-0210-9.

[69] N.J. Tarp-Johansen. *Examples of fatigue lifetime and reliability evaluation of larger wind turbine components*. 2003. ISBN: 87-550-3236-2 (Internet).

[70] H.S. Toft and J.D. Sørensen. “Probabilistic fatigue design of composite material for wind turbine blades”. und. In: *Applications of Statistics and Probability in Civil Engineering -proceedings of the 11th International Conference on Applications of Statistics and Probability in Civil Engineering* (2011), pages 1185–1192.

[71] H.S. Toft and J.D. Sørensen. “Reliability-based design of wind turbine blades”. In: *Structural Safety* 33.6 (2011), pages 333 –342. ISSN: 0167-4730. DOI: https://doi.org/10.1016/j.strusafe.2011.05.003. URL: http://www.sciencedirect.com/science/article/pii/S0167473011000452.

[72] J. Tong et al. “On matrix crack growth in quasi-isotropic laminates - I. Experimental investigation”. eng. In: *Composites Science and Technology* 57.11 (1997), pages 1527–1535. ISSN: 18791050, 02663538. DOI: 10.1016/S0266-3538(97)00080-8.

[73] J. Varna et al. “Crack opening geometry in cracked composite laminates”. eng. In: *International Journal of Damage Mechanics* 6.1 (1997), pages 96–118. ISSN: 15307921, 10567895. DOI: 10.1177/105678959700600107.

[74] J. Varna et al. “Damage in composite laminates with off-axis plies”. eng. In: *Composites Science and Technology* 59.14 (1999), pages 2139–2147. ISSN: 18791050, 02663538. DOI: 10.1016/S0266-3538(99)00070-6.

[75] A.P. Vassilopoulos and T. Keller. “Macroscopic fatigue failure theories for multiaxial stress states”. In: *Fatigue of Fiber-reinforced Composites*. London: Springer London, 2011, pages 155–197. ISBN: 978-1-84996-181-3. DOI: 10.1007/978-1-84996-181-3_6. URL: http://dx.doi.org/10.1007/978-1-84996-181-3_6.

[76] A.P. Vassilopoulos, B.D. Manshadi, and T. Keller. “Influence of the constant life diagram formulation on the fatigue life prediction of composite materials”. In: *International Journal of Fatigue* 32.4 (2010), pages 659 –669. ISSN: 0142-1123. DOI: https://doi.org/10.1016/j.ijfatigue.2009.09.008. URL: http://www.sciencedirect.com/science/article/pii/S0142112309002795.

[77] A.P. Vassilopoulos, B.D. Manshadi, and T. Keller. "Piecewise non-linear constant life diagram formulation for FRP composite materials". In: *International Journal of Fatigue* 32.10 (2010), pages 1731 –1738. ISSN: 0142-1123. DOI: https://doi.org/10.1016/j.ijfatigue.2010.03.013. URL: http://www.sciencedirect.com/science/article/pii/S0142112310000794.

[78] D. Veldkamp. "A probabilistic evaluation of wind turbine fatigue design rules". In: *Wind Energy* 11.6 (2008), pages 655–672. ISSN: 1099-1824. DOI: 10.1002/we.287. URL: http://dx.doi.org/10.1002/we.287.

[79] J. Wang, Z. Huang, and Y. Li. "Computation method on fatigue life of a full composite wind turbine blade". eng. In: *Asia-pacific Power and Energy Engineering Conference* (2010). ISSN: 21574847, 21574839.

[80] *Wind turbines Part 1 Design requirements*. Standard. IEC, 2005-2008.

[81] J. Zangenberg, P. Brøndsted, and R. Ostergaard. "The effects of fibre architecture on fatigue life-time of composite materials". PhD thesis. Denmark, 2013.

[82] Z. Zou et al. "Application of a delamination model to laminated composite structures". eng. In: *Composite Structures* 56.4 (2002), pages 375–389. ISSN: 18791085, 02638223. DOI: 10.1016/S0263-8223(02)00021-1.

Part II

Publications

CHAPTER 6

Paper 1

Accepted for publication:
Oscar Castro, Kim Branner, and Nikolay Dimitrov. *Assessment and propagation of mechanical property uncertainties in fatigue life prediction of composite laminates.* Journal of Composites Materials (2017).

Assessment and propagation of mechanical property uncertainties in fatigue life prediction of composite laminates

Oscar Castro[+], Kim Branner[+] and Nikolay Dimitrov[+]

[+]DTU Wind Energy, Technical University of Denmark, Frederiksborgvej 399, 4000 Roskilde, Denmark. E-mail: osar@dtu.dk , kibr@dtu.dk , nkdi@dtu.dk

Abstract

A probabilistic model for estimating the fatigue life of laminated composite materials considering the uncertainty in their mechanical properties is developed. The uncertainty in the material properties is determined from fatigue coupon tests. Based on this uncertainty, probabilistic constant life diagrams are developed which can efficiently estimate probabilistic ε-N curves at any load level and stress ratio. The probabilistic ε-N curve information is used in a reliability analysis for fatigue limit state proposed for estimating the probability of failure of composite laminates under variable amplitude loading cycles. Fatigue life predictions of uni-directional and multi-directional Glass/Epoxy laminates are carried out to validate the proposed model against experimental data. The probabilistic fatigue behaviour of laminates is analyzed under constant amplitude loading conditions as well as under both repeated block tests and spectral fatigue using the WISPER, WISPERX and NEW WISPER load sequences for wind turbine blades.

Keywords: uncertainty, probabilistic, fatigue, mechanical properties, laminates, composite

1 Introduction

The properties of materials are varying in their nature. This variation may be even higher for composite materials due to the difficulty to do a highly controlled manufacturing process for applications such as wind turbine blades. This variability in the material properties together with the inherently random nature of other factors (e.g. loading, geometry, environmental conditions, etc.) is reflected in the variability in the fatigue behaviour of this type of materials. Nevertheless, fatigue life prediction methods are most often based on deterministic material properties. This research explores what benefits can

be gained in the fatigue lifetime estimation of composite materials by taking uncertainties in their mechanical properties into account.

The uncertainty in the mechanical properties of composite materials is mainly influenced by the uncertainty in their constituent elements (fibres and matrix) and in the manufacturing process. Some of the main sources of uncertainty related to the manufacturing process are the volume fractions of matrix and fibres, voids and porosity of the matrix, bonding defects, ply misalignment, ply cracking, delaminations and cure cycle [39, 10, 37, 8, 36, 35, 43, 23].

The uncertainties related to the mechanical properties can, in general, be classified as aleatory and epistemic. The aleatory uncertainty, also denoted physical uncertainty, refers to the inherent randomness in the different physical parameters such as static and fatigue strengths. Whereas the epistemic uncertainty, also denoted systematic uncertainty, appears due to limited data and knowledge of the problem. This type of uncertainty can be related to experimental processes and modelling methods. Another possible type of uncertainty is the error (e.g. gross-errors, instrumentation error, etc.), which is often considered as part of the aleatory uncertainty.

The aleatory uncertainty of composite materials can be analyzed through two approaches according to Sriramula and Chryssanthopoulos [41]: micro-scale and macro-scale. At the micro scale, the macroscopic material properties and their uncertainties are built up from the fibre and matrix properties [39, 3]. Whereas at the macro scale, the uncertainty in material properties is determined by experimental tests at coupon/component level [17, 45]. Some researchers also suggest the mesoscale (ply or lamina level) as an advantageous scale to define the variability behaviour of the mechanical properties [44].

Using the macro-scale approach, the uncertainties of static and fatigue properties of composite materials have been quantified and then propagated in fatigue methods in order to obtain probabilistic fatigue lifetime estimations. Liu and Mahadevan [25], for example, suggested a damage accumulation model for laminated composites under multi-axial stress states, which was extended to a probabilistic analysis by using the Monte Carlo simulation and treating the material properties as random variables based on experimental data. Kang et al. [18] also developed a probabilistic fatigue life prediction model based on a damage accumulation process. In this work, the static stress-strain curves and the developed fatigue damage accumulation curves of the materials were assumed as random variables. Xiang and Liu [48] proposed a critical plane-based model for multi-axial fatigue reliability analysis in which the identification of the critical plane not only depended on the stress state but also on the material properties. In this study, the uncertainties of the material properties as well as of the ply configurations and volume fractions were assumed to have a coefficient of variation of 0.05 and then were propagated by using the Inverse First-Order Reliability Method

(IFORM). Dimitrov et al. [6] also developed a probabilistic fatigue life model for laminated composites under multi-axial stress state. This model was based on the mean value and the uncertainty of the mechanical properties of the individual lamina and calibrated to test results using Bayesian inference, allowing the prediction of the fatigue behaviour of a wide range of laminate configurations.

Most of these probabilistic fatigue life models are able to predict the fatigue response of composite materials at any stress ratio and load level; however, they require iterative processes that could make them slow. Kawai and Yano [22] recently developed probabilistic constant fatigue life diagrams that allow efficiently predicting probabilistic S-N curves without using any iterative process. The probabilistic constant life diagrams were built based on the stochastic behaviour of the static strengths and the S-N curve at the critical stress ratio of the laminates, which is obtained from experimental coupon tests. Then, any probabilistic S-N curve can be predicted based on this information by using a probabilistic scaling law. Nevertheless, these probabilistic constant fatigue life diagrams were developed based on the two-segment anisomorphic constant life diagrams [19], which do not describe well the sensitivity zone in which the mean stress changes from tension-dominated level to compression-dominated level presented in matrix-dominated off-axis and transverse laminated composites [20].

Moreover, less attention has been given on predicting the probabilistic fatigue lifetime of composite materials under variable loading conditions.

The purpose of this paper is to investigate if reliable fatigue life predictions of composite materials under constant and variable loading conditions can be obtained by considering the variability in their mechanical properties and propagating it through the fatigue life prediction method.

For that, the material properties and their uncertainties are estimated from experimental coupon test data. We develop probabilistic constant life diagrams by propagating these uncertainties in linear and non-linear constant life diagrams that consider the fatigue behaviour of composite materials under any combination of tension and compression loading conditions. The information given by the developed probabilistic diagrams is used to carry out a reliability analysis using the Monte Carlo simulation, with which the probabilistic fatigue response of the composite materials under different types variable loading conditions is evaluated. The probabilistic fatigue lifetime predicted by using the different probabilistic constant life diagrams is further analyzed and compared with experimental data.

2 Theoretical considerations

2.1 Assessment of uncertainty in ε-N curves

S-N or ε-N curves have been used for more than one century to predict the fatigue behavior of materials based on an interpolation process between experimental constant amplitude fatigue data. In the present work, ε-N curves (where ε is the normalized stress respect to the static elastic modulus, $\varepsilon = \sigma/E_0$) are used instead of S-N curves. In the following, it is described how uncertainties in the ε-N curves are determined from experimental data. These uncertainties are further propagated through the entire fatigue lifetime estimation process.

The variability in the ε-N curves is estimated based on constant amplitude fatigue coupon tests at different R-ratios, where the R-ratio is the ratio between the minimum and maximum cyclic stress, $R = \sigma_{min}/\sigma_{max}$. A log-log ε-N curve based on the Basquin equation that follows the form below is assumed to fit experimental data pairs $(\hat{N}_1, \hat{\varepsilon}_{amp_1})$, $(\hat{N}_2, \hat{\varepsilon}_{amp_2})$, ..., $(\hat{N}_n, \hat{\varepsilon}_{amp_n})$ and model the fatigue behaviour of the material [45].

$$\log N = \log I - b \log \varepsilon_{amp} + \hat{\epsilon} \tag{1}$$

where N is the number of cycles to failure, ε_{amp} is the normalized stress amplitude respect to the static elastic modulus (i.e. $\varepsilon_{amp} = \sigma_{amp}/E_0$) and $\hat{\epsilon}$ is the fitting error. The material parameters $\log I$ and b are the intercept and the slope of the curve respectively.

Based on Eq. 1, the following equation is considered from now onwards in order to facilitate the propagation of the ε-N curve uncertainty in constant life diagrams (CLDs), as described in section 2.2:

$$\log \varepsilon_{amp} = \log K - m \log N + \epsilon \tag{2}$$

where

$$\log K = \frac{\log I}{b}; \quad m = \frac{1}{b}; \quad \epsilon = \frac{\hat{\epsilon}}{b} \tag{3}$$

It may be noted that Eq. 2 is only valid in the region between approximately 10^3 and 10^6 cycles, where a linear fatigue behaviour of the material in a log-log plot is expected. The fatigue behaviour in the low-cycle regime or for stresses under an eventual fatigue limit is not considered in this study.

In Eq. 2, the fitting error ϵ is assumed normally distributed with standard deviation s_ϵ. The parameters $\log K$ and m, and the parameter s_ϵ, are estimated by the Maximum Likelihood method by maximizing the LogLikelihood function $L(\log K, m, s_\epsilon^2) = \sum_{j=1}^{n} \log(p(\log \hat{\varepsilon_{amp}}_j | \log \hat{N}_j; \log K, m, s_\epsilon^2))$. The slope m is assumed deterministic since it is usually strongly dependent on $\log K$ [6] and the parameters $\log K$ and s_ϵ are assumed uncorrelated. The parameter $s_{\log K}$, which represents the

physical uncertainty of the material properties, and the parameter s_{s_ϵ}, which represents the model uncertainty (i.e., the "unexplained" variance that cannot be attributed to changes in the intercept of the ε-N curve), are estimated by using the covariance matrix $\mathbf{C}$, see e.g. [24], as follows:

$$\mathbf{C} = [-\mathbf{H}]^{-1} \tag{4}$$

where $\mathbf{H}$ is the Hessian matrix of second order derivatives of the log-likelihood function.

Based on this, the variability in the parameter $\log \varepsilon_{amp}$, $s_{\log \varepsilon_{amp}}$, which represents the total uncertainty in the ε-N curve, can be expressed as:

$$s_{\log \varepsilon_{amp}} = \sqrt{s^2_{\log K} + s^2_\epsilon} \tag{5}$$

Moreover, the variability in the normalized stress amplitude, $s_{\varepsilon_{amp}}$, of an ε-N curve can be approximated by the following expression:

$$s_{\varepsilon_{amp}} \approx |\varepsilon_{amp}(\ln(10) s_{\log \varepsilon_{amp}})| \tag{6}$$

And the variability in the number of cycles to failure, s_N, for a given normalized stress amplitude ε_{amp} can be thus estimated by:

$$s_N = \frac{1}{m} \frac{(K)^{\frac{1-m}{m}}}{\varepsilon_{amp}^{1/m}} s_{\varepsilon_{amp}} \tag{7}$$

2.2 Uncertainty propagation in constant life diagrams

In the following, we demonstrate how probabilistic constant life diagrams (P-CLDs) are developed by propagating the above uncertainty in ε-N curves in modified constant life diagrams. The developed P-CLDs provide a predictive tool for the estimation of probabilistic ε-N curves for any R-ratio for which no experimental data is available and provide the option of evaluating the response of the material under any percentage of survival probability.

2.2.1 Modified constant life diagrams

Constant life diagrams (CLDs) provide a graphical representation of given fatigue lives and their corresponding safe regime of constant amplitude loading at any R-ratio, see Fig. 1. By using the CLDs, any S-N curve (or ε-N curve) at R-ratios in which experimental data has not been taken can be estimated doing an interpolation process as explained below. The CLDs are commonly divided in four regions: tension-tension (T-T), tension-compression (T-C), compression-tension (C-T) and

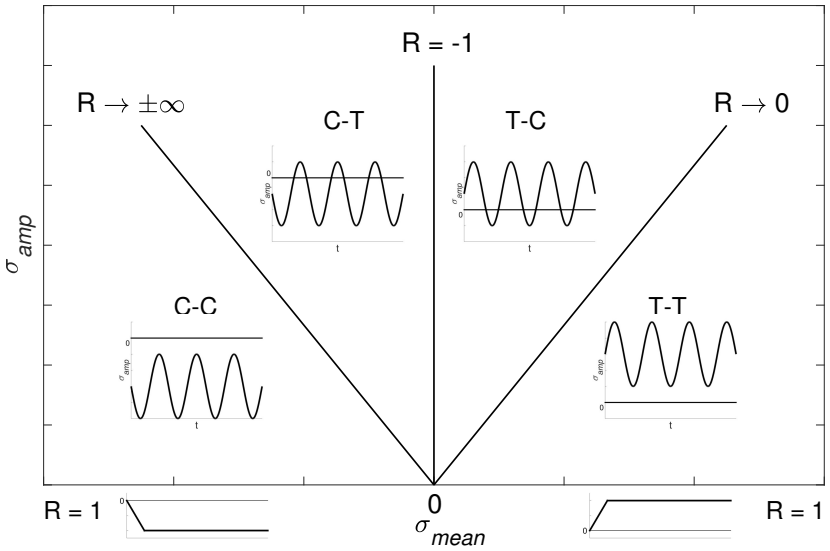

Figure 1: Common representation of deterministic constant life diagrams (CLDs) with four regions shown from left to right: compression-compression (C-C), compression-tension (C-T), tension-compression (T-C), and tension-tension (T-T).

compression-compression (C-C), which are bounded by radial lines that represent known S-N curves (or ε-N curves) at $R = -1$, $R \to 0$ (e.g., $R = 0.1$), $R \to \pm\infty$ (e.g., $R = 10$) and at the static case $R = 1$, usually determined by experimental tests. Note that $R = 1$ can indicate either tensile or compressive stress amplitude. Based on this, any known S-N curve (or ε-N curve) can be estimated by doing an interpolation process between the known S-N curves and the static strengths σ_{D_O} (where D is X, Y and S for on-axis, transverse and in-plane shear fiber direction respectively, and O is T and C for tension and compression respectively).

The static strengths σ_{D_O} in common CLDs (see a summary of common CLDs in [46]) has been adopted due to the lack of information about the fatigue behaviour of the material at stress amplitude close to zero and high stress mean loading conditions (i.e. $R \to 1$). This assumption represents a deficiency of common CLDs that lead to no accurate fatigue life predictions at R-ratios close to $R = 1$ at T-T and C-C loading conditions, see e.g. [14]. This can be explained from a material point of view, in which the damage mechanisms developed in the material under static loading conditions are different than those developed under fatigue loading conditions. For example, Huther and Brøndsted showed in [14] that the quasi-static mechanical properties of unidirectional glass fiber reinforced composites are not influenced by the curing cycle. However, when elevated temperatures are applied during the curing and higher residual stresses are generated, the fatigue performance of the UD material decreases considerably.

Taking into account the implication of this deficiency in common CLDs, a modified

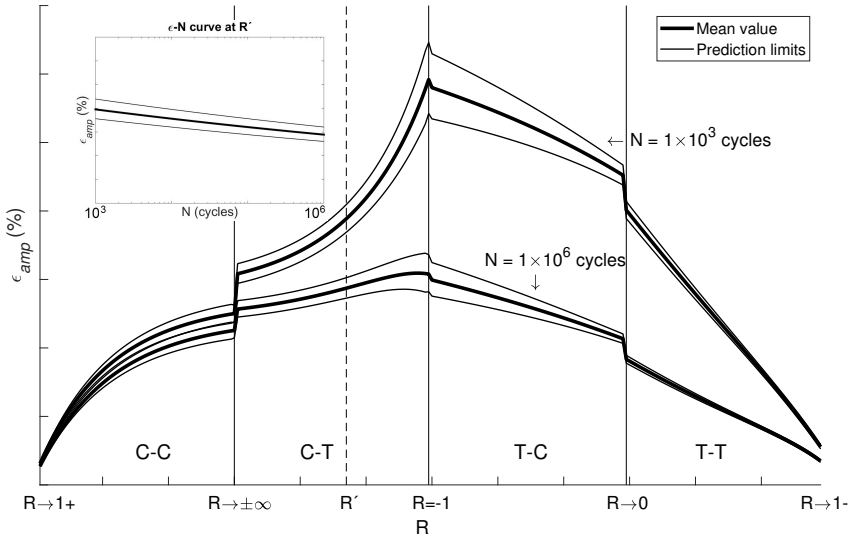

Figure 2: Probabilistic constant life diagram (P-CLD). Thick lines represent the mean. Thin lines represent the predictions limits corresponding to the desired number of standard deviations from the mean.

CLD is proposed in this study, see Fig. 2. The proposed CLD is represented on the $\varepsilon_{amp} - R$ plane to provide a better visualization of the variability in the predicted fatigue behavior, as described in section 2.2. In this CLD, the normalized static strengths ε_{D_O} (i.e., $\varepsilon_{D_O} = \sigma_{D_O}/E_0$) in tension and compression are replaced by experimental ε-N curves at R-ratios that tend to 1 from the left and the right (i.e. at T-T and C-C loading conditions), respectively. In this way, the interpolation process at T-T and C-C regions is carried out based only on fatigue input data, eliminating the need of using the static strengths. Selecting ε-N curves at R-ratios closer to 1 (e.g. $R = 0.9$ and $R = 1.1$) will allow covering a wider range of loading conditions.

By using the proposed CLD, any ε-N curve is determined as vertical lines proceeding from the corresponding R' ratio on the x-axis. As an example, the ε-N curve shown at the upper-left corner of Fig. 2 corresponds to the ε-N curve represented as a vertical dashed line emerging from the R' ratio on the x-axis in the P-CLD diagram.

As shown in Fig. 2, the values of R-ratio vary depending on the load condition region. For C-C region, for example, the R-ratio values increase from $R \to 1+$ to $R \to +\infty$; whereas for C-T region, the R-ratio values vary from $R \to -\infty$ to $R = -1$. For T-C region, the R-ratio values increase from $R = -1$ to $R \to 0$; and for T-T region, the R-ratio values vary from $R \to 0$ to $R \to 1-$. They were plotted in this way to provide a better visualization of the constant life lines.

Moreover, the mean value of the constant life lines is represented as thick lines, whereas the number of standard deviation values from the mean are represented as thin

lines. The behaviour of these constant life lines varies with each fatigue loading condition (i.e. C-C, C-T, T-C, T-T) depending on the known ε-N curves used as input data and on the implemented interpolation method.

In this work, two different interpolation methods are analyzed: piecewise linear (PWL) and piecewise non-linear (PWNL). The PWL and PWNL methods were implemented by Philippidis and Vassilopoulos [33, 34] and Vassilopoulos etal [47] respectively, to create CLDs in which the interpolation process is carried out between multiple sub-regions defined by known S-N curves. These CLDs have shown good accuracy of the fatigue predictions compared with other CLDs, see e.g. in [47]. Based on these CLDs, modified PWL and PWNL interpolation equations at T-T and C-C loading conditions are developed in present work, see Appendix A.

It is worth mentioning that discontinuities at $R=\pm\infty$ and $R=0$ might appear if the deterministic CLD used to build the P-CLD implements an independent interpolation process at each loading condition region (i.e., C-C, C-T, T-C and T-T), as the PWL and PWNL CLDs used in this work, see e.g., Fig. 2. In those cases, non-accurate estimations might be obtained if the $R-$ratio to be analyzed, R', is located between the known ε-N curve at $R\rightarrow\pm\infty$ (e.g., $R=10$) and $R=\pm\infty$, and between the known ε-N curve at $R\rightarrow 0$ (e.g., $R=0.1$) and $R=0$. In this sense, the range of $R-$ratios affected by this limitation can be minimized by using known ε-N curves at $R-$ratios as close as possible to $R=\pm\infty$ and $R=0$.

2.2.2 Probabilistic constant life diagrams

Based on modified PWL and PWNL constant life diagrams, two different probabilistic constant life diagrams, P-CLDs, were developed: probabilistic piecewise linear (P-PWL) and probabilistic piecewise non-linear (P-PWNL). The P-CLDs were developed by propagating the uncertainty in the ε-N curves in the deterministic CLDs by using first-order Taylor series, see e.g. [13]. In this method, a quantity $z=f(x_1,x_2,...,x_{N_x})$ depending on N_x stochastic variables is linearized by approximation to a first-order Taylor series expansion, as follows:

$$z-\mu_z=\sum_{i=1}^{N_x}\frac{\partial f}{\partial x_i}(x_i-\mu_{x_i}) \tag{8}$$

where all higher-order terms are assumed to be negligible and $\mu_z=f(\mu_1,\mu_2,...,\mu_{N_x})$.

The variance of z is estimated by the expectation of the squared deviation $(z-\mu_z)^2$, i.e. $E[(z-\mu_z)^2]=s_z^2$, which can be written as:

$$s_z^2=\sum_{i=1}^{N_x}\Big(\frac{\partial f}{\partial x_i}\Big)^2 s_i^2+2\sum_{i=1}^{N_x-1}\sum_{j=i+1}^{N_x}\frac{\partial}{\partial x_i}\frac{\partial}{\partial x_j}s_i s_j\rho_{ij} \tag{9}$$

where $s_i^2 = E[(x_i - \mu_{x_i})^2]$ is the variance of x_i and ρ_{ij} is the correlation coefficient of x_i and x_j.

For the construction of the P-CLDs, the normalized stress amplitude of an unknown ε-N curve, ε'_{amp}, is assumed as the quantity z in Eqs. (8) and (9). The function f and the parameters x_i depend on the interpolation method used by each deterministic CLD in each of the four regions (i.e. T-T, C-C, T-C, C-T). For example, by using the modified PWL diagram, any normalized stress amplitude ε'_{amp} at a corresponding stress ratio R' can be estimated by interpolating between the known normalized stress amplitudes ε_{ampi} and corresponding known stress ratios R_i, see Eq. 16 in Appendix A. Whereas by using the PWNL diagram, the estimation of any ε'_{amp} also depends on these parameters except on R_i, see Eqs. 17-20 in Appendix A.

$$\varepsilon'_{amp,PWL} = f(\varepsilon_{ampi}, R_i, R') \tag{10}$$

$$\varepsilon'_{amp,PWNL} = f(\varepsilon_{ampi}, R') \tag{11}$$

The R_i and R' ratios are assumed as deterministic values as their uncertainty is typically small compared to the contribution from the other factors. Then, it can be demonstrated that any normalized stress amplitude ε'_{amp} can be estimated as a function only of the known normalized stress amplitude ε_{ampi}, which is considered as the stochastic variable. Based on this, it can be shown that Eq. 9 leads to the following equation which can be used to estimate the model uncertainty $s_{\varepsilon'_{amp}}$ in each region (i.e. at T-T, T-C, C-T, C-C) of the selected CLDs:

$$s^2_{\varepsilon'_{amp}} = \sum_{i=1}^{2} \Big(\frac{\partial f}{\partial \varepsilon_{ampi}}\Big)^2 s^2_{\varepsilon_{ampi}} \tag{12}$$

where $\partial f / \partial \varepsilon_{ampi}$ is the partial derivative of the interpolation function used by each CLD with respect to the known normalized stress amplitude ε_{ampi} and $s_{\varepsilon_{ampi}}$ is the variability in the ε-N curves defined in Eq 6.

The variability in the number of cycles to failure, s_N, for a given normalized stress amplitude ε'_{amp} from an interpolated ε-N curve can be estimated by Eq. 7.

2.3 Uncertainty propagation in cumulative damage models

The P-CLDs discussed in the previous section give an estimation of the variability in the number of cycles to failure s_N. This variability is the propagated physical uncertainty in the fatigue capacity of materials subjected to uni-axial stress state and under constant-amplitude loading. Applying the model based on multiple constant-amplitude tests to variable amplitude loading requires a cumulative damage model (e.g. Palmgren-Miner's rule, [32, 26]) which is also associated with a certain model uncertainty.

Several cumulative damage models have been suggested previously by different authors, see summary in [9]. However, most of them are not well suited for design purposes since they must be fitted to a specific loading condition to gain more accuracy. Even though the level of accuracy of the Palmgren-Miner's rule for predicting the fatigue lifetime of composite materials under variable loading may be objected due that it is based on the assumption of linear damage accumulation, this rule is considered in the present study since it is currently the most widely used damage accumulation model. Eventual inaccuracy in the Palmgren-Miner's rule should not have a significant impact on the outcomes of the present study where the proposed model only considers the reliability level of the rule, as described further.

Based on the Palmgren-Miner's rule, a reliability analysis using the Monte Carlo simulation method was carried out to propagate the model uncertainties of the P-CLDs in the cumulative damage model. Performing a reliability analysis, the probability of failure, P_f, of the composite laminates corresponding to a specified structural requirement is evaluated considering the uncertainties that may influence it. This methodology is suggested for this analysis because it can be applied as a starting point for more detailed analyses of composite structures under variable amplitude loading (e.g. wind turbine blades, etc.), in which the probability of failure corresponding to a specified reference period and its consequences in terms of costs may be of interest.

In a reliability analysis, the failure events are described by a functional relation called limit state function $g(\mathbf{x})$ [7]. In the present study, the following limit state function is implemented, which relates the resistance (or structural requirement) r of the laminate with the load effect q to which the laminate is subjected, as a function of the stochastic variables $\mathbf{x}$:

$$g(\mathbf{x}) = r - q(\mathbf{x}) = r - \sum_i \frac{n_i}{N_i(\mathbf{x})} \tag{13}$$

where n_i is the number of cycles with a normalized stress amplitude ε_{ampi} and stress ratio R_i, and N_i is the number of cycles to failure at ε_{ampi} and R_i.

As shown, the load effect q is assumed equal to the Palmgren-Miner's cumulative fatigue damage $\sum_i n_i/N_i$, which assumes a proportionality of the damage fraction at each stress level in a variable amplitude loading and then adding the damage fractions for all the levels together. The actual number of cycles n_i at each stress level is assumed deterministic and determined as described in section 3.2, whereas the number of cycles to failure N_i at each stress level is assumed stochastic with standard deviation s_{N_i}. For uni-axial stress states the main value of N_i is determined by using Eq. 2 once the corresponding ε-N curve is estimated by implementing any desired deterministic CLD, whereas the standard deviation s_{N_i} is estimated by using Eq. 7 .

In addition, the resistance r is assumed deterministic and equal to the

Palmgren-Miner's limit damage fraction. This limit damage fraction is commonly adopted equal to the unity (i.e. $r = 1$); however, several studies have shown that the limit damage fraction may take other values for composite materials, especially under variable-amplitude loading [45, 21, 5, 4]. According to these studies, the limit damage fraction could be smaller or larger than the value of unity depending on the stress amplitude, the R-ratio and the load sequence; however, it is still not well understood how the limit factors affect the variable loading fatigue life of composites.

Based on this limitation, the resistance r is assumed equal to the experimental limit damage fraction to make possible a comparison between the estimated and the empirical probabilities of failure. The resistance r is calculated then using the following equation:

$$r = \sum_i \frac{n_{i(exp)}}{N_i(\mathbf{x})} \tag{14}$$

where $n_{i(exp)}$ are the experimental number of cycles at the time of failure for each normalized stress amplitude ε_{ampi} and stress ratio R_i, and $N_i(\mathbf{x})$ are the stochastic allowable number of cycles to failure calculated by using the P-CLDs.

Once q and r in Eq. 13 are established, the probability of failure P_f can be estimated by:

$$P_f = \frac{1}{N_x} \sum_{j=1}^{N_X} \mathbb{1}_{g(\mathbf{x}_j)\leq 0} \tag{15}$$

where N_x is the number of random trials and $\mathbb{1}_{g(\mathbf{x}_j)\leq 0}$ is the zero-one indicator function. In order to limit the uncertainty in the failure probability to a coefficient of variation of less than 10%, a number of random trials equal to $100/P'_f$ was taken [40], where P'_f is the expected probability of failure. The expected probability of failure was assumed equal to $P'_f = 5 \times 10^{-4}$, which is similar to what is expected from the IEC 61400-1 standard [15] for applications in wind turbines blades. The random trials were carried out by generating pseudorandom, independent, Normally distributed samples with zero mean and unit variance, which were then transformed to represent the required statistical distributions of the random variables in the reliability model.

3 Experimental data

3.1 Materials

The test data used in this study were taken from the OptiDat database [29]. Tests on two different Glass/Epoxy laminates were analyzed. The first one was an uni-directional (UD) E-glass/epoxy laminate and the second one was a multi-directional (MD) $[[\pm 45/0]_4/\pm 45]$ E-glass/epoxy laminate, both characterized by the Knowledge Centre - Wind turbine Materials and Constructions (WMC). The ε-N curves at $R = -1, 10$ and 0.1 were used in

both cases to build the P-CLDs. In addition, for the UD material, ε-N curves at $R = 0.9$ and 1.1 were used as the ε-N curves at R-ratios that tend to 1 from the left and the right; whereas for the MD material, ε-N curves at $R = 0.5$ and 2.0 were used for this purpose, respectively.

Furthermore, experimental ε-N curves at different $R-$ratios were utilized to validate the prediction capabilities of the developed P-CLDs and the propagated uncertainties in the cumulative damage at the different loading conditions regions (i.e., C-C, C-T, T-C, and T-T). For the UD material, experimental ε-N curves at $R = 2.0, -2.5, -0.4$ and 0.5 were used for this purpose; whereas for the MD material, experimental ε-N curves at $R = -2.5$ and -0.4 were used in this sense. Unfortunately, no experimental ε-N curves at C-C and T-T loading conditions were available to validate the predicted response of the MD material in these regions.

3.2 Loading conditions

Different cycle loading conditions were analyzed in order to validate the output of the P-CLDs and the cumulative damage model. Tests under constant amplitude cycle loading at different R-ratios were used with the P-CLDs, while two different variable amplitude cycle loading sequences were applied in evaluating the cumulative damage model: repeated block tests (RBT) and spectrum tests.

The RBTs presented in OptiDat database [29] were a sequence of two types of alternating constant amplitude cyclic load blocks, each under different R-ratios and load levels, which were repeated until failure. Three R-ratios were evaluated: $R = -1, 10$ and 0.1. Three load levels were also evaluated referred to as level 1b, 2 and 3, which led to a mean lifetime of 5×10^3, 5×10^4 and 10^6 cycles respectively.

The summary of the RBTs analyzed in this study is presented in Table 1. The RBTs were carried out for the MD material. The first column of the table indicates the letter code used in OptiDat database [29] for the different RBTs. For example, the letter code 'RBTC1b2' corresponds to a RBT coded 'C', which has a first block at $R = -1$ and level 1b, and a second block at $R = -1$ and level 2. The second and third columns of the Table 1 indicates the R-ratios of the first and second block respectively. The fourth and fifth columns indicate the load level in terms of the maximum normalized stresses, ε_{max}, which were assumed equal to the mean value of the maximum normalized stresses applied during the experiments. Note that the normalized stress amplitude can be easily compute as $\varepsilon_{amp} = \varepsilon_{max}(1 - R)/2$. The sixth and seventh columns correspond to the block lengths, n_{len}, which are repeated until failure. The total amount of these cycles for each R_i-ratio correspond to the actual number of cycles n_i in Eq. 13.

Besides the RBTs, three types of standardized loading spectrum were analyzed for the UD and MD materials: WISPER (W), WISPERX (WX) and NEW WISPER

Table 1: Summary of analyzed repeated block tests for MD material. Data taken from OptiDat database [29]

Test ID	R_1	R_2	$\varepsilon_{max}^{(R_1)}$ (%)	$\varepsilon_{max}^{(R_1)}$ (%)	$n_{len}^{(R_1)}$ (cycles)	$n_{len}^{(R_2)}$ (cycles)
RBTC1b2	-1	-1	0.846	0.662	50	500
RBTD1b3	-1	-1	0.847	0.485	50	10.000
RBTE1b2	0.1	0.1	1.249	0.991	50	500
RBTF1b3	0.1	0.1	1.237	0.727	50	10.000
RBTG21b	-1	0.1	0.672	1.235	500	50
RBTI1b1b	10	0.1	-0.116	1.230	50	50

(NW), see Fig. 3. WISPER (WInd turbine reference SPEctRum) is a standardized loading spectrum developed by an international working group formed by 14 different institutes and manufactures in 1988 [42]. It is based on flapwise blade bending data on nine horizontal-axis wind turbines with blades made of different materials and with different swept areas and installation sites. The spectrum is defined by 132,711 cycles subjected mainly to T-T loading conditions, see Fig. 3-a. The cycles are grouped in 64 spectrum-load levels with the maximum at spectrum-load level 64 and the zero-load at spectrum-load level 25 (defining the spectrum-load levels as non-dimensional range-sizes obtained from a rainflow counting procedure on the analyzed spectrum). WISPERX is a shortened version of WISPER in which all cycles with magnitude smaller than 17 (expressed in WISPER levels) are discarded, yielding a smaller sequence of 12,831 cycles [42]. NEW WISPER was developed in 2005 by a work group consisting of five representatives from the wind energy industry [27]. It was developed to consider new tendencies of the wind turbine technology based on an extensive database with more than 2600 hours of measurements. The spectrum is composed by 47,733 cycles subjected mainly to T-C and T-T loading conditions, see Fig. 3-b. The cycles are grouped in 54 spectrum-load levels with the maximum at spectrum-load level 37 and the minimum at spectrum-load level -17. All spectra are non-dimensional, which allows scaling them to reach desired loading conditions by multiplying the spectrum-load levels by a suitable factor.

The summary of the spectrum tests analyzed in this study is shown in Table 2. Both UD and MD materials were evaluated under two load levels referred to as level 1 (L1) and level 3 (L3), which lead to a mean lifetime of 10^3 and 10^6 cycles respectively [28] (note that these load levels are different than the spectrum-load levels described previously). Cycles at T-T loading condition with R-ratios higher than 0.5 were not considered for the MD material case since the experimental ε-N curves used for the interpolation process in this loading condition region are at $R = 0.1$ and 0.5. The effect of the suppressed cycles on the fatigue life predictions is assumed negligible since they are few compared with the

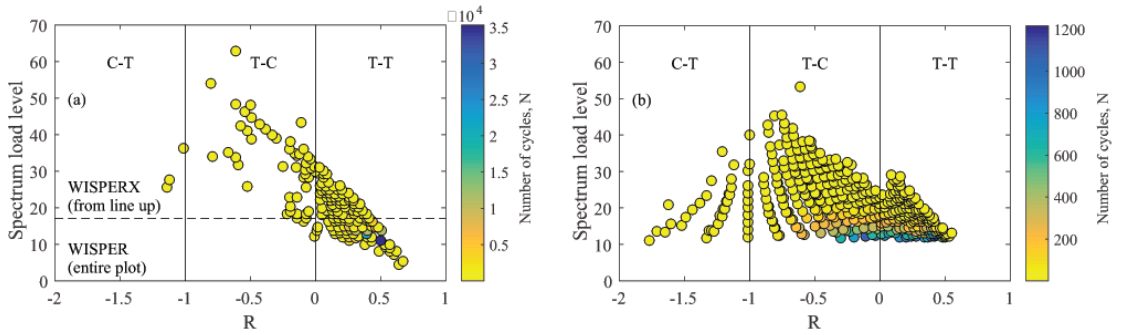

Figure 3: Spectrum load level-R-N matrix of (a) WISPER and WISPERX and (b) NEW WISPER spectra

Table 2: Summary of analyzed spectrum tests for UD and MD materials. Data taken from OptiDat database [29]

Material	Test ID	ε_{max} (%)	n_{len} (cycles)
UD	W-L1	1.195	132,711
UD	W-L3	0.930	132,711
MD	W-L1	1.296	132,544
MD	W-L3	0.982	132,544
MD	WX-L3	0.905	12,831
MD	NW-L1	0.971	47,704
MD	NW-L3	0.867	47,704

total number of applied cycles: 167 cycles for WISPER spectrum and 29 cycles for NEW WISPER spectrum (i.e. 0.12% and 0.06% of the total number of cycles, respectively) and the load levels are small compared with the ones attained at other load ratios, see Fig. 3.

In Table 2, the first column indicates the analyzed material. The second column indicates the letter code of the test, which relates the type of test (i.e. W, WX and NW) with the load level (i.e. L1 and L3). The third column indicates the factors used to scale the spectra, which were assumed equal to the mean value of the maximum stresses applied during the experiment tests. The fourth column corresponds to the spectrum length, n_{len}, which is repeated until failure. The total amount of these cycles for each stress level in the spectrum correspond to the actual number of cycles n_i in Eq. 13.

Table 3: Variability in on-axis ε-N curves at different R-ratios estimated from fatigue coupon tests for UD and MD materials.

	R	m (-)	$\log K$ (-)	s_ϵ (-)	$s_{\log K}$ (-)	$\mathsf{CoV}_{(s_\epsilon)}$ (%)	$\mathsf{CoV}_{(\log K)}$ (%)	$s_{\log \varepsilon_{amp}}$ (-)	Test n
UD	1.1	0.02	-3.15	0.0087	0.0223	27.59	-0.71	0.0093	8
	10.0	0.01	-2.26	0.0206	0.0344	22.82	-1.52	0.0215	11
	-1.0	0.09	-1.64	0.0362	0.0629	24.31	-3.83	0.0380	10
	0.1	0.11	-1.76	0.0131	0.0228	19.08	-1.30	0.0135	15
	0.9	0.07	-2.75	0.0233	0.0657	24.46	-2.39	0.0244	10
MD	2.0	0.03	-2.30	0.0104	0.0301	29.81	-1.31	0.0111	7
	10.0	0.01	-2.24	0.0137	0.0354	25.55	-1.58	0.0145	9
	-1.0	0.08	-1.80	0.0280	0.0289	18.57	-1.61	0.0288	16
	0.1	0.09	-1.96	0.0249	0.0494	22.89	-2.52	0.0260	11
	0.5	0.12	-2.00	0.0134	0.0717	38.06	-3.59	0.0147	5

4 Results

4.1 Uncertainty in the $\varepsilon - N$ curves

The ε-N curve parameter m and $\log K$ and the corresponding coefficient of variation, CoV_m and $\mathrm{CoV}_{\log K}$, for the evaluated materials subjected to uni-axial fatigue loading conditions at different R-ratios are presented in Table 3. According to Eq. 5 and considering the slope m of the ε-N curves deterministic as described in section 2.1, Table 3 also presents the variability in the intercept parameter K, $s_{\log K}$, the variability of the residuals, s_ϵ, and the total variability of the ε-N curves, $s_{\log \varepsilon_{amp}}$. Note that these uncertainties represent the uncertainty in the fatigue material properties (i.e. in the ε-N curves) and that the uncertainties in the static material properties, in the load and in the geometry were not taken into account in this work.

As shown in Table 3, the fitting residuals which represent the physical uncertainty due to material variation seem to have the largest contribution to the total model variance of the ε-N curves, since the variability of the residuals s_ϵ is almost identical to the total variability of the model $s_{\log \varepsilon_{amp}}$, see Eq. 5. For both materials the highest $s_{\log \varepsilon_{amp}}$ variability was reported at T-C loading cases (i.e. $R = -1$).

4.2 Propagated uncertainties in constant life diagrams

Probabilistic constant life diagrams (P-CLDs) were developed by propagating the uncertainty in the mechanical properties of the materials in deterministic CLDs, see e.g. in Fig 4. As shown, the behaviour the fatigue life predictions of the developed P-PWL and P-PWNL diagrams varies with each fatigue loading condition. For T-C loading conditions, the fatigue life predictions of both P-CLDs are the same because they use

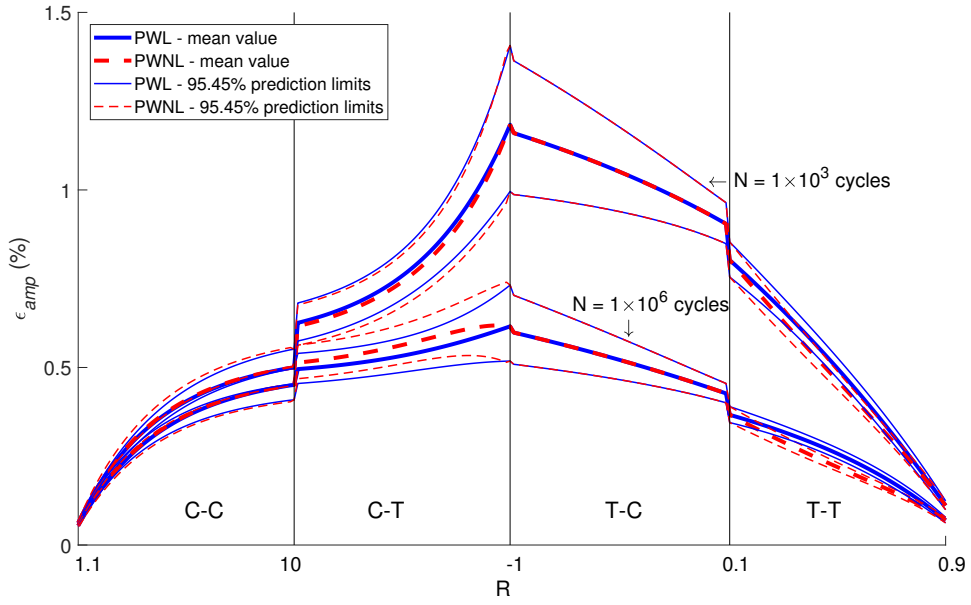

Figure 4: P-PWL and P-PWNL constant life diagrams for UD material. Thick lines represent the mean, thin lines represent ±2 standard deviations from the mean.

the same linear interpolation method in this region, as explained in Appendix A. Whereas for the other loading conditions, both P-CLDs use different interpolation methods leading to different fatigue life predictions. In the following, the validation of predicted fatigue lifetime with respect to experimental data is presented.

4.2.1 Validation with experimental data

A comparison between the variability in the different ε-N curves of the materials estimated by using the developed P-PWL and P-PWNL diagrams, $s'_{\log\varepsilon_{amp}}$, and the variability obtained from the experimental ε-N curves by using the Maximum Likelihood method, $s^{exp}_{\log\varepsilon_{amp}}$, is presented in Table 4 and represented graphically in Fig. 4-6. In Fig. 4-6, the experimental and estimated probabilistic ε-N curves are plotted, as an example, with 95.45% prediction limits (i.e., within two standard deviations of the mean); however, other prediction limits can be used according to the design needs.

As shown in Table 4 and Fig. 4-6, the variability estimated by the P-CLDs is similar to each other and comparable with the variability obtained from the experimental data. In most of the cases, the estimated variability is lower than the experimental one except for the UD material at $R = -2.5$.

In addition, the ability of the developed P-CLDs to predict accurate ε-N curves depends on the material and varies with the loading conditions, see Fig. 5 and 6. For the UD material, predicted ε-N curves are accurate at T-C and C-C loading conditions

Table 4: Comparison between the variability in the ε-N curves estimated by using the P-CLDs, $s'_{\log\varepsilon_{amp}}$,

and the variability fitted from experimental data, $s^{exp}_{\log\varepsilon_{amp}}$, for UD and MD materials.

			$s^{exp}_{\log\varepsilon_{amp}}$	$s'_{\log\varepsilon_{amp}}$	
	R	Test n		P-PWL	P-PWNL
UD	2.0[1]	11	0.0273	0.0126	0.0212
	-2.5[2]	8	0.0185	0.0215	0.0230
	-0.4[3]	7	0.0320	0.0216	0.0216
	0.5[4]	9	0.0202	0.0129	0.0122
MD	-2.5[5]	4	0.0385	0.0274	0.0254
	-0.4[6]	14	0.0376	0.0297	0.0297

for both low-cycle (LCF) and high-cycle (HCF) fatigue, see Fig. 5-a and 5-b. For C-T loading conditions, the P-PWL diagram predicts accurate values for all normalized stress levels, whereas the P-PNWL diagram predicts accurate values only at LCF fatigue, see Fig. 5-d. For T-T loading conditions, the accuracy level of the P-PNWL diagram is good and higher than the accuracy level of the P-PWL diagram, see Fig. 5-c.

For the MD material, the levels of accuracy of the P-CLDs decreases compared to the UD material, see Fig.6. For evaluated loading conditions (i.e. T-C and C-T), predictions are more accurate at LCF regimens, being the ones obtained from the P-PWNL diagram the most accurate in general.

4.3 Propagated uncertainties in cumulative damage models

4.3.1 Validation with experimental data for repeated block loading

The reliability level of predicted fatigue lifetime of MD coupons under different repeated block loading tests (RBTs) described in section 3.2 is presented in Fig. 7. In most cases the estimated variability is in good agreement with the variability in the experimental data, except for the estimations of the RBTI1b1b tests which showed high variability.

Furthermore, different Palmgren-Miners limit damage fractions r were found in the repeat block tests, see Fig. 7. The RBTF1b3 test presented the smallest limit damage fraction (i.e. $r = 0.40$) and the RBTI1b1b test presented the highest one (i.e. $r = 3.93$), whereas the RBTE1b2 test had a limit damage fraction $r = 1.16$ which was the closest to the unity value.

4.3.2 Validation with experimental data for spectrum loading

The reliability level of estimated fatigue lifetime of the UD and MD materials under different spectrum loading conditions described in section 3.2 is presented in Fig. 8. The estimated variability was lower than the experimental variability for most of the

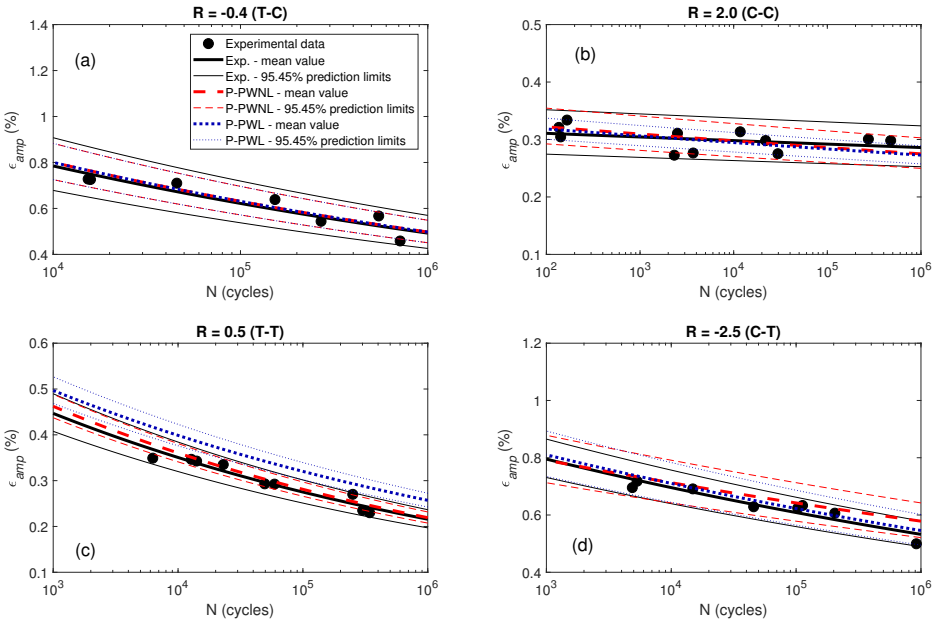

Figure 5: Propagated uncertainties in predicted ε-N curves and experimental data for UD material. Thick lines represent the mean, thin lines represent ± 2 standard deviations from the mean. Same legend for all figures.

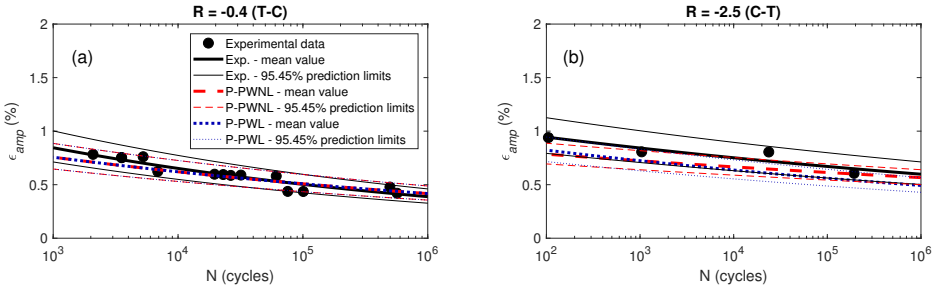

Figure 6: Propagated uncertainties in predicted ε-N curves and experimental data for MD material. Thick lines represent the mean, thin lines represent ± 2 standard deviations from the mean. Same legend for both figures.

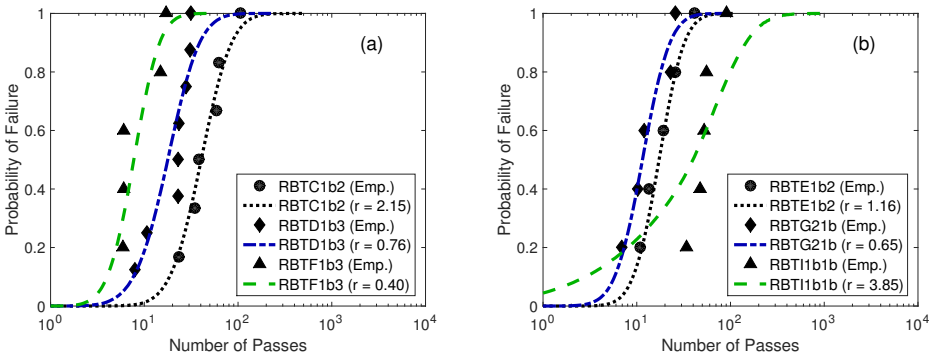

Figure 7: Comparison of estimated variability in Palmgren-Miner's rule and experimental data for repeated block tests for MD material.

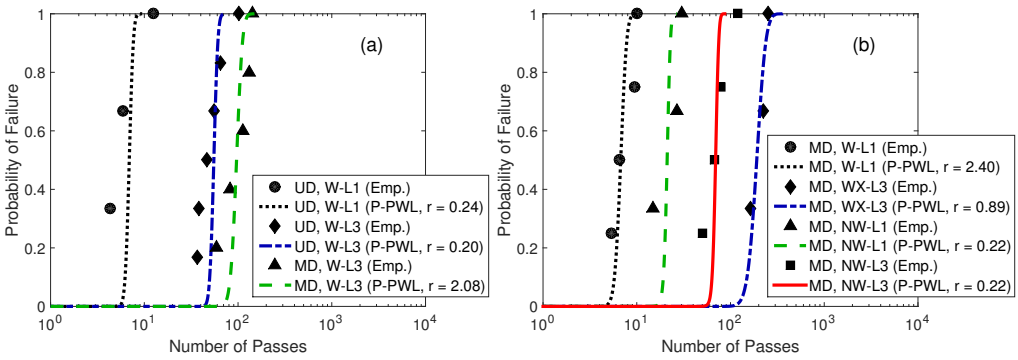

Figure 8: Comparison of estimated variability in Palmgren-Miner's rule and experimental data for spectrum tests for UD and MD materials.

evaluated cases. However, for W-L1, W-L3, WX-L3 and NW-L1 cases (see test ID in Table 2) of the MD material the estimated variability and the experimental variability were in very good agreement.

In addition, the predicted reliability levels were not considerably affected by the different P-CLDs. For WISPER and WISPERX spectra the P-PWNL diagram presented a slightly more variability than the P-PWL diagram, whereas for NEW WISPER spectrum the variability of both P-CLDs was very similar to each other, see e.g. in Fig. 9.

Table 5: Estimated Palmgren-Miner's limit damage fraction in spectrum tests for UD and MD materials for developed P-CLDs.

		$r(-)$	
Material	Test ID	P-PWNL	P-PWL
UD	W-L1	0.24	0.08
UD	W-L3	0.20	0.06
MD	W-L1	2.40	1.77
MD	W-L3	2.08	1.81
MD	WX-L3	0.89	0.77
MD	NW-L1	0.22	0.20
MD	NW-L3	0.22	0.21

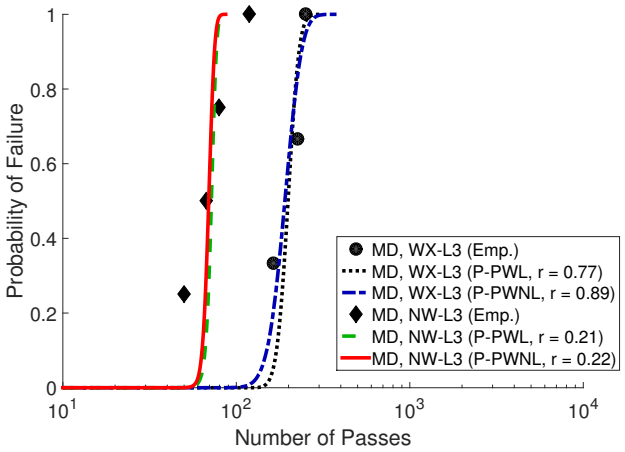

Figure 9: Comparison of variability in Palmgren-Miner's rule estimated by using different P-CLDs and experimental data for spectrum tests.

On the other hand, different Palmgren-Miner's limit damage fractions r were also found in the spectrum tests, see Table 5. The limit damage fractions depended not only on the type of test but also on the P-CLDs. For all spectra the r fractions related to the P-PWNL diagram were much higher than that for the P-PWL diagram. Moreover, a big difference between the calculated r-fractions for the UD and MD materials was found, in which for W-L1 load level the r-fractions of the UD material were between 10 and 20 times smaller than that of the MD material as shown in Table 5.

It is worth mentioning that the estimated probabilities of failure obtained in all the evaluated cases shown in Fig. 7-9 vary from 5×10^{-4} to 1, which are consistent with the assumption made in section 2.3 regarding the expected probability of failure, P'_f, used to calculate the number of random trials N_x.

5 Discussion

5.1 Evaluation of the probabilistic constant life diagrams

The results presented in section 4.2 show that reliable fatigue life predictions of composite materials subject to constant amplitude and uni-axial loading can be obtained by using the proposed P-CLDs, which were developed by propagating the uncertainty in ε-N curves in common constant life diagrams.

By using the developed P-CLDs, probabilistic fatigue lifetime estimations can be efficiently calculated by doing an interpolation process between known ε-N curves, see section 2.2. This means that the allowable number of cycles and their variability under different load levels and R-ratios can be estimated instantaneously without using any iterative process.

Comparisons of the estimated probabilistic ε-N curves and the experimental data in Table 4 and Fig. 5 and 6 show a good agreement with each other. In most of the cases, the predicted variability was lower than that predicted from the experiments, which could be due to the fact that only the uncertainty in the mechanical properties of the materials was taken into account. Deeper studies considering other uncertainty sources during the manufacturing and testing process as those described in [28] (e.g. geometry, fibre alignment, loading conditions, etc.) may lead to even more reliable fatigue life predictions.

Moreover, the performance of the P-CLDs depends not only on the reliability level of the predictions but also on their level of accuracy, understanding as level of accuracy the closeness of the mean of the estimations to the mean of the experimental data. For T-T and C-C loading conditions, for example, high level of accuracy was obtained by replacing the static strengths for ε-N curves at R-ratios close to 1 (as described in section 3.1), especially when the P-PWNL diagram was used, see Fig. 5-b and 5-c.

For T-C and C-T loading conditions, proposed P-CLDs also predict allowable number of cycles with high level of accuracy for UD materials (see Fig. 5); however, the level of accuracy seems to decrease for MD materials (see Fig. 6), especially at low-cycle (LCF) fatigue and C-T loading conditions. This could be due to the fact that different damage mechanisms are involved in both materials under fatigue loading conditions. For UD materials, for example, fiber-bridged matrix cracking and interfacial debonding between the fibers and the matrix seem to be the damage mechanisms that lead to the final failure [11]; whereas for MD materials, transverse cracks and delaminations are the driving damage mechanisms [38]. This makes the fatigue behavior of both materials different and, therefore, creates the needed of designing further improved P-CLDs for MD materials.

According to obtained results, a new P-CLD diagram that combines the prediction capabilities of the P-PWL and P-PWNL diagrams at the different loading conditions in

only one P-CLD could improve even more the accuracy level and the reliability level of the predictions. For UD materials, for example, a good combination would be: a P-PWNL diagram at T-T and C-C loading conditions; a P-PWL diagram at C-T loading conditions; and either P-PWL or P-PWNL diagrams at T-C loading conditions since they are both the same in this region. For MD material, the P-PWNL diagram seems to provide better predictions at T-C and C-T loading conditions. Unfortunately, experimental data to evaluate and validate the predictions capabilities of the P-CLDs was available only for T-C and C-T loading conditions and, therefore no conclusions in this regards could be obtained at T-T and C-C loading conditions.

In addition, note that Fig. 4-6 were plotted with 95.45% prediction limits, which correspond to data values within two standard deviations of the mean (i.e.,$\mu \pm 2s$). This was plotted in this way only as an example; however, the designer can used the developed P-CLDs to evaluate the response of the material under any percentage of survival probability depending on the desired application.

5.2 Evaluation of predicted probabilistic fatigue lifetime for variable amplitude loading

Comparisons between the estimated probability of failure and the empirical cumulative distribution functions presented in the section 4.3, show that reliable fatigue life predictions of composite materials under variable amplitude loading conditions can be obtained when the variability in ε-N curves is propagated in the Palmgren-Miner's rule through the Monte Carlo simulation.

The probability of failure estimated by implementing the proposed methodology seems to be affected by the variability in the input ε-N curves (i.e. the experimental ε-N curves). The higher accuracy of the variability in the input ε-N curves, the higher reliability level of the fatigue life estimations. This can be observed by doing a comparison between the results obtained from the repeated block tests and the ones obtained from the spectrum tests. For the repeated block tests, the estimated probability of failure was accurate in most of the cases (see Fig. 7) because the estimations were carried out based on the variability in the experimental ε-N curves at $R = 0.1$, -1 and 10 (i.e. based on the real variability), see Table 1. Whereas for the spectrum tests, the estimated probability of failure was lower than the experimental one in most of the cases (see Fig. 8) because the probabilistic ε-N curves at the R-ratios that conform the evaluated spectra (see Fig. 3) were predicted by using the P-CLDs. And, as described in section 5.1, the variability predicted by the P-CLDs can be lower than the real one (see Fig. 5 and 6) because the P-CLDs only consider the uncertainty in the ε-N curves.

The estimated probability of failure is also affected by the slope m of the ε-N curves as

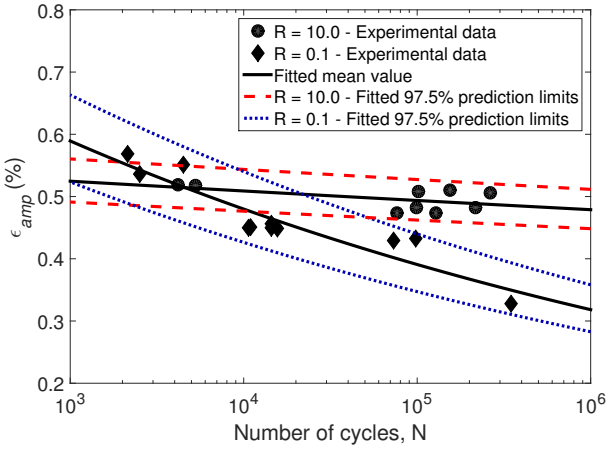

Figure 10: Experimental ε-N curves of MD material at $R = 10$ and $R = 0.1$

also discussed in [22]. The lower the ε-N curve slope, the greater effect on the estimated reliability level. This can be observed, for example, with the high variability predicted in the RBTI1b1 test case, see Fig. 7-b. The RBTI1b1 tests were carried out with alternating R-ratios at $R = 10$ and $R = 0.1$ (see Table 1), being the slope of the known ε-N curve at $R = 10$ much lower than that at $R = 0.1$, see Fig. 10. Even though the variability in the known ε-N curve at $R = 10$ is lower than the variability in the known ε-N curve at $R = 0.1$ (see Table 3), its effect on the predicted fatigue lifetime is much higher because for any given loading level the failure could occur in a very wide range of cycles.

This effect of the slope of the $\varepsilon-$N curves on the predicted fatigue life is more critical at $R-$ratios in the C-C loading region where the slopes are very low (see e.g. in Fig. 4). This explains why reliable predictions were obtained in general for the evaluated spectrum tests (see. Fig. 8), since not $R-$ratios at C-C loading conditions are presented in these spectra, see Fig. 3. Further improvements of the prediction capabilities of the proposed reliability model at the C-C loading conditions are, therefore, needed in order to obtain more realistic predictions at this fatigue loading region.

Furthermore, the effect of the selected P-CLD on the predicted reliability level is in general small as shown in Fig. 9. The small differences between the predictions obtained from the P-PWL and P-PWNL diagrams seem to depend on the loading conditions (i.e. R-ratios) that the laminate is subjected to during the loading. For WISPER and WISPERX spectrum loading, for example, the variability estimated by both P-CLDs is a bit different because the laminate is subjected mainly to T-T loading conditions, in which predictions obtained from the P-PWNL diagram are different than those obtained from the P-PWL diagram, see e.g. in Fig. 4. Whereas for the NEW WISPER spectrum, the variability estimated by both P-CLDs is similar to each other because many of the R-ratios in the spectrum are in T-C (see e.g. Fig. 3-b) and the P-CLDs predict the same

fatigue behavior under this loading condition, see e.g. in Fig. 4.

Moreover, the efficiency of predicting fatigue lifetime using the developed P-CLDs is very useful for this type of analysis in which several load levels and R-ratios are involved during the loading, see e.g. Fig. 3. By using the developed P-CLDs, probabilistic ε-N curves for all load conditions in the spectrum can be instantaneously estimated as described in section 5.1. This may be also useful for structural reliability analysis and reliability-based structural design of composite structures under complex loading conditions (e.g. wind turbine blades) in which complex geometries, layups and different types of materials are also involved.

5.2.1 Comments about the accuracy of Palmgren-Miner's rule for composite materials

The level of accuracy of the Palmgren-Miner's rule for predicting the fatigue lifetime of composite materials is still questionable in the composite field since it does not consider possible non-linearities during the progressive damage of the material when it is subject to different fatigue loading conditions. Even though the understanding of the level of accuracy of the Palmgren-Miner's rule in composite materials is not the aim of this paper, few comments in this regard can be made based on obtained results.

The results presented in Fig. 7-8 and Table 5 show that the Palmgren-Miner's fatigue limit r can take either higher or lower values than the one at failure, which agrees with several studies about the effect of the load sequence on variable loading fatigue life of composites [2, 49, 12, 16, 31, 1].

Kawai et al showed in [21], for example, that the Palmgren-Miner's rule predicts satisfactorily the fatigue failure of woven fabric carbon/epoxy laminates under alternating R-ratios, R_1 and R_2, with an accuracy of a factor of two, i.e. $0.5 < r < 2$. However, this range seems not be applicable to unidirectional and multi-directional E-glass/Epoxy laminates according to the results found in present work, in which values of r out of this range were obtained for the RBTC1b2 and RBTI1b1b block tests, see Fig. 7. Moreover, a similar behavior was also obtained for the spectrum tests as shown in Table 9.

Even though most of the r-limits estimated in this work by using Eq. 14 were in good agreement with the predicted Miner's sum presented in [30], it is not possible to establish a clear statement of the level of accuracy of the Palmgren-Miner's rule for composite materials based on analyzed experimental data. Further studies that consider the damage evolution of composite materials with different layup configurations and under different loading conditions are still needed in order to get a better understanding of the accuracy of the Palmgren-Miner's rule for these materials.

6 Conclusions

The fatigue behaviour of composite materials could be highly affected by the variability in the material properties and in other factors, such as loading, geometry and environmental conditions. In this paper, we analyzed the benefits of considering the variability in the ε-N curves during the fatigue lifetime estimation of composite laminates. Uni-directional and multi-directional Glass/Epoxy laminates under different stress ratios, load levels and cycle loading conditions were analyzed.

We developed probabilistic fatigue lifetime diagrams, P-CLDs, by propagating the variability of the ε-N curves in existing linear and non-linear constant lifetime diagrams. By using the developed P-CLDs, probabilistic ε-N curves at any load level and R-ratio could be efficiently estimated without using any iterative process. It was shown that the variability in the ε-N curves estimated by the P-CLDs is comparable with that estimated from the experimental data. Moreover, compared with common CLDs, better predictions at T-T and C-C loading conditions were obtained with the developed P-CLDs because they use experimental ε-N curves at R-ratios that tend to 1 from the left and the right to carry out the interpolation process instead of the static strengths. In addition, it was found that the probabilistic piecewise non-linear diagram provides more accurate estimations than the probabilistic piecewise linear diagram.

We also carried out a reliability analysis for fatigue limit state in order to estimate the probability of failure of composite laminates under variable amplitude loading cycles, considering the variability in their mechanical properties. By applying the Monte Carlo simulation method, the reliability of the laminate is determined using a limit state equation based on the Palmgren-Miner's rule. The limit equation contains as stochastic variables the number of cycles to failure related to the different load level and R-ratio in the loading, which are estimated by using the developed P-CLDs. The reliability analysis was evaluated for repeated block tests and spectrum fatigue data using WISPER, WISPERX and NEW WISPER standardized load spectra for wind turbine blades. By doing a comparison with experimental data, this study showed that reliable fatigue lifetime predictions of composite materials under variable amplitude loading cycles can be efficiently obtained by using the proposed reliability analysis.

Further research should be done in order to consider the uncertainty in other factors that may affect the fatigue behavior of the composite materials such as the geometry and the loading conditions. Moreover, probabilistic fatigue analysis of composite under multi-axial stress state may be also of interest within the framework of an industrial application, such as wind turbine blades. Finally, further studies regarding the application of the Palmgren-Miner's rule in composite materials are also needed to improve the accuracy of theoretical calculations.

Acknowledgements

This work was supported by the Danish Centre for Composite Structures and Materials for Wind Turbines (DCCSM), grant no. 09-067212 from the Danish Strategic Research Council.

Notes

[1] see Fig. 5-b.
[2] see Fig. 5-d.
[3] see Fig. 5-a.
[4] see Fig. 5-c.
[5] see Fig. 6-b.
[6] see Fig. 6-a.

References

[1] H. Atsushi, K. Hiroyuki, and Y. Hiromichi. Fatigue characteristics of quasi-isotropic cfrp laminates subjected to variable amplitude cyclic two-stage loading. *International Journal of Fatigue*, 28(10):1284–1289, 2006.

[2] L.J. Broutman and S. Sahu. A new theory to predict cumulative fatigue damage in fiberglass reinforced plastics. volume 1972, pages 170–188. ASTM International, 100 Barr Harbor Drive, PO Box C700, West Conshohocken, PA 19428-2959, 1972.

[3] C.C. Chamis. Probabilistic simulation of multi-scale composite behavior. *Theoretical and Applied Fracture Mechanics*, 41(1-3):51–61, 2004.

[4] N.K. Dimitrov. *Structural Reliability of Wind Turbine Blades*. PhD thesis, 2013.

[5] N.K. Dimitrov and A.D. Kiureghian. *Probabilistic modelling of fatigue life of composite laminates using Bayesian inference*, pages 2586–2597. American Society of Civil Engineers, 2014.

[6] N.K. Dimitrov, A.D. Kiureghian, and C. Berggreen. Bayesian inference model for fatigue life of laminated composites. *Journal of Composite Materials*, 50(2):131–143, 2016.

[7] O.D. Ditlevsen and H.O. Madsen. *Structural Reliability Methods*. Tongji University Press, 2005.

[8] A. Endruweit and A.C. Long. Influence of stochastic variations in the fibre spacing on the permeability of bi-directional textile fabrics. *Composites Part A: Applied Science and Manufacturing*, 37(5):679 – 694, 2006.

[9] A. Fatemi and L. Yang. Cumulative fatigue damage and life prediction theories: a survey of the state of the art for homogeneous materials. *International Journal of Fatigue*, 20(1):9 – 34, 1998.

[10] G. Fernlund, N. Rahman, R. Courdji, M. Bresslauer, A. Poursartip, K. Willden, and K. Nelson. Experimental and numerical study of the effect of cure cycle, tool surface, geometry, and lay-up on the dimensional fidelity of autoclave-processed composite parts. *Composites Part A: Applied Science and Manufacturing*, 33(3):341 – 351, 2002.

[11] E.K. Gamstedt and R. Talreja. Fatigue damage mechanisms in unidirectional carbon-fibre-reinforced plastics. *Journal of Materials Science*, 34(11):2535–2546, 1999.

[12] N. Gathercole, H. Reiter, T. Adam, and B. Harris. Life prediction for fatigue of t800/5245 carbon-fibre composites: I. constant-amplitude loading. *International Journal of Fatigue*, 16(8):523 – 532, 1994.

[13] GUM. Evaluation of measurement data - guide to the expression of uncertainty in measurement, 2008.

[14] J. Huther and P. Brøndsted. Influence of the curing cycles on the fatigue performance of unidirectional glass fiber reinforced epoxy composites. *I O P Conference Series: Materials Science and Engineering*, 139, 2016.

[15] Wind turbines part 1 design requirements. Standard, IEC, 2005-2008.

[16] M.-H.R. Jen, Y.S. Kau, and I.C. Wu. Fatigue damage in a centrally notched composite laminate due to two-step spectrum loading. *International Journal of Fatigue*, 16(3):193 – 201, 1994.

[17] H.K. Jeong and R.A. Shenoi. Probabilistic strength analysis of rectangular {FRP} plates using monte carlo simulation. *Computers & Structures*, 76(1âĂŞ3):219 – 235, 2000.

[18] K.W. Kang, D.M. Lim, and J.K. Kim. Probabilistic analysis for the fatigue life of carbon/epoxy laminates. *Composite Structures*, 85(3):258 – 264, 2008.

[19] M. Kawai and M. Koizumi. Nonlinear constant fatigue life diagrams for carbon/epoxy laminates at room temperature. *Composites Part A: Applied Science and Manufacturing*, 38(11):2342 – 2353, 2007. CompTest 2006.

[20] M. Kawai and T. Teranuma. A multiaxial fatigue failure criterion based on the principal constant life diagrams for unidirectional carbon/epoxy laminates. *Composites Part A: Applied Science and Manufacturing*, 43(8):1252 – 1266, 2012.

[21] M. Kawai, K. Yang, and S. Oh. Effect of alternating r-ratios loading on fatigue life of woven fabric carbon/epoxy laminates. *Journal of Composite Materials*, 49(27):3387–3405, 2015.

[22] M. Kawai and K. Yano. Probabilistic anisomorphic constant fatigue life diagram approach for prediction of p-s-n curves for woven carbon/epoxy laminates at any stress ratio. *Composites Part A: Applied Science and Manufacturing*, 80:244–258, 2016.

[23] J.S. Lightfoot, M.R. Wisnom, and K. Potter. Defects in woven preforms: Formation mechanisms and the effects of laminate design and layup protocol. *Composites Part A: Applied Science and Manufacturing*, 51:99 – 107, 2013.

[24] D.V. Lindley. *Introduction to probability and statistics from a Bayesian viewpoint:*. Cambridge University Press, Cambridge, 001 1965.

[25] Y. Liu and S. Mahadevan. Probabilistic fatigue life prediction of multidirectional composite laminates. *Composite Structures*, 69(1):11 – 19, 2005.

[26] M.A. Miner. Cumulative damage in fatigue. *Journal of Applied Mechanics-transactions of the Asme*, 12(3):A159–A164, 1945.

[27] R. Nijssen. (new) wisper(x) test results and analysis. Technical Report 10313, 2005.

[28] R. Nijssen. *Fatigue life prediction and strength degradation of wind turbine rotor blade composites*. Thesis, 2006.

[29] R. Nijssen. Optidat reference document. Technical report, WMC knolwedge centre, 2006.

[30] R. Nijssen, O. Krause, and C. Kensche. Block tests: Results and analysis of simple load spectrum tests. Technical report, WMC knolwedge centre, 2005.

[31] N. Otani and D.Y. Song. Fatigue life prediction of composites under two-stage loading. *Journal of Materials Science*, 32(3):755–760, 1997.

[32] A. Palmgren. Die lebensdauer von kugellagern. *Zeitschrift der Vereines Deutches Ingenieure*, 68(14):339 – 341, 1924.

[33] T.P. Philippidis and A.P. Vassilopoulos. Complex stress state effect on fatigue life of grp laminates.: part i, experimental. *International Journal of Fatigue*, 24(8):813 – 823, 2002.

[34] T.P. Philippidis and A.P. Vassilopoulos. Life prediction methodology for {GFRP} laminates under spectrum loading. *Composites Part A: Applied Science and Manufacturing*, 35(6):657 – 666, 2004.

[35] K. Potter, B. Khan, M. Wisnom, T. Bell, and J. Stevens. Variability, fibre waviness and misalignment in the determination of the properties of composite materials and structures. *Composites Part A: Applied Science and Manufacturing*, 39(9):1343 – 1354, 2008.

[36] K. Potter, C. Langer, B. Hodgkiss, and S. Lamb. Sources of variability in uncured aerospace grade unidirectional carbon fibre epoxy preimpregnate. *Composites Part A: Applied Science and Manufacturing*, 38(3):905 – 916, 2007.

[37] K.D. Potter, M. Campbell, C. Langer, and M.R. Wisnom. The generation of geometrical deformations due to tool/part interaction in the manufacture of composite components. *Composites Part A: Applied Science and Manufacturing*, 36(2):301 – 308, 2005. 7th International Conference on the Deformation and Fracture of Composites (DFC-7).

[38] K.L. Reifsnider, E.G Henneke, W.W. Stinchcomb, and J.C. Duke. Damage mechanics and nde of composite laminates. In Z. Hashin and C.T. Herakovich, editors, *Mechanics of Composite Materials: Recent Advances*, pages 399–420. Peraamon Press. New York, 1983.

[39] M.C. Shiao and C.C. Chamis. Probabilistic evaluation of fuselage-type composite structures. *Probabilistic Engineering Mechanics*, 14(1âĂŞ2):179 – 187, 1999.

[40] M.L. Shooman. *Probabilistic Reliability: an Engineering Approach*. McGraw-Hill Book Company, 1968.

[41] S. Sriramula and M.K. Chryssanthopoulos. Quantification of uncertainty modelling in stochastic analysis of {FRP} composites. *Composites Part A: Applied Science and Manufacturing*, 40(11):1673 – 1684, 2009.

[42] A.A. ten Have. Wisper and wisperx final definition of two standardised fatigue loading sequences for wind turbine blades. Technical report, National Aerospace Laboratory NRL, 1988.

[43] H.S. Toft, K. Branner, P. Berring, and J.D. Sørensen. Defect distribution and reliability assessment of wind turbine blades. *Engineering Structures*, 33(1):171 – 180, 2011.

[44] H.S. Toft, K. Branner, L. Jr Mishnaevsky, and J.D. Sørensen. Uncertainty modelling and code calibration for composite materials. *Journal of Composite Materials*, 47(14):1729–1747, 2013.

[45] H.S. Toft and J.D. Sørensen. Reliability-based design of wind turbine blades. *Structural Safety*, 33(6):333 – 342, 2011.

[46] A.P. Vassilopoulos, B.D. Manshadi, and T. Keller. Influence of the constant life diagram formulation on the fatigue life prediction of composite materials. *International Journal of Fatigue*, 32(4):659 – 669, 2010.

[47] A.P. Vassilopoulos, B.D. Manshadi, and T. Keller. Piecewise non-linear constant life diagram formulation for frp composite materials. *International Journal of Fatigue*, 32(10):1731 – 1738, 2010.

[48] Y. Xiang and Y. Liu. Inverse first-order reliability method for probabilistic fatigue life prediction of composite laminates under multiaxial loading. *Journal of Aerospace Engineering*, 24(2):189 – 198, 2011.

[49] J.N. Yang and D.L. Jones. Effect of load sequence on the statistical fatigue of composites. *AIAA Journal*, 18(12):1525–1531, 1980.

A Appendix

A simplified version of the Piecewise Linear CLD developed by Philippidis and Vassilopoulos [33, 34] and a modified version of the Piecewise Non-Linear CLD developed by Vassilopoulos etal [47] are presented in this section. The proposed versions do not consider the static strengths during the interpolation process at T-T and C-C loading conditions. Instead, experimental ε-N curves at R-ratios that tend to 1 from the left and the right, $R_{\rightarrow 1-}$ and $R_{\rightarrow 1+}$, are used as input data as described in section 2.2.

A.1 Modified Piecewise Linear CLD

Any ε-N curves at any R-ratio, R', located between any two known ε-N curves at R-ratios, R_i and R_{i+1}, can be estimated by using the following simplified version of the Piecewise Linear CLD:

$$\varepsilon'_{amp} = \frac{\varepsilon_{amp,i}(r_i - r_{i+1})}{(r_i - r')\frac{\varepsilon_{amp,i}}{\varepsilon_{amp,i+1}} + (r' - r_{i+1})} \tag{16}$$

where ε'_{amp} is the normalized stress amplitude corresponding to R', $\varepsilon'_{amp,i}$ and $\varepsilon'_{amp,i+1}$ are the normalized stress amplitudes corresponding to R_i and R_{i+1} respectively, and $r' = (1+R')/(1-R')$, $r_i = (1+R_i)/(1-R_i)$ and $r_{i+1} = (1+R_{i+1})/(1-R_{i+1})$.

A.2 Modified Non-Piecewise Linear CLD

In the following modified version of the Piecewise Non-Linear CLD, the expressions used to estimate ε-N curves at R-ratios at C-T and T-C loading conditions (i.e. $-\infty \leq R' \leq -1$ and $-1 \leq R' \leq 0$ respectively) remain as the ones suggested by Vassilopoulos etal in [47].

However, new expressions are proposed to estimate ε-N curves at R-ratios at C-C and T-T loading conditions.

A.2.1 C-C loading conditions:

$R_{\to 1+} \leq R' \leq R_{\to \pm\infty}$

$$\varepsilon'_{amp} = \frac{(1-R')}{R'^2}\Big(\varepsilon_{amp}^{R_{\to\pm\infty}}(R_{\to 1+} - R') + \varepsilon_{amp}^{R_{\to 1+}}\Big(\frac{R^2_{\to 1+}}{1+R_{\to 1+}}\Big)\Big) \tag{17}$$

where $\varepsilon_{amp}^{R_{\to\pm\infty}}$ and $\varepsilon_{amp}^{R_{\to 1+}}$ are the normalized stress amplitudes corresponding to the ε-N curves at $R_{\to\pm\infty}$ and $R_{\to 1+}$ respectively.

A.2.2 C-T loading conditions:

$R_{\to\pm\infty} \leq R' \leq -1$

$$\varepsilon'_{amp} = \frac{(1-R')}{R'^2}\Big(\frac{\varepsilon_{amp}^{R_{-1}}}{2}\Big(\frac{1-R'}{1+R_{\to\pm\infty}}\Big) - \varepsilon_{amp}^{R_{\to\pm\infty}} R^2_{\to\pm\infty}\Big(\frac{1+R'}{1-R^2_{\to\pm\infty}}\Big)\Big) \tag{18}$$

where $\varepsilon_{amp}^{R_{-1}}$ is the normalized stress amplitude corresponding to the ε-N curve at $R=-1$.

A.2.3 T-C loading conditions:

$-1 \leq R' \leq R_{\to 0}$

$$\varepsilon'_{amp} = \frac{\varepsilon_{amp}^{R_{\to 0}}(1-R')}{-2R'\Big(\frac{\varepsilon_{amp}^{R_{\to 0}}}{\varepsilon_{amp}^{R_{-1}}}\Big) + (1+R')} \tag{19}$$

where $\varepsilon_{amp}^{R_{\to 0}}$ is the normalized stress amplitude corresponding to the ε-N curve at $R_{\to 0}$.

It worth mentioning that Eq. 19 is equivalent to the equation used by the Piecewise Linear CLD at the T-C region. This can be easily demonstrated by substituting $\varepsilon_{amp,i}$, $\varepsilon_{amp,i+1}$, R_i, R_{i+1} in Eq. 16 for $\varepsilon_{amp}^{R_{\to 0}}$, $\varepsilon_{amp}^{R_{-1}}$, $R_{\to 0}$ and R_{-1}, respectively.

A.2.4 T-T loading conditions:

$R_{\to 0} \leq R' \leq R_{\to 1-}$

$$\varepsilon'_{amp} = \frac{\varepsilon_{amp}^{R_{\to 1-}}(1-R')R^3_{\to 1-}}{R'^3(1-R_{\to 1-}) + (R^3_{\to 1-} - R'^3)\frac{\varepsilon_{amp}^{R_{\to 1-}}}{\varepsilon_{amp}^{R_{\to 0}}}} \tag{20}$$

where $\varepsilon_{amp}^{R_{\to 1-}}$ is the normalized stress amplitude corresponding to the ε-N curves at $R_{\to 1-}$.

CHAPTER 7

Paper 2

In manuscript:
Oscar Castro and Kim Branner. *Damage mechanics-based multiscale model for wind turbine blades under fatigue: Part 1. Effect of off-axis cracks on the blade stiffness degradation.*

Damage mechanics-based multiscale model for wind turbine blades under fatigue: Part 1. Effect of off-axis cracks on the blade stiffness degradation

Oscar Castro[+] and Kim Branner[+]

[+]DTU Wind Energy, Technical University of Denmark, Frederiksborgvej 399, 4000 Roskilde, Denmark. E-mail: osar@dtu.dk, kibr@dtu.dk

Abstract

A damage mechanics-based multiscale approach for wind turbine blades under fatigue loading conditions is proposed in this study. In this approach, damage mechanics fatigue models are used to predict the initiation and propagation of the damage at the micro/macro-length scales. Then the effect of this damage is efficiently propagated at the subcomponent and full-length scales of the blade by a using a 2D finite-element-based cross-section analysis. The proposed multiscale approach is used in this first paper to analyze the effects of off-axis cracks on the stiffness degradation of these structures, as a first step in the development of a model that allows predicting the entire fatigue response of wind turbine blades. The effects of the off-axis cracks are analyzed at the macro, subcomponent, and full-length scales of the blade. The ability of the proposed multiscale approach for making reliable predictions is demonstrated at the different length scales by doing comparisons against experimental and analytical data related to different types of laminates and a full commercial wind turbine blade.

Keywords: wind turbine blades, fatigue, multiscale approach, damage mechanics, stiffness degradation, off-axis cracks

1 Introduction

Wind turbines are still growing in size and it is expected to see turbines with blades above 100 m soon. The high investments related to the installation and operation of these enormous turbines demand more accurate and reliable lifetime prediction methods that ensure an operational life of minimum 20-30 years, while at the same time continuing to decrease the cost of energy.

During this operational lifetime, the wind turbine blades, which are the largest rotating component of the wind turbines, are subjected to complex loading conditions as a result of the combination of gravity, inertia, and aeroelastic forces. As the blades rotate during operation, the combination of these forces changes with the time, which leads to cyclic loading conditions that induce fatigue in the blades. This is why the design against fatigue is one of the most important requirements during the design of these structural members. However, the current fatigue design requirements suggested by the IEC 61400-1 international standard [21] and certification guidelines [13] are still based on methods developed for metals and the blades are mainly made of composite materials. In this sense, this paper deals with a new fatigue method for wind turbine blades which considers the actual fatigue behavior of composite materials.

A variety of models have been proposed to analyze the fatigue behavior of composite materials, which can be categorized into three groups [12]: fatigue-life models, phenomenological models, and damage mechanics models. The fatigue-life models predict the cumulative damage and fatigue lifetime of the composite materials based on empirical relations; however, they do not consider any physical damage mechanisms inside the material and do not provide either any detail about the material property degradation. The phenomenological models predict the material property degradation regarding stiffness and/or strength. Nevertheless, the evolution laws used by these models for predicting the property degradation are based on macroscopically observable properties and not on the physical damage mechanisms. Moreover, the applicability of the phenomenological models is limited to the laminates that were tested to develop the model. Contrary to previous models, the damage mechanics models predict the fatigue lifetime and the material property degradation of the composite materials by correlating the physical damage mechanisms to macroscopically measurable material properties. However, these models require much more computational resources than the fatigue-life and phenomenological models.

Most of the published studies regarding fatigue in full wind turbine blades are based on fatigue-life models [34, 28, 52, 45, 22, 11] due to their simplicity. In fact, the prediction methods suggested by the IEC 61400-1 international standard [21] and certification guidelines [13] are also based on this type of model. In [52, 22, 11], for example, the fatigue lifetime of wind turbine blades under different loading conditions was predicted by applying fatigue-life models. In these studies, Goodman diagrams were implemented to quantify the interaction of mean and alternating stresses on the fatigue lifetime of the structure. These diagrams assume a symmetric and linear fatigue behavior of the material from tension to compression, which leads to inaccurate estimations for composite materials whose fatigue response is different under tension and compression due to, among others, buckling of fibres under compression loads, misalignments between plies, etc. Moreover, these models do not predict the stiffness

degradation of the blade, which can be a critical design variable for these structures because collisions with the tower and structural instabilities, such as local or global buckling, should be prevented along their lifetime [13].

Moreover, only one study has applied phenomenological models for predicting the fatigue response of full wind turbine blades [41]. In this study, the fatigue lifetime of a wind turbine blade under different loading conditions was estimated based on a stiffness degradation technique developed in [40]. In this technique, the Hashin's failure criterion [20] was used to estimate the failure of the different plies and, based on that, evaluate the accumulated fatigue damage of the blade. However, the use of this type of failure criteria might lead to inaccurate estimations especially under multiaxial loading conditions, as shown in [9], due to lack of any physical basis. Furthermore, even though the technique implemented in this study was based on the material stiffness degradation, the stiffness degradation of the entire blade was not estimated.

In this sense, if the aim is to predict the stiffness degradation and final failure of wind turbine blades under different fatigue loading conditions, it is first necessary to identify the different fatigue damage mechanisms developed in the material and then predict how these damage mechanisms affect the structural response of the blades. This should be done considering the fact that the length scale in which the damage initiates and propagates in composite materials is not unique [44] and vary depending on the microstructural configuration of the material (i.e. matrix, reinforcements, etc.) and on the driving forces that the material is subjected.

As discussed in [43], a better description of the structural response of wind turbine blades could be obtained if a multiscale approach is implemented, in which the effects of the damage progression at different length scales, such as the microscale (material), macroscale (test specimen), subcomponent scale (blade sections, spars, shell, etc.), and full scale (wind turbine rotor blade) are sequentially coupled.

Based on the above considerations, the implementation of damage mechanics models in a multiscale approach might lead to more accurate and reliable fatigue-life predictions of wind turbine blades because the damage mechanics models would allow predicting the damage evolution and its effects on the material response at different length scales [42, 17, 30, 49]. In addition, as explained above, the multiscale approach would allow coupling all these effects to predict the full structural response of the blade and its final failure.

The ability of this type of model for predicting the damage evolution in wind turbine blades and its effect on the final structure response was recently demonstrated in [32]. In this study, a physics-based multiscale progressive damage model was proposed for predicting the evolution of off-axis matrix cracks in different regions of the blade and their effects on the blade tip flap-wise displacement evolution by combining computational micromechanics and continuum damage mechanics in a 3D finite element model.

The off-axis matrix cracks are one of the first damage mechanisms that take place in multidirectional composite laminates, which are the main materials used in the wind turbine blades. Normally, the multidirectional laminates used in these structures consist of unidirectional UD non-crimp fabric (NCF) plies orientated in different directions. The NCF materials are made of bundles of normal UD fibers reinforced with backing fiber bundles, which provide the UD material slightly higher strength in other directions and easier handling. When the multidirectional laminates are made of pure UD fiber, the stiffness degradation of the material is caused mainly by the onset and propagation of the off-axis matrix cracks together with the onset of delaminations between the different plies [39]. However, when the UD fibers are reinforced with backing fiber bundles, the initiation and propagation off-axis cracks in backing bundles provide an additional drop of the stiffness, as described in [54, 23]. Moreover, the structural load-bearing capacity of the multidirectional laminates is determined by the UD fibers located in the on-axis plies, in which different damage mechanisms, such as fiber breakage, fiber/matrix debond, fiber fragmentation, etc. can be developed and lead to the catastrophic failure of the laminate [10].

Consequently, in order to predict the stiffness degradation and the final failure of wind turbine blades it is necessary to predict, among others, the following damage mechanisms developed in multidirectional laminates made of NCF plies:

- The initiation and propagation of off-axis matrix cracks (the crack density evolution) in off-axis plies,
- The initiation and propagation of delaminations induced by the off-axis matrix cracks,
- The initiation and propagation off-axis cracks in backing bundles, and
- The fiber-related damage at the load-bearing regions, such as UD bundles and on-axis plies.

It is worth mentioning that above framework is an expansion of the framework for designing composite structures against fatigue made of pure UD fibers proposed by Quaresimin in [35], in which the damage mechanisms caused by the presence of backing fiber bundles are not considered. Further studies about the behavior of multidirectional laminates made of NCF plies could improve this framework.

Modelling all above damage mechanisms developed in this type of multidirectional laminate to obtain the full fatigue response of the blades would increase considerably the computational resource demand if 3D finite element models are used; which would make the implementation of multiscale progressive damage models unfeasible for wind turbine blades.

In the present study, a damage mechanisms-based multiscale approach implemented by using 2D finite-element-based cross-section analysis instead of 3D finite element models is proposed for analyzing and predicting the fatigue behavior of composite wind turbine blades. By using a 2D finite-element-based cross-section analysis, the full blade is modeled as a beam composed of several cross-sections; which simplifies the complexity of the blade regarding geometry and material distribution compared with the 3D finite element models [4] and allows saving considerably computational time [3]. Moreover, the 2D finite-element-based cross-section analysis also provide confidence in the implementation of damage mechanisms models because their accuracy when calculating stresses/strains is comparable to that obtained from 3D finite element models [4].

Accordingly, the aims of the paper are, first, to describe the proposed damage mechanisms-based multiscale approach and, second, apply this multiscale approach in order to analyze the effect of the off-axis cracks on the stiffness degradation of wind turbines blades. As a second part of this paper, the evolution of the off-axis cracks evolve in the wind turbine blade under fatigue loading conditions is analyzed [8]. This study is the first step towards future models that allow predicting the full fatigue response of wind turbine blades, in which the effect of other damage mechanisms, such as delaminations, off-axis cracks in backing bundles, and fiber-related damage, are also considered.

2 Multiscale damage mechanics approach

In the present section, a new multiscale approach based on damage mechanics models is proposed for analyzing and predicting the fatigue behavior of composite wind turbine blades. In the first part of the section, a general description of the proposed multiscale approach is presented; whereas in the second part, a description of the damage mechanics model used to predict the effect of off-axis cracks on the stiffness degradation of wind turbine blades is given.

2.1 General approach description

Wind turbine blades normally consist of subcomponents made of composite materials due to the high strength-to-weight ratio of these materials. Some of these subcomponents are, for example, spar caps, shear webs, leading-edge, and trailing-edge panels, which are often bonded together by means of adhesive joints. These subcomponents are subjected to different loading conditions during the wind turbine service life, which causes different damage types on the material and, therefore, a change in the structural response of the blades.

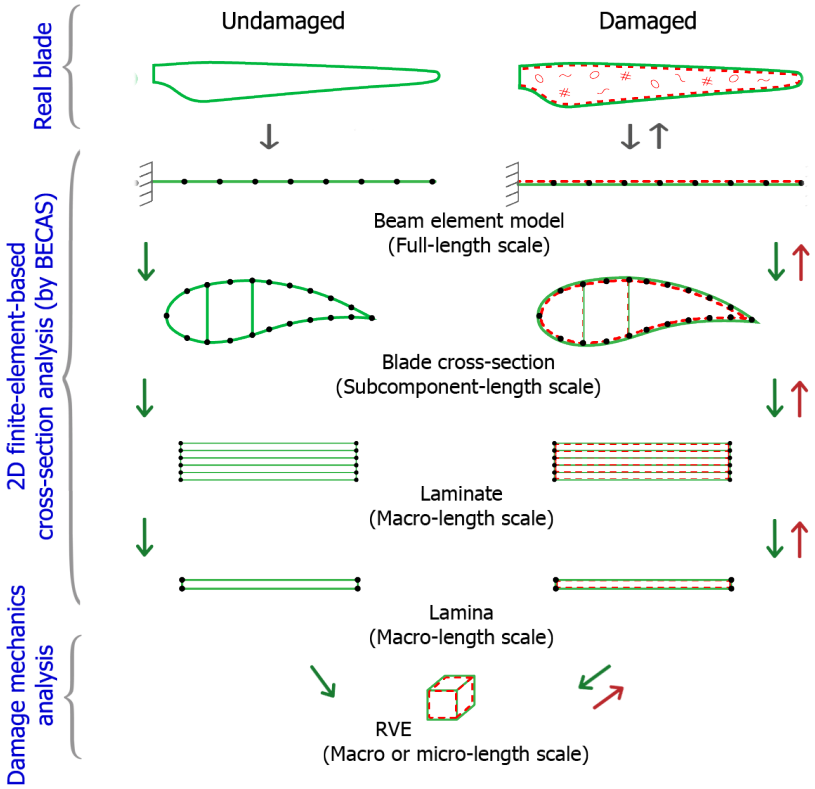

Figure 1: Damage mechanics-based multiscale model for wind turbine blades under fatigue implemented by using a 2D finite-element-based cross-section analysis.

Some of these damages can be detected visually, such as delaminations, laminate failure in compression and adhesive joint failure between skins [43]. However, other types of damage might develop at other length scales in the different materials used in the wind turbine blades, as discussed in [44]. For example, fiber-matrix debonding can develop at micro-length scales in unidirectional laminates; whereas, off-axis matrix cracks can appear at macro-length scales in multidirectional laminates.

Hence, the initiation and propagation of damage in composite wind turbine blades can be assumed as a multiscale process that might initiate and propagate from a micro-length scale (material) and/or a macro-length scale (test specimen), passing through the subcomponent-length scale (spars caps, shells, shear webs, etc.), and ending at the full-length scale (wind turbine rotor blade). This means that, if the full structure fails or its mechanical response degrades, it might be due to the propagation of the damage at all the smaller length scales.

In order to consider this multiscale damage evolution process in wind turbine blades during the fatigue analysis of these structures, a damage mechanics-based multiscale approach using a 2D finite-element-based cross-section analysis is proposed in the present study (see Fig. 1).

In the proposed multiscale approach, the damage evolution of the real blade is modeled by using two types of analysis (see Fig. 1): i) a 2D finite-element-based cross-section analysis; and ii) a damage mechanics analysis. During the first analysis, the blade is modeled as a cantilever beam composed of several cross-sections by using BECAS (BEam Cross-section Analysis Software) tool developed by DTU Wind Energy [4]. BECAS is a general-purpose cross-section analysis tool developed to analyze efficiently and accurately the mechanical response of complex beam-like structures, such as wind turbine blades. During this analysis, the response of the blade can be predicted from the full-length scale to the macro-length scale or vice versa. Then, based on the estimated state of the blade at the macro-length scale, a damage mechanics analysis is carried out in which the initiation and propagation of the damage are estimated. Subsequently, the effects of the estimated damage on the structural response of the blade at the different length scales are sequentially coupled by using the 2D finite-element-based cross-section analysis (i.e., by BECAS).

In this sense, the proposed model initiates by defining the geometry, material configuration, material properties and applied loading conditions of the blade, which can be assumed undamaged in this first step.

Based on this input information, the beam finite element model of the blade (full-length scale) is carried out using Frans, which is an extension beam finite element code of BECAS. By using Frans, the beam finite element static equilibrium equations are given as [4]

$$\hat{\mathbf{K}}\hat{\mathbf{u}} = \hat{\mathbf{f}} \tag{1}$$

where $\hat{\mathbf{u}}$ is the vector of the three displacements u and rotations r with respect to the x, y, and z axis (being z the longitudinal beam axis) of the b nodes of the beam finite element assembly; $\hat{\mathbf{f}}$ is the vector of the three external forces $\hat{f}$ and external moments $\hat{m}$ with respect to the x, y, and z axis of the b nodes of the beam finite element assembly; and $\hat{\mathbf{K}}$ is defined as

$$\hat{\mathbf{K}} = \sum_{e=1}^{n_b} \hat{\mathbf{K}}_{\mathbf{e}} = \sum_{e=1}^{n_b} \int_0^{L_e} \hat{\mathbf{B}}_{\mathbf{e}}^{\mathbf{T}} \mathbf{K}_{\mathbf{s}} \hat{\mathbf{B}}_{\mathbf{e}} dz \tag{2}$$

where the summation is related to a typical finite element assembly with n_b number of elements, in which the element e has a length L_e. Whereas, $\hat{\mathbf{K}}_{\mathbf{e}}$ is the beam finite element stiffness matrix, which is a function of the cross-section stiffness matrix $\mathbf{K}_{\mathbf{s}}$ and the strain-displacement matrix $\hat{\mathbf{B}}_{\mathbf{e}}$. More details about the beam finite element model can be found in [4].

As seen in Eq. 2, the stiffness matrix of the different cross-sections, $\mathbf{K}_{\mathbf{s}}$, must be first estimated in order to develop the beam finite element model. For that, the number of cross-sections to consider during the model along with their geometry and material

configuration must be defined. Once this is done, the stiffness matrix of the different cross-sections can be estimated using BECAS.

In BECAS, each cross-section is discretized in finite elements and its stiffness matrix $\mathbf{K_s}$ is obtained according to the virtual work principle explained in [15], which leads to the following equation:

$$\mathbf{K_s} = (\mathbf{W}^T \mathbf{G} \mathbf{W})^{-1} \tag{3}$$

where $\mathbf{G}$ is a system matrix that depends, among others, on the material constitutive matrices, $\mathbf{Q}_{e'}$, defined at the different cross-section elements, e'; whereas $\mathbf{W}$ is a vector containing the warping displacements $\mathbf{u}$, the internal strains $\boldsymbol{\psi}$ and the corresponding Langrange multipliers $\boldsymbol{\lambda}$. More details about the estimation of the cross-section stiffness matrix can be found in [4, 15].

Furthermore, each finite element of the discretized cross-section (see Fig. 1) represents either a laminate, a ply, a sandwich structure or a joint. The 3D stress/strain components at each of these elements can be calculated using BECAS [4], if the cross-section forces and moments are known. The cross-section forces and moments can be obtained, for example, from aeroelastic simulations.

Note that, so far, an analysis of the undamaged state of the blade has been carried out from the full-length scale to the macro-length scale using continuum mechanics theories. However, as described above, the damage in the wind turbine blades might initiate at different length scales depending on the microstructural configuration of the material and on the driving forces. This suggests, on the one hand, that the finite elements in the cross-sections discretized by BECAS must be further discretized in structural elements in which the damage evolution can be analyzed and, on the other hand, that this damage evolution analysis should be done by using damage mechanics models.

In this sense, the discretization of the cross-section finite elements can be done using representative volume elements (RVEs), in which a sample of the damage can be contained [5]. The shape and length scale of the RVEs can vary depending of the damage type to be analyzed. For example, micro axisymmetric multi-cylinder RVEs were used in [56] to study the progression of failure from broken fibers; whereas, a macro RVE of a segment of a laminate containing one crack was used in [7] to study the effect of off-axis matrix cracks on composite laminates.

Having discretized the cross-section finite elements in RVEs, the regions where the damage might develop can be identified taking into account the stress states of the undamaged cross-section obtained from BECAS. The identification of this regions is done by using damage mechanics models, which can vary according to the damage type to be analyzed.

In this work, the damage type studied is the off-axis matrix cracks and the damage mechanics models used to model how this type of crack evolves and affects the structural

response of the wind turbine blades are described in section 2.2.

Back to the general model description, whatever the type of damage to be analyzed, a re-calculation of the stresses at the RVE level must be carried out because the local stresses might change as a result of the damage. Moreover, the damage also might cause a degradation in the stiffness of the damaged RVEs and, therefore, a degradation in the stiffness properties of the damaged cross-section finite elements and in the cross-section itself. Then, the degraded cross-section matrix stiffness, $\mathbf{K_{s,dam}}$, can be calculated using BECAS through Eq. 3. Because BECAS specifies the material properties at each element of the cross-section finite element discretization, the $\mathbf{K_{s,dam}}$ matrix must be calculated after the material properties of the damaged cross-section finite elements, $\mathbf{Q_{e',dam}}$, are updated.

Once this process is done for all cross-sections, the degraded beam finite element stiffness matrix, $\hat{\mathbf{K}}_{\mathbf{e,dam}}$, can be calculated using the beam finite element model (i.e. by Frans) through Eq. 2. In addition, the response of the full blade in terms of failure characteristics, critical regions, stress-strain response, deflections, and vibration (i.e., natural frequencies) characteristics can also be calculated using the beam finite element model.

In the case of the fatigue loading conditions, in which it is expected that the damage propagates as the number of load cycles are applied, the method described above can be used to estimate the propagation of the damage and its effect on the structural response of the blade over time. In this sense, for each applied cycle (or block of cycles), it must be checked if there are damaged cross-section elements. If so, the calculation of the stress/strain states must be calculated based on the stress re-distribution due to the presence of damage. Then, the propagation of the damage can be calculated along with the corresponding stiffness degradation. All this process is schematically presented in Fig. 2

In this work, the proposed damage mechanics-based multiscale approach for wind turbine blades under fatigue loading conditions is implemented to analyze the effect of off-axis matrix cracks on the structural response of a commercial wind turbine blade. During this analysis, the following assumptions are made:

- The effect of the backing fiber bundles in the non-crimp UD materials is not considered. This means that only pure UD materials are assumed;
- The effect of material imperfections (e.g. voids, inclusions, etc.) on the structural response of the blade is not considered; and
- Adhesive joints are not taken into account as perfect bonding is assumed.

In addition to these assumptions, the effects of other types of damage, such as delaminations or damage in the load-bearing plies on the structural response of the

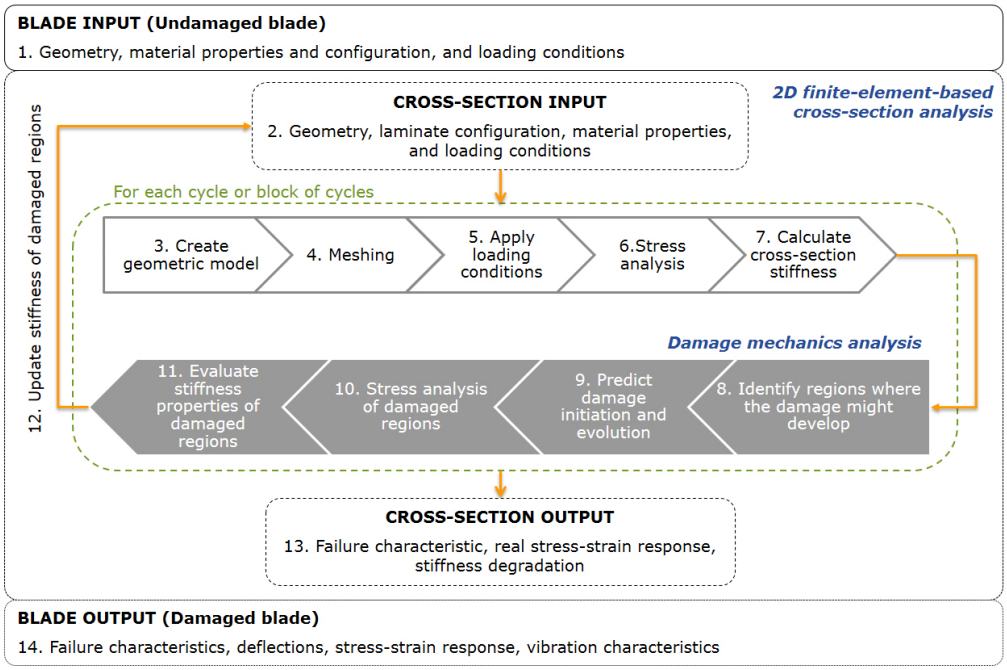

Figure 2: Flow chart of the proposed multiscale approach for fatigue design of wind turbine blades based on damage mechanics models

blade are not considered in this work. All of these assumptions may cause omissions of possible additional stiffness drops in the blade, which must be considered in future extensions of the model proposed in this work.

In the next section, a description of the damage mechanics model implemented in this work to predict the stiffness degradation of the blade as a function of off-axis cracks is presented.

2.2 Stiffness degradation model for matrix-cracked laminates

One of the main causes of the stiffness degradation in multidirectional laminates is the initiation and propagation of matrix cracks along the fibers in the off-axis plies [39], normally called off-axis cracks. This phenomenon has been analyzed experimentally over many years in different studies, e.g., [39, 46, 2, 36, 37]. These studies have showed that the development of the off-axis cracks initiates during the early fatigue lifetime and propagates quickly as the number of cycles increases until reaching a saturation point in which the mechanical response of the laminate tends to a stable condition.

Based on these studies, different analytical and numerical models have been proposed in order to predict the degradation of the elastic properties of the material as a function of the off-axis crack density, e.g., [38, 19, 17, 31, 29, 50].

Considering some limitations of these models, Carraro and Quaresimin [7] proposed an

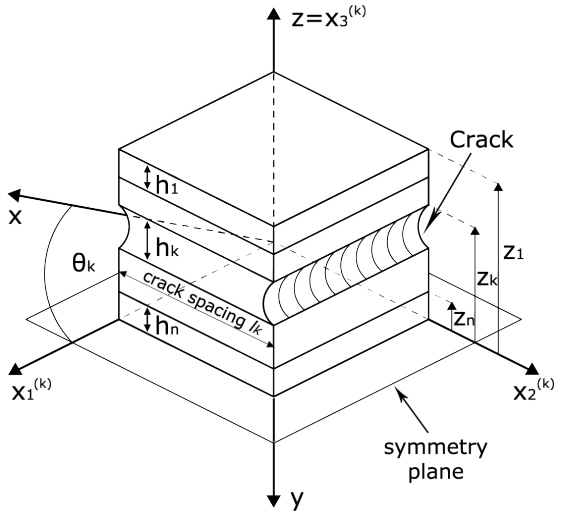

Figure 3: Representative volume element, RVE, assumed in the present work.

accurate analytical model based on a bi-dimensional optimal shear lag analysis (as defined in [33]), which allows predicting the elastic property degradation of any multidirectional symmetric laminate with off-cracks in different plies. This model was then extended in order to account for the interaction between all off-axis cracks [7].

According to Carraro and Quaresimin [7], any symmetric laminate made of $2n-1$ plies made of unidirectional (UD) fiber-reinforced composites, each orientated to θ_i angle respect to the global $x-$axis and with thickness h_i, can be analyzed using this model (see Fig. 3). In this model, symmetry conditions are applied in the middle of the nth ply and only the n plies of the superior half of the laminate are considered. Moreover, each damaged ply can have different number of off-axis cracks; however, it is assumed that all off-axis cracks in each ply are equally spaced. Hence, a segment of the laminate containing a crack spacing l_k in the kth ply is assumed as the representative volume element (RVE), see Fig. 3. This RVE is periodically repeated along the direction $x_2^{(k)}$, where $x_1^{(k)}$, $x_2^{(k)}$, and $x_3^{(k)}$ is the material coordinate system of the cracked ply rotated an angle θ_k around the z-axis of the global coordinate system x, y, z. Note that, in this case, the damage length scale corresponds to the total thickness, h, of the laminate, meaning to a macro-length scale.

Based on the *superposition of solutions* method suggested by Tsai and Daniel in [48], Carraro and Quaresimin [7] assumed that, if no interaction between cracks in the different plies is considered, the compliance matrix of the damaged laminate, $[S_{dam}]$, can be calculated as the sum of the compliance matrix of the undamaged laminate, $[S_0]$, and the sum of the contributions $[\Delta S(\rho_k)]$ for each cracked ply, as follows:

$$[S_{dam}] = [S_0] + \sum_{k=1}^{n} [\Delta S(\rho_k)] \tag{4}$$

where ρ_k is the off-crack density in the k-th ply, which is defined as $\rho_k = 1/l_k$. The contributions $[\Delta S(\rho_k)]$ for each cracked ply can be calculated as

$$[\Delta S(\rho_k)] = [S^{(k)}(\rho_k)] - [S_0] \tag{5}$$

where $[S^{(k)}(\rho_k)]$ is the total compliance matrix of the laminate assuming cracks only in the kth ply.

According to Carraro and Quaresimin [7], the $[S^{(k)}(\rho_k)]$ compliance matrix can be calculated as follows:

$$[S^{(k)}(\rho_k)] = [R][T(\theta_k)]^{-1}[R]^{-1}[\hat{S}]^{(i\neq k)}[\Omega(\rho_k)]^{(i\neq k)} \tag{6}$$

where $[\hat{S}]^{(i\neq k)}$ is the compliance matrix of any ith ply excepted the kth ply, $[T(\theta_k)]$ is the rotation matrix of the kth ply to the global coordinate system, $[R]$ is defined as

$$[R] = \begin{bmatrix} 1 & 0 & 0 \\ 0 & 1 & 0 \\ 0 & 0 & 2 \end{bmatrix} \tag{7}$$

and $[\Omega(\rho_k)]$ are the stresses of any ith ply averaged over the entire volume of the ply in the coordinate system of the cracked kth ply corresponding to the global loading conditions $\sigma_g = \{1,0,0\}^T, \{0,1,0\}^T, \{0,0,1\}^T$, as follows (see more details in [7]):

$$[\Omega(\rho_k)] = \begin{bmatrix} \gamma_{k,x}^{(i)}(\rho_k) & \gamma_{k,y}^{(i)}(\rho_k) & \gamma_{k,xy}^{(i)}(\rho_k) \\ \lambda_{k,x}^{(i)}(\rho_k) & \lambda_{k,y}^{(i)}(\rho_k) & \lambda_{k,xy}^{(i)}(\rho_k) \\ \beta_{k,x}^{(i)}(\rho_k) & \beta_{k,y}^{(i)}(\rho_k) & \beta_{k,xy}^{(i)}(\rho_k) \end{bmatrix} \tag{8}$$

On the other hand, Carraro and Quaresimin [7] found that, if the interaction between cracks in different plies is considered, the compliance matrix of the damaged laminate, $[S_{dam}]$, can be calculated as follows:

$$[S_{dam}] = [S_0] + \sum_{k=1}^{n} ([\Delta S(\rho_k)] \cdot IM) \tag{9}$$

in which the contributions $[\Delta S(\rho_k)]$ for each cracked ply are affected by the following IM matrix, which contains unknown global stress $\sigma_{x,k}$ and $\sigma_{xy,k}$ to be calculated as explained in [7].

$$IM = \left[\left\{ \begin{matrix} \sigma_{x,k} \\ 0 \\ \sigma_{xy,k} \end{matrix} \right\} \middle| \sigma_g = \{1,0,0\}^T \quad \left\{ \begin{matrix} \sigma_{x,k} \\ 0 \\ \sigma_{xy,k} \end{matrix} \right\} \middle| \sigma_g = \{0,1,0\}^T \quad \left\{ \begin{matrix} \sigma_{x,k} \\ 0 \\ \sigma_{xy,k} \end{matrix} \right\} \middle| \sigma_g = \{0,0,1\}^T \right] \tag{10}$$

Once the compliance matrix of the damaged laminate $[S_{dam}]$ is calculated using Eq. 4 for the no-interaction case, or Eq. 9 for the interaction case, the degraded mechanical properties of the damaged laminate, such as the in-plane Young's modules in the axial and transverse directions, E_x and E_y, the shear modulus, G_{xy}, the Poisson's ratio, ν_{xy}, and the traction-shear coupling coefficients, can be easily calculated as a function of the ρ_k density.

In order to apply this damage mechanics model in the multiscale approach for wind turbine blades proposed in this study, it must be assumed that the blade to be analyzed is made of symmetric laminates because the applied damage mechanics model can be only used in this type of laminate. This assumption might affect the stiffness matrix of the different cross-sections and the bend-twist coupling effects in the blade [14]. However, according to the knowledge of the authors, currently, there is no model that accurately predicts the effect of off-axis cracks on the response of any type of cracked multidirectional laminate. Therefore, further damage mechanics models that can be applied in a generic cracked multidirectional laminate are needed to overcome this limitation.

Based on this assumption, the RVE shown in Fig. 3 would correspond to segments of the representative laminates, l', in the discretized cross-section containing a crack spacing l_k in the kth ply, as shown in Fig. 4. because the damage mechanics model assumes cracks equally spaced in the laminate, the degraded compliance matrix of each of the damaged representative laminates in the cross-section, $[S_{dam,l'}]$, can be calculated using Eq. 4 for the no-interaction case, or Eq. 9 for the interaction case. In addition, determined $[S_{dam,l'}]$, the degraded stiffness matrix of each of the damaged representative laminates in the cross-section, $[K_{dam,l'}]$, can also be calculated as $[K_{dam,l'}] = [S_{dam,l'}]^{-1}$

Moreover, in order to estimate the degraded cross-section matrix $\mathbf{K_{s,dam}}$, an equivalent discretization of the cross-section has to be done because, in BECAS, the materials properties are specified at each cross-section finite element e' and the damage mechanics model provides the degraded compliance matrix $[S_{dam,l'}]$ (or the degraded stiffness matrix $[K_{dam,l'}]$) of the entire representative laminate l'. In this sense, each group of cross-section finite elements e' contained in the representative laminate l' is replaced by finite elements e'' contained in an equivalent representative laminate l'' (see Fig. 4). Note that each cross-section finite elements e' represents a different ply in the undamaged representative laminate l'; whereas, each cross-section finite elements e'' is part of the equivalent representative laminate l''. This means that each e'' element has either a stiffness matrix $[K_{dam,l'}]$, if the equivalent representative laminate is damaged (which can be calculated using Eq. 4 or Eq. 9), or a stiffness matrix $[K_{0,l'}]$, if the equivalent representative laminate is undamaged (which can be easily calculated using, for example, the Classical Laminate Theory [24]). In this way, each cross-section is now discretized in a number of finite elements e'' and its degraded cross-section matrix can

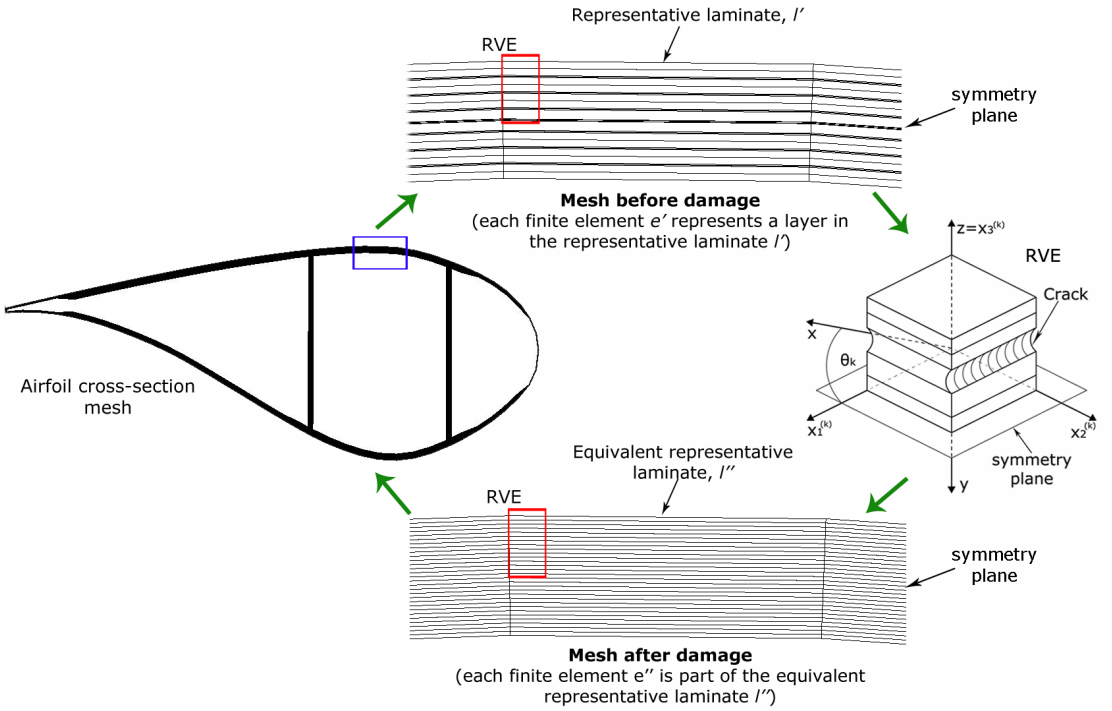

Figure 4: Cross-section mesh before and after the damage is estimated.

be calculated as described in Eq. 3.

Furthermore, Carraro and Quaresimin [7] showed that an improvement in the accuracy of the predictions can be obtained if the interaction between the off-axis cracks in different plies is accounted. However, the fact of taking into account this interaction between cracks requires an additional step in the model because the IM matrix presented in Eq. 10 has to be calculated. This additional step demands an additional computational effort which could be increased considerably when analyzing all the representative laminates in a cross-section and, even more, in all cross-sections of the blade.

In this sense, because one of the goals of the proposed damage mechanics-based multiscale model is to make efficient predictions, the interaction between off-axis cracks in different plies is not considered in the present work. Nevertheless, the capabilities of the no-interaction model used in this work to accurately predict the response of the material as a function of the off-axis crack density is demonstrated in section 4.1. This savings in computational resources will become more relevant in a future when other types of damage, such as delaminations and fiber-related damage, are included in the proposed multiscale approach.

3 Validation and implementation

3.1 Validation of the applied damage mechanics model

The validation of the applied damage mechanics model is carried out at the macro-length scale (i.e., material length scale) based on data presented in the literature, see section 4.1. Symmetric multidirectional laminates with cracks in only one ply [46, 47, 26, 27], and symmetric multidirectional laminates with cracks in multiple plies [55], are analyzed. In all cases, the elastic properties of the damaged laminate are normalized with the corresponding elastic properties of the undamaged laminate and plotted as a function of the density of off-axis cracks.

3.2 Implementation of the proposed multiscale approach

In order to show the capabilities of the cross-section beam model used in the proposed damage mechanics-based multiscale approach and the capabilities of the multiscale approach itself, the structural response of a 34m long blade designed for a wind turbine with a power capacity of 1.5MW is analyzed as a function of the off-axis crack density.

The effect of the off-axis cracks on the degradation properties of the blade cross-sections was evaluated varying the values of ρ_k from 0 crack/mm to 5 crack/mm in all off-axis plies. Assuming that all off-axis plies in the blade have the same crack density is indeed no real because the damage might develop differently along the blade depending on the material configuration and the internal forces; however, this allows analyzing what would be the maximum effect of this type of damage on the structural response of the blade. Nevertheless, the evolution of the off-axis cracks in the different blade regions and their consequences on the structural blade response by considering the effect of fatigue loading conditions will be presented as the second part of this work [8].

Furthermore, the stiffness degradation of the blade as a function of the off-axis crack density was evaluated in terms of blade deflections, see section 4.2. For that, the proposed multiscale approach was implemented to model a static test carried out to the blade at DTU Risø Campus [18], in which the blade deflections caused by quasi-static loads applied at four load points along the blade were measured. The bending moment distribution caused by the applied loads corresponded to a bending moment distribution obtained from aeroelastic simulations, which took into account all relevant Design Load Cases (DLCs) suggested by the IEC 61400-1 international standard [21]. More details about the experimental setup modeled in this analysis can be found in [18].

Moreover, an evaluation of the capabilities of the 2D finite-element-based cross-section analysis implemented in the proposed multiscale model to make reliable estimations of damaged blades at the full-length scale was carried out by doing a comparison between the estimated analytical blade deflections and the experimental ones, see section 4.2.

In order to build the beam finite element model, cross-sections located every 2m from the root (i.e., 0m span) to the tip (i.e., 34m span) of the blade were analyzed. The airfoil characteristics were modeled according to manufacturer specifications. However, some modifications in the materials and laminate layups were carried out according to the assumptions made in the applied damage mechanics model (see section 2). On the one hand, as discussed in the previous section, the blade was assumed to be made of symmetric laminates. For that, special attention was given to each laminate in the different cross-sections regions (i.e. spar caps, trailing-edge, leading-edge, shear webs, shell panels) in order to keep as similar as possible the assumed symmetric laminates to the original ones.

On the other hand, because the applied damage mechanics model only considers multidirectional laminates made of unidirectional (UD) plies, biaxial and triaxial plies used in the blade were replaced by $[+45/-45]$ and $[0/+45/-45]$ UD laminates respectively; which was done keeping the thickness of the original plies. The mechanical properties of all UD plies were assumed equal to the mechanical properties of the UD material used by the manufacturer in the blade. By doing this, it was found a good agreement between the mechanical properties of the original biaxial and triaxial plies and the ones of the assumed UD laminates. Moreover, the adhesive material used in the blade by the manufacturer was omitted in the model in agreement with the assumptions made in section 2.

Furthermore, a 2D finite element mesh in BECAS was developed for each of the cross-sections using linear four node elements Q4 (see examples in Fig. 5); whereas, four node beam finite elements with cubic Lagrangean interpolation functions were used in the beam finite element model.

4 Results

4.1 Validation at macro-length scale

The damage mechanics model applied in the proposed multiscale approach was validated by using experimental and analytical data taken from the literature related to matrix-cracked symmetric multidirectional laminates.

Tong et al. [46], for example, presented results about the effect of off-axis cracks in the 90° plies of a quasi-isotropic glass/epoxy $[0/90/-45/+45]_s$ laminate on the degradation of its mechanical properties. A comparison between the degraded Young's modulus and Poisson's ratio estimated by the damage mechanics model applied in current work and the ones obtained from the experiments reported by Tong et al. [46] is presented in Fig. 6-a. As shown in this figure, a good agreement between the estimated and experimental results was obtained for values of ρ_k less than 0.6 cracks/mm; however, from this value, some

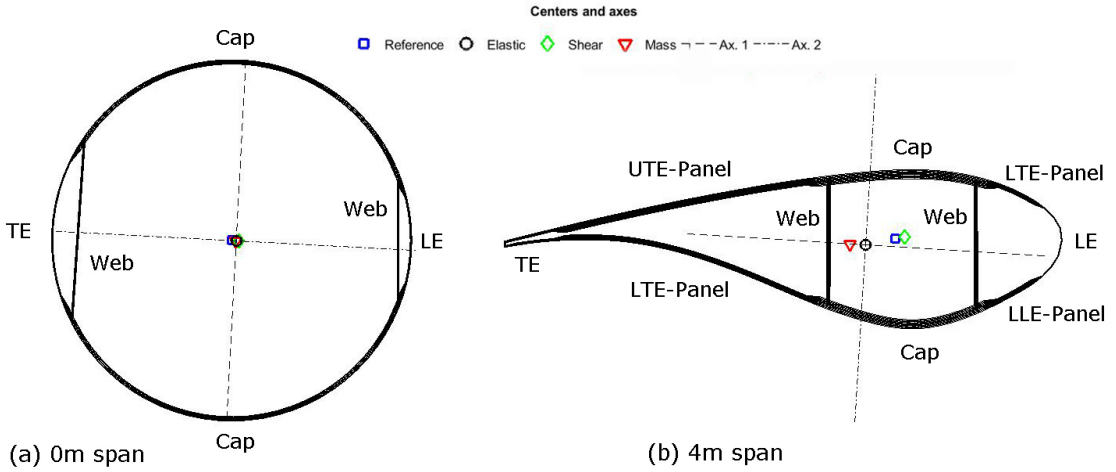

Figure 5: Cross-section finite element mesh examples developed by BECAS [4] at: (a) 0m blade span, and (b) 4m blade span. Reference, elastic, shear, and mass center positions, and elastic axis orientations. And cross-section regions: spar caps (Caps), shear webs (Webs), leading-edge (LE), trailing-edge (TE), lower and upper trailing-edge panels (LTE-Panel and UTE-Panel respectively), and lower and upper leading-edge panels (LLE-Panel and ULE-Panel respectively).

differences can be seen between the results. These differences are due to the occurrence of off-axis cracks at the $-45°$ and $+45°$ plies during the experiments, which took place when the crack density at the $90°$ plies was between 0.6 and 0.8 cracks/mm [46]. As a result of these cracks at the $-45°$ and $+45°$ plies, the laminate suffered an additional property degradation; which was not considered in the current analysis because the crack densities at these plies were not reported in [46].

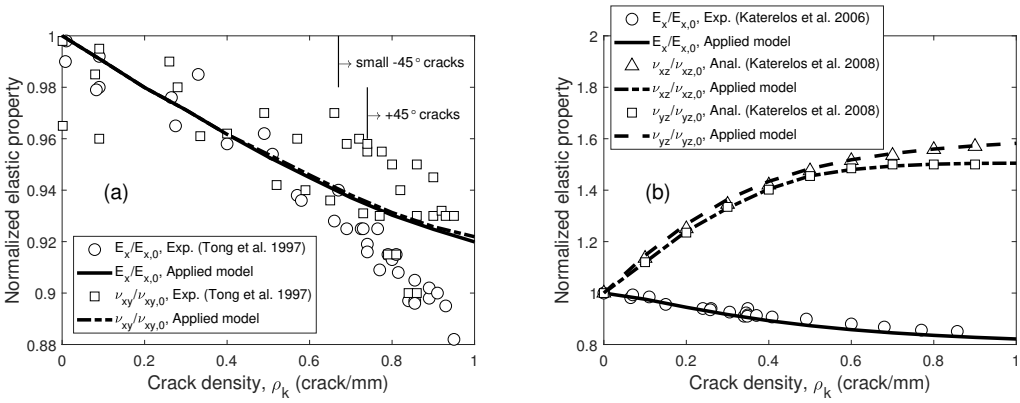

Figure 6: Comparison between the material property degradation of matrix-cracked symmetric laminates estimated by the applied damage mechanics model and the results reported by: a) Tong et al. [46]; and b) Katerelos et al. [26].

Moreover, Katerelos et al. [26] presented results about the effect of off-axis cracks on the longitudinal Young's modulus of a $[0/45]_s$ laminate. The degradation of the

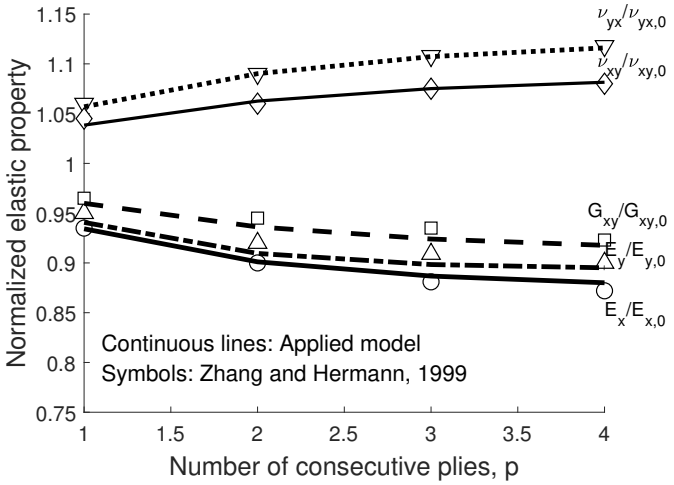

Figure 7: Comparison between the material property degradation of $[0_p/90_p/\pm 45_p]_s$ laminates with $\rho_2 = \rho_3 = \rho_4 = 2$ cracks/mm estimated by the applied damage mechanics model and the model developed by Zhang and Herrmann [55].

Poisson's ratios ν_{xz} and ν_{yz} of this laminate was also reported by Katerelos et al. [27], which were estimated by using an analytical model developed by Kashtalyan and Soutis [25] for unbalanced symmetric $[0/\theta]_s$ composite laminates. As shown in Fig. 6-b, a good agreement between the applied damage mechanics model and the experimental and analytical results reported in [26, 27] was achieved.

Furthermore, the capabilities of the applied damage mechanics model for predicting the material response of symmetric laminates with off-axis cracks in different plies was evaluated against the results reported by Zhang and Herrmann [55] about carbon/epoxy $[0_p/90_p/\pm 45_p]_s$ laminates with different values of p. As shown in Fig. 7, for the longitudinal Young's modulus E_x, and the Poisson's ratios ν_{yx} and ν_{xy}, a good agreement between the results estimated from the applied damage mechanics model and the ones reported in [55] was obtained; whereas for the transverse Young's modulus E_y and the shear modulus G_{xy}, an acceptable agreement between the two models was achieved. The small differences in the E_y and G_{xy} results may be due to the fact that the applied damage mechanics model does not consider the interaction between cracks in different layers. Indeed, as shown in [7], a better agreement was obtained for the E_y case when the interaction between cracks was accounted in the damage mechanics model used in this work.

However, despite these small differences, it can be concluded that the applied damage mechanics model predicts well the behavior of cracked symmetric laminates, even though the interaction between cracks in different layers is not considered. An extended validation of the applied damage mechanics model can be found in [7].

Additionally, note that this validation is made at a macro-length scale and that, in the

case of wind turbine blades, the response of the material can be affected by the presence of, for example, material imperfections, backing fiber bundles, adhesive joints, etc. Even though these factors are not considered in this work (as described in section 2.1), future experimental studies that allow evaluating their effect on the damage evolution of off-axis cracks from the macro-length scale to the full-length scale may be useful to improve the proposed multiscale model.

In the next section, the results about the effect of the off-axis cracks estimated by the applied damage mechanics at the macro-length scale on the structural response of a wind turbine blade obtained using the proposed multiscale model are presented.

4.2 Structural response of damaged wind turbine blades

The effects of the matrix crack density ρ_k on the cross-section stiffness degradation in the edge-wise and flap-wise directions of the analyzed blade are presented in Fig. 8. In this figure, the edge-wise and flap-wise stiffness of the damaged blade cross-sections, $E_{edgewise}$ and $E_{flapwise}$ respectively, are normalized with the corresponding stiffness of the undamaged blade cross-sections, $E_{0,edgewise}$ and $E_{0,flapwise}$ respectively, and plotted as a function of the off-axis crack density.

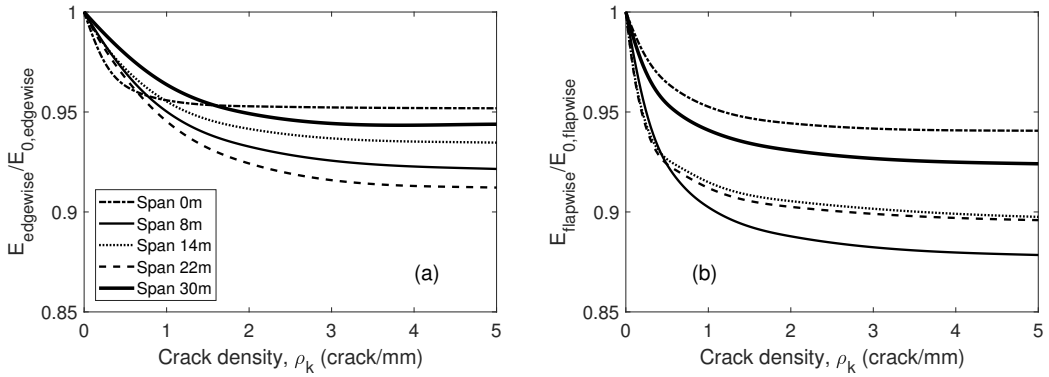

Figure 8: Blade cross-section stiffness degradation as a function of the off-axis crack density ρ_k in the: (a) edge-wise direction; and (b) flap-wise direction.

As shown in Fig. 8, for all analyzed cases, the cross-section stiffness decreases as the off-axis crack density ρ_k increases until a saturation condition is reached.

Moreover, the level of the stiffness degradation seems to change along the blade and also within the in-plane of each cross-section. This can be seen in Fig. 8, in which the value of both edge-wise and flap-wise stiffness of all analyzed cross-sections vary from one cross-section to another. In addition, it can also be observed that, for the same value of ρ_k, the flap-wise stiffness seems to degrade more than the edge-wise stiffness in each cross-section.

On the other hand, as shown in Figs. 9 and 10, the way in which the cross-section stiffness degrades is reflected in the structural response of the blade. In Fig. 9, for example, it can be seen that the higher the off-axis crack density, the higher the total blade deflection, u_{total}, as a result of the decrease in the cross-section stiffness, being the total blade deflection u_{total} defined as

$$u_{total}^2 = u_{edgewise}^2 + u_{flapwise}^2 \tag{11}$$

where $u_{edgewise}$ and $u_{flapwise}$ are the blade deflections in the edge-wise and flap-wise directions respectively. However, when the off-axis crack saturation condition is reached, it seems that the blade deflection does not increase more. This level of deflection can be assumed as the maximum one caused by this type of damage since it was assumed that all off-axis plies in the blade have the same off-axis crack density (as described in section 3.2).

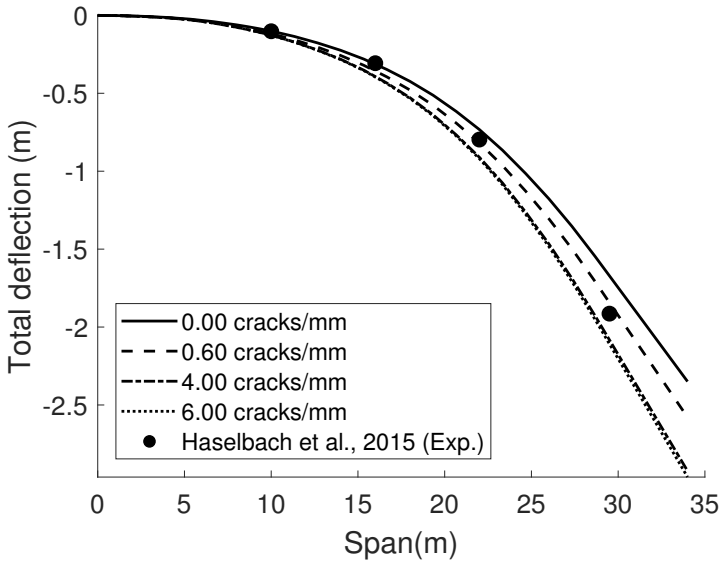

Figure 9: Comparison between the total blade deflection, u_{total}, obtained from the experiment test reported in [18] with the ones obtained from the proposed damage mechanics-based multiscale model for different values of the off-axis crack density.

Furthermore, a similar behavior is also observed in Fig. 10, where the effects of the off-axis cracks on the blade displacements, u, and curvatures, r, in the edge-wise, flap-wise, and torsional directions of the blade (i.e., $u_{edgewise}$, $u_{flapwise}$, $u_{torsional}$, $r_{edgewise}$, $r_{flapwise}$, and $r_{torsional}$) are presented. As shown in Fig. 10, the different displacements and curvatures of the blade also increase as the off-axis crack density increases until the saturation condition is achieved. These effects of the off-axis cracks seem to be significant for most of displacements and curvatures of the blade except for the torsional curvature, in which there is no appreciable change with the increase in ρ_k (see Fig. 10-f).

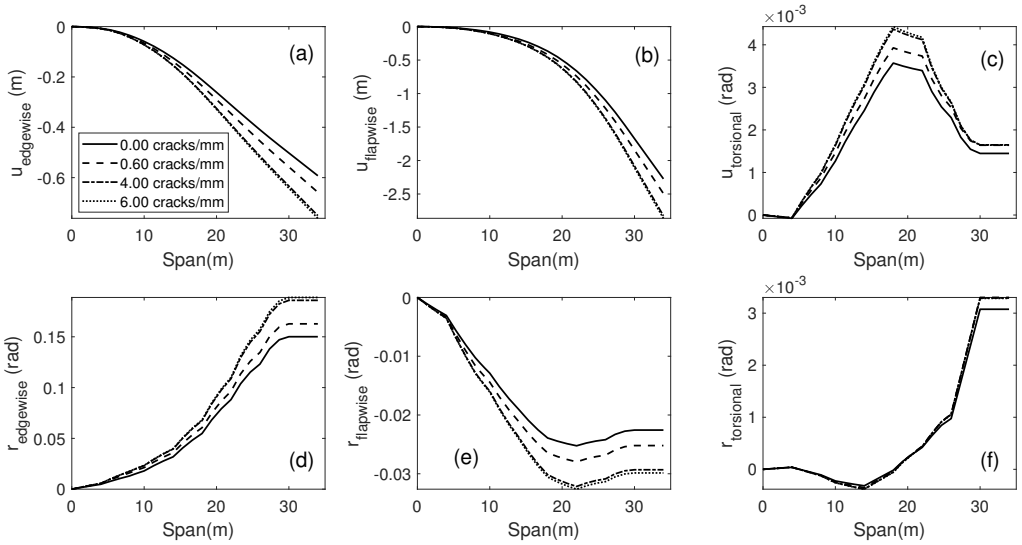

Figure 10: Effect of off-axis crack density on the degradation of: a) edge-wise deflection; b) flap-wise deflection; c) torsional displacement; d) edge-wise curvature; e) flap-wise curvature; and f) torsional curvature of the blade.

Additionally, as observed in Fig. 9, the total deflections of the blade for different values of ρ_k estimated using the proposed damage mechanics-based multiscale model are consistent with the total deflections obtained from the static test reported in [18]. This can be concluded because the experimental deflection is between the minimum and maximum analytical deflections caused by off-axis cracks, which correspond to $\rho_k = 0$ crack/mm and the crack saturation condition respectively.

5 Discussion

The results presented in section 4 show that reliable estimations about the effect of off-axis cracks on the structural response of wind turbine blades can be obtained by using the proposed damage mechanics-based multiscale approach. In this section, an analysis about these results at the macro, subcomponent, and full-length scales is presented.

5.1 Material property degradation (macro-length scale)

Comparisons of the property degradation at the macro-length scale estimated using the damage mechanics model [7] implemented in the proposed multiscale approach and the experimental and analytical data reported in the literature showed a good agreement with each other (see section 4.1). By using this damage mechanics model, the effects of the off-axis cracks on the change in the mechanical properties of the material (i.e., Young's modules, shear modulus, and the Poisson's ratios) are accurately predicted for

different types of multidirectional symmetric laminates.

One of these effects is related to the laminate thickness and the number of damaged off-axis plies in the laminate. As shown in Fig 7, the thinner the laminate and the lower number of damaged off-axis plies in it, the lower the change in the material properties. The capability of the implemented damage mechanics model to predict this phenomenon is especially important when analyzing the behavior of wind turbine blades, whose laminate thickness and layups vary along the blade and at each region of the different cross-sections (e.g., spar caps, shear webs, etc.), as discussed in the next sections.

Another effect that can be predicted by the implemented damage mechanics model is the off-axis crack saturation condition that multidirectional laminates could experience under quasi-static and fatigue loading conditions, see example in Fig. 6-b. Under quasi-static loading conditions, the mechanical properties of the laminates change considerably for low values of the off-axis crack density; however, when the saturation condition of multiple off-axis cracks with near-regular spacing is achieved, the mechanical properties of the material tend to a stable-state in which no further significant changes occur [51, 50]. The capability of the implemented damage mechanics model to predict this phenomenon in laminates under quasi-static loading conditions was extensive demonstrated in [7].

Moreover, in the case of laminates under fatigue loading conditions, a similar saturation condition of the off-axis cracks has also been identified in several studies [2, 53, 1, 36, 37]. Normally, the off-axis cracks initiate and propagate in the laminate during the early stages of the fatigue lifetime causing the main drop of stiffness. However, as the applied number of cycles increases and the saturation condition is reached, the stiffness tends to a stable-state and new damages, such as delaminations, start developing [53, 37].

The evolution of the off-axis cracks as a function of the applied number of cycles has been recently modeled in [6, 16], in which this crack saturation condition has also been predicted. In fact, the damage mechanics model implemented in the proposed multiscale approach was used by Carraro et al. in [6] to account for the retribution of stresses as a result of the occurrence of off-axis cracks in laminates under fatigue. That is why the evolution model developed by Carraro et al. in [6] will be used in the second part of this work [8] for predicting the off-axis crack evolution in wind turbine blades under fatigue loading conditions.

In the next section, the effects of the damage at the macro-length scale discussed in this section on the structural response of the blade at the subcomponent-length scale are analyzed.

5.2 Cross-section stiffness degradation (subcomponent-length scale)

By using the proposed damage-based multiscale approach, the effects of the different matrix-crack-related phenomena developed at the macro-length scale, such as the laminate thickness effect and the crack saturation condition, on the structural response of the blade at the subcomponent-length scale are reflected.

An example of this can be observed in Fig. 8, where both the edge-wise and flap-wise stiffness of all analyzed cross-sections decrease as the off-axis crack density increases until a saturation condition is achieved. As the blade is made of several multidirectional laminates, this saturation condition at the subcomponent scale can be related to the saturation condition of the off-axis cracks at the macro-length scale discussed in the previous section. Following this damage connection between the different length scales, it would be interesting to analyze experimentally if the delaminations driven by tensional loads, as the ones found in skin and main spar flanges at the subcomponent-length scale in [43], also initiate and propagate when the off-axis crack saturation condition is reached (as at the macro-length scale [53, 37]). In addition, it would be also interesting to analyze how other types of damage presented in wind turbine blades [43], such as delaminations, adhesive joint failure, splitting along fiber, etc., contribute to the cross-section stiffness degradation.

Moreover, as shown in Fig. 8, the cross-section stiffness degrades differently along the blade. One of the factors that seems to affect this stiffness degradation level is the laminate thickness of the different cross-section regions. To analyze this factor, Fig. 11-a presents the laminate thickness of the different cross-section regions normalized with the maximum thickness of the corresponding region along the blade for the cross-sections analyzed in Fig. 8. As shown in Fig. 11-a, the 30m span cross-section has the lowest thickness in all cross-section regions compared with the other airfoil cross-sections (i.e., excluding the 0m span cross-section which has a tubular cross-section geometry), and, as shown in Fig. 8, it is the airfoil cross-section that degrades the least. This agrees with what was discussed in the previous section at the macro-length scale, in which the laminates with less thickness seem to be less degraded.

Furthermore, another factor that seems to affect the stiffness degradation level along the blade is the cross-section geometry. As shown in Fig. 8, the 0m span cross-section (i.e., the blade root) is the cross-section that degrades the least of all cross-sections. This may be due in part to the thickness of its cross-section regions, which are thin compared with the same regions in other cross-sections (except for the leading-edge (LE) which, as shown in Fig. 5, is a small region in the cross-section and thereby does not affect considerably its stiffness). Moreover, the stiffness degradation level of this cross-section seems to be also affected by its geometry, which is tubular and, therefore, can provide a higher stiffness than airfoil geometries.

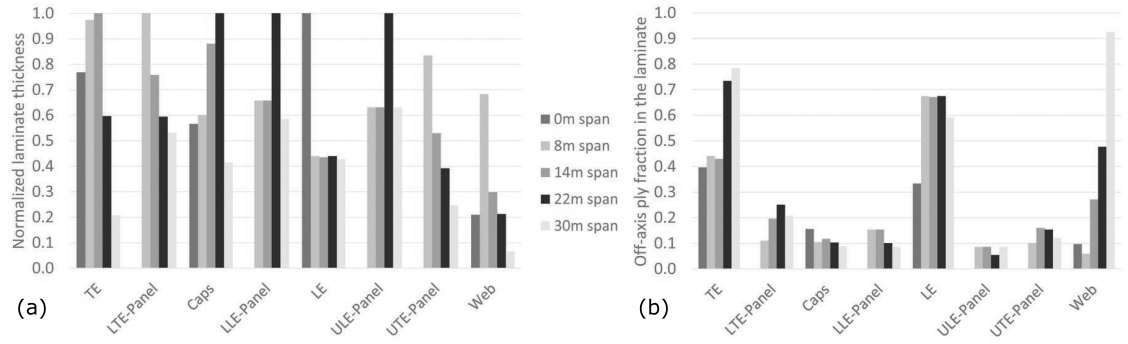

Figure 11: (a) Normalized laminate thickness and (b) off-axis ply fraction in the laminate for the different cross-section regions: spar caps (Caps), shear webs (Webs), leading-edge (LE), trailing-edge (TE), lower and upper trailing-edge panels (LTE-Panel and UTE-Panel respectively), and lower and upper leading-edge panels (LLE-Panel and ULE-Panel respectively).

In addition, another factor that might affect this stiffness degradation level is the number of damaged plies in the different cross-section regions. However, this variable seems not to influence as much as, for example, the laminate thickness. This can be deducted from Fig. 11-b, which presents the fraction of off-axis plies (which are also assumed damaged in this work, see section 3.2) in the different regions of the cross-sections analyzed in Fig. 8. One example of this is the 30m span cross-section, which has the highest number of off-axis plies in the shear webs and in the trailing-edge, and it is the airfoil cross-section whose stiffness is the least degraded, see Fig. 8. Another example of this is the 8m span cross-section, whose percentage of off-axis plies in all cross-section regions is lower or comparable to the ones from the other cross-sections; however, it is one of the cross-sections that degrades the most.

On the other hand, as shown in Fig. 8, the cross-section stiffness degrades more in the flap-wise direction than in the edge-wise direction. This may due to the area moment of inertia of each cross-section because the centroid of many of the cross-section regions (e.g., leading-edge, trailing-edge, leading-edge panels, and trailing-edge panels) are located farther from the y-axis than from the x-axis causing that the area moment of inertia around the y-axis is higher than the one around the x-axis. Consequently, the stiffness in the edge-wise direction becomes higher than the one in the flap-wise direction.

In the next section, the effects of the damage at the macro and subcomponent-length scales on the structural response of the blade at the full-length scale are analyzed.

5.3 Blade stiffness degradation (full-length scale)

The ability of the proposed damage mechanics-based multiscale approach for wind turbine blades to predict reliable estimations about the effect of the damage developed at the macro-length scale on the structural response of the blade at the full-length scale is

demonstrated in section 4.2.

As discussed in the previous sections, the increasing of off-axis cracks causes a degradation in both the material properties and the cross-section stiffness until a saturation condition is achieved. These damage effects are also reflected in the blade response at the full-length scale (see Figs. 9 and 10), in which the deflections, torsional displacements, and curvatures of the blade increase with the increase of the off-axis crack density until the saturation condition is reached, from which no more appreciable changes occur.

Note that the blade displacements and curvatures when the saturation state is achieved would correspond to the maximum blade displacements and curvatures caused by the occurrence of off-axis cracks because the same crack density was assumed for all off-axis plies. In this sense, for example, the increase in the deflection between the undamaged state and the maximum one obtained when the saturation condition is reached corresponds to 28.56% in the edge-wise direction and 25.90% in the flap-wise direction, according to the results showed in Figs. 10-a and 10-b respectively.

These results seem to be consistent with the ones reported by Mortesano et al. in [32], in which the effects of the off-axis crack evolution in different regions of a wind turbine blade under quasi-static loading conditions were estimated combining computational micromechanics and continuum damage mechanics in a 3D finite element model. In this work [32], an additional flap-wise deflection of approximately 10% was found under the applied loading conditions; however, the crack saturation state was not reached in all off-axis plies in the blade at the end of the numerical model, meaning that even higher flap-wise deflections could be reached.

The possibility of estimating the maximum blade deflection caused by the presence of off-axis cracks in the blade may be important during the design of these structures because it would allow predicting the occurrence of possible collisions with the tower, or possible instabilities, such as local or global buckling; which are, in fact, design requirements requested by current standards [21] and certification guidelines [13]. However, it must be also considered, among other factors, the off-axis cracks evolution in the wind turbine blade under fatigue loading conditions in order to make more reliable and accurate designs, as analyzed in the second part of this work [8].

On the other hand, the reliability of the predictions obtained from the proposed multiscale approach can be observed in Fig. 9, in which a comparison between the estimated total deflections of the blade as a function of the off-axis crack density and the experimental deflection reported in [18] is presented. As shown in Fig. 9, the analytical and experimental results are consistent each other because the experimental deflection is located between the minimum estimated deflection corresponding to the undamaged state of the blade and the maximum one corresponding to the off-axis crack saturation state. This might indicate that, under the applied loading conditions, the real blade

could experience a degradation of its stiffness as a result of the development of off-axis cracks.

Nevertheless, it is worth noting that some differences between the analytical and experimental results can occur because the modeled blade layup was altered by assuming symmetric multidirectional laminates, which could provide some changes in the estimated blade stiffness. In addition, other factors that could also induce additional changes in the predicted blade behavior, such as the occurrence of both adhesive joints and other damage types, were also omitted.

Finally, the proposed damage mechanics-based approach is an efficient alternative to 3D finite element models for structural analysis of wind turbine blades because a 2D finite-element-based cross-section analysis is carried out instead. This efficiency of the proposed approach is demonstrated in the second part of this work [8], where the effects of applied loading cycles obtained from time series analyses on the initiation and propagation of the off-axis cracks in wind turbine blades are studied, along with the fatigue structural response of the blade itself.

6 Conclusions

In this paper, a new damage mechanics-based multiscale approach implemented by using a 2D finite-element-based cross-section model was proposed for analyzing and predicting the fatigue behavior of composite wind turbine blades. The relevance of this approach lies in considering the natural damage evolution of composite materials on the structural response of the blades, which is expected to improve the accuracy and reliability in the fatigue-life predictions of these structures.

As a first step in the implementation of this multiscale approach, the effect of off-axis cracks on the structural response of the blade was analyzed. Based on this analysis, it was found that the stiffness of the different cross-sections and, consequently the stiffness of the entire blade, decreases as the number of off-axis cracks increases. However, when a saturation condition of the off-axis cracks is reached at the macro-length scale, a stoppage in the degradation of the blade stiffness at the full-length scale is also reached. Furthermore, it was found that the degradation level of the blade stiffness varied along the blade and in the flap-wise and edge-wise directions. This variation in the stiffness degradation level seemed to be affected by mainly the cross-section geometry and the laminate thickness of the different cross-section regions.

Moreover, it was shown that reliable predictions can be obtained with the proposed multiscale model, which was demonstrated doing a comparison between the estimated structural response of the blade and the one obtained from experiments at the full-length scale. Furthermore, this approach also provides a high computational efficiency because 2D finite-element-based cross-section models are carried out as an alternative of

3D finite element models. The importance of this saving in computational resources is demonstrated in the second part of this work, in which the evolution of the off-axis cracks in the blade under fatigue loading conditions, and the blade response itself, are analyzed. In fact, the potential of implementing 2D finite-element-based cross-section analysis in damage mechanics-based multiscale approaches will be even more relevant when other damage types, such as delaminations, fiber-related damage, and off-axis cracks in backing bundles, are included in the model.

Acknowledgements

This work was supported by the Danish Centre for Composite Structures and Materials for Wind Turbines (DCCSM), grant no. 09-067212 from the Danish Strategic Research Council.

References

[1] S. Adden and P. Horst. Stiffness degradation under fatigue in multiaxially loaded non-crimped-fabrics. *International Journal of Fatigue*, 32(1):108–122, 2010.

[2] J. Bartley-Cho, S.G. Lim, H.T. Hahn, and P. Shyprykevich. Damage accumulation in quasi-isotropic graphite/epoxy laminates under constant-amplitude fatigue and block loading. *Composites Science and Technology*, 58(9):1535–1547, 1998.

[3] J.P.A.A. Blasques, R.D. Bitsche, V. Fedorov, and B.S. Lazarov. Accuracy of an efficient framework for structural analysis of wind turbine blades. *Wind Energy*, 19(9):1603–1621, 2016.

[4] J.P.A.A. Blasques and M. Stolpe. Multi-material topology optimization of laminated composite beam cross sections. *Composite Structures*, 94(11):3278–3289, 2012.

[5] V.N. Bulsara, R. Talreja, and J. Qu. Damage initiation under transverse loading of unidirectional composites with arbitrarily distributed fibers. *Composites Science and Technology*, 59(5):673–682, 1999.

[6] P.A. Carraro, L. Maragoni, and M. Quaresimin. Prediction of the crack density evolution in multidirectional laminates under fatigue loadings. *Composites Science and Technology*, 145:24–39, 2017.

[7] P.A. Carraro and M. Quaresimin. A stiffness degradation model for cracked multidirectional laminates with cracks in multiple layers. *International Journal of Solids and Structures*, 58:34–51, 2015.

[8] O.G. Castro and K. Branner. Damage mechanics-based multiscale model for wind turbine blades under fatigue: Part 2. prediction of off-axis crack evolution. *In manuscript.*

[9] O.G. Castro, K. Branner, and P. Brøndsted. *Fatigue strength of composite wind turbine blade structures.* PhD thesis, Denmark, 2018.

[10] O.G. Castro, P.A. Carraro, L. Maragoni, and Quaresimin. Fatigue damage evolution in unidirectional glass/epoxy composites under a longitudinal cyclic load. *Polymer Testing. Submitted.*

[11] O.G. Castro, M. Lennie, K. Branner, G. Pechlivanoglou, C. Nayeri, and C.O. Paschereit. Comparing fatigue life estimations of composite wind turbine blades using different fatigue analysis tools. *Proceedings of the 20th International Conference on Composite Materials*, 2015.

[12] J. Degrieck and W. Van Paepegem. Fatigue damage modeling of fibre-reinforced composite materials: Review. *Applied Mechanics Reviews*, 54(4):279–300, 2001.

[13] Rotor blades for wind turbines. Standard, DNV GL, 2015.

[14] V. Fedorov, C. Berggreen, S. Krenk, and K. Branner. *Bend-Twist Coupling Effects in Wind Turbine Blades.* PhD thesis, Denmark, 2012.

[15] V. Giavotto, M. Borri, P. Mantegazza, and G. Ghiringhelli. Anisotropic beam theory and applications. *Computers and Structures*, 16(1-4):403–413, 1983.

[16] J. Glud, J. Dulieu-Barton, O.T. Thomsen, and L.C.T. Overgaard. A stochastic multiaxial fatigue model for off-axis cracking in frp laminates. 2017.

[17] P. Gudmundson and W.L. Zang. An analytic model for thermoelastic properties of composite laminates containing transverse matrix cracks. *International Journal of Solids and Structures*, 30(23):3211–3231, 1993.

[18] P.U. Haselbach and K. Branner. *Effect of trailing edge damage on full-scale wind turbine blade failure.* ICCM20 Secretariat, 2015.

[19] Z. Hashin. Analysis of cracked laminates - a variational approach. *Mechanics of Materials*, 4(2):121–136, 1985.

[20] Z. Hashin and A. Rotem. A fatigue failure criterion for fiber reinforced materials. *Journal of Composite Materials*, 7(4):448 – 464, 1973.

[21] Wind turbines part 1 design requirements. Standard, IEC, 2005-2008.

[22] Y.J. Jang, C.W. Choi, J.H. Lee, and K.W. Kang. Development of fatigue life prediction method and effect of 10-minute mean wind speed distribution on fatigue life of small wind turbine composite blade. *Renewable Energy*, 79(1):187–198, 2015.

[23] K.M. Jespersen, J. Zangenberg, T. Lowe, P.J. Withers, and L.P. Mikkelsen. Fatigue damage assessment of uni-directional non-crimp fabric reinforced polyester composite using x-ray computed tomography. *Composites Science and Technology*, 136:94–103, 2016. CC BY-NC-ND 3.0.

[24] R.M. Jones. *Mechanics of composite materials*. Taylor & Francis,, 1999.

[25] M. Kashtalyan and C. Soutis. Modelling off-axis ply matrix cracking in continuous fibre-reinforced polymer matrix composite laminates. *Journal of Materials Science*, 41(20):6789–6799, 2006.

[26] D.G. Katerelos, L.N. McCartney, and C. Galiotis. Effect of off-axis matrix cracking on stiffness of symmetric angle-ply composite laminates. *International Journal of Fracture*, 139(3-4):529–536, 2006.

[27] D.T.G. Katerelos, M. Kashtalyan, C. Soutis, and C. Galiotis. Matrix cracking in polymeric composites laminates: Modelling and experiments. *Composites Science and Technology*, 68(12):2310–2317, 2008.

[28] C. Kong, T. Kim, D. Han, and Y. Sugiyama. Investigation of fatigue life for a medium scale composite wind turbine blade. *International Journal of Fatigue*, 28(10):1382–1388, 2006.

[29] S. Li, C.V. Singh, and R. Talreja. A representative volume element based on translational symmetries for fe analysis of cracked laminates with two arrays of cracks. *International Journal of Solids and Structures*, 46(7-8):1793–1804, 2009.

[30] P. Lundmark and J. Varna. Constitutive relationships for laminates with ply cracks in in-plane loading. *International Journal of Damage Mechanics*, 14(3):235–259, 2005.

[31] L.N. McCartney. Theory of stress transfer in a $0^\circ - 90^\circ - 0^\circ$ cross-ply laminate containing a parallel array of transverse cracks. *Journal of the Mechanics and Physics of Solids*, 40(1):27–68, 27–68, 1992.

[32] J. Montesano, H. Chu, and C. V. Singh. Development of a physics-based multi-scale progressive damage model for assessing the durability of wind turbine blades. *Composite Structures*, 141:50–62, 2016.

[33] J.A. Nairn and D.A. Mendels. On the use of planar shear-lag methods for stress-transfer analysis of multilayered composites. *Mechanics of Materials*, 33(6):335–362, 2001.

[34] R.P.L. Nijssen and D.R.V. Van Delft. Alternative fatigue formulations for variable amplitude loading of fibre composites for wind turbine rotor blades. *Esis Publication*, 32:563–574, 2003.

[35] M. Quaresimin. A damage-based approach for the fatigue design of composite structures. *Iop Conference Series: Materials Science and Engineering*, 139(1):012006, 2016.

[36] M. Quaresimin and P.A. Carraro. Damage initiation and evolution in glass/epoxy tubes subjected to combined tension-torsion fatigue loading. *International Journal of Fatigue*, 63:25–35, 2014.

[37] M. Quaresimin, P.A. Carraro, L.P. Mikkelsen, N. Lucato, L. Vivian, P. Brøndsted, B.F. Sørensen, J. Varna, and R. Talreja. Damage evolution under cyclic multiaxial stress state: A comparative analysis between glass/epoxy laminates and tubes. *Composites Part B: Engineering*, 61:282–290, 2014.

[38] K.L. Reifsnider. Some fundamental aspects of the fatigue and fracture response of composite materials. 1977.

[39] K.L. Reifsnider. *Fatigue of composite materials*, volume 4. Elsevier„ 1991.

[40] M.M. Shokrieh and L.B. Lessard. Progressive fatigue damage modeling of composite materials, part i: Modeling. *Journal of Composite Materials*, 34(13):1056–1080, 2000.

[41] M.M. Shokrieh and R. Rafiee. Simulation of fatigue failure in a full composite wind turbine blade. *Composite Structures*, 74(3):332–342, 2006.

[42] C.V. Singh and R. Talreja. A synergistic damage mechanics approach for composite laminates with matrix cracks in multiple orientations. *Mechanics of Materials*, 41(8):954–968, 2009.

[43] B.F. Sørensen, E. Jorgensen, C.P. Debel, F.M. Jensen, H.M. Jensen, T.K. Jacobsen, and K. Halling. Improved design of large wind turbine blade of fibre composites based on studies of scale effects (phase 1). summary report, 2004.

[44] R. Talreja. Multi-scale modeling in damage mechanics of composite materials. *Journal of Materials Science*, 41(20):6800–6812, Oct 2006.

[45] H.S. Toft and J.D. Sørensen. Probabilistic fatigue design of composite material for wind turbine blades. *Applications of Statistics and Probability in Civil Engineering -proceedings of the 11th International Conference on Applications of Statistics and Probability in Civil Engineering*, pages 1185–1192, 2011.

[46] J. Tong, F.J. Guild, S. L. Ogin, and P.A. Smith. On matrix crack growth in quasi-isotropic laminates - i. experimental investigation. *Composites Science and Technology*, 57(11):1527–1535, 1997.

[47] J. Tong, F.J. Guild, S.L. Ogin, and P.A. Smith. On matrix crack growth in quasi-isotropic laminates - ii. finite element analysis. *Composites Science and Technology*, 57(11):1537 – 1545, 1997.

[48] C.L. Tsai and I.M. Daniel. The behavior of cracked cross-ply composite laminates under shear loading. *International Journal of Solids and Structures*, 29(24):3251–3267, 1992.

[49] J. Varna, L.A. Berglund, A. Krasnikovs, and A. Chihalenko. Crack opening geometry in cracked composite laminates. *International Journal of Damage Mechanics*, 6(1):96–118, 1997.

[50] J. Varna, R. Joffe, N.V. Akshantala, and R. Talreja. Damage in composite laminates with off-axis plies. *Composites Science and Technology*, 59(14):2139–2147, 1999.

[51] J. Varna, R. Joffe, N.V. Akshantala, and R. Talreja. Damage in composite laminates with off-axis plies. *Composites Science and Technology*, 59(14):2139–2147, 1999.

[52] J. Wang, Z. Huang, and Y. Li. Computation method on fatigue life of a full composite wind turbine blade. *Asia-pacific Power and Energy Engineering Conference*, 2010.

[53] A.W. Wharmby and F. Ellyin. Damage growth in constrained angle-ply laminates under cyclic loading. *Composites Science and Technology*, 62(9):1239–1247, 2002.

[54] J. Zangenberg, P. Brøndsted, and R. Ostergaard. *The effects of fibre architecture on fatigue life-time of composite materials*. PhD thesis, Denmark, 2013.

[55] J.Q. Zhang and K.P. Herrmann. Stiffness degradation induced by multilayer intralaminar cracking in composite laminates. *Composites Part A-applied Science and Manufacturing*, 30(5):683–706, 1999.

[56] L. Zhuang, R. Talreja, and J. Varna. Tensile failure of unidirectional composites from a local fracture plane. *Composites Science and Technology*, 133:119–127, 2016.

CHAPTER 8

Paper 3

Submitted:
Oscar Castro, Paolo A. Carraro, Lucio Maragoni and Marino Quaresimin. *Fatigue damage evolution in unidirectional glass/epoxy composites under a cyclic load.* Polymer Testing (2018)

Fatigue damage evolution in unidirectional glass/epoxy composites under a cyclic load

Oscar Castro[+], Paolo A. Carraro[*], Lucio Maragoni[*] and Marino Quaresimin[*]

[+]DTU Wind Energy, Technical University of Denmark, Frederiksborgvej 399, 4000 Roskilde, Denmark. E-mail: osar@dtu.dk

[*]Department of Management and Engineering, University of Padova, Italy. E-mail: paoloandrea.carraro@unipd.it , lucio.maragoni@gmail.com , marino.quaresimin@unipd.it

Abstract

In the present work, the initiation and progression of the fiber damage in on-axis UD glass/epoxy materials under fatigue loading conditions are studied. Uniaxial tension-tension fatigue tests at different load levels were carried out to monitor the fiber damage evolution through the fatigue lifetime. The damage evolution was quantified by initial fiber breaks, evolution of the density of broken fibers, and fragmentation progression. Through qualitative and quantitative analyses, it is shown how the fiber damage evolution depends on the number of cycles, the applied load level, and the number of broken fibers during the first cycle. In addition, it is also analyzed how the damage affects the stiffness variation of the material.

Keywords: fatigue damage, damage evolution, glass/epoxy materials, broken fibers

1 Introduction

Fatigue life estimation of composite materials has been a demanding research field in the last 40 years, as most structures made partially or totally of these materials in the industry, such as wind turbine blades, are subjected to cyclic loadings. These composite structures are mainly made of multidirectional laminates consisting of unidirectional (UD) plies with different orientations. The stiffness degradation of these laminates is principally caused by the onset and propagation of matrix cracks in the off-axis UD plies together with the initiation and propagation of delaminations between the different plies. Nevertheless, their structural load-bearing capacity is determined by the on-axis UD plies, which have higher fatigue strength than the off-axis ones. Accordingly, if the

objective is to predict the fatigue stiffness degradation and failure of multidirectional laminates, it is necessary to predict [25]

- the initiation and propagation of off-axis cracks (the crack density evolution),
- the initiation and propagation of delaminations induced by off-axis cracks, and
- the failure of the fibers of the load-bearing plies.

Carraro et al. [4] presented a procedure for predicting the crack density evolution, whereas an approach and preliminary results for the prediction of delamination onset were shown in [5]. In the present work, the attention is focused on the fiber-related damage mechanisms under on-axis fatigue loadings, as a fundamental step toward the prediction of the final fatigue life of a multidirectional laminate.

The progressive fiber failure process under cyclic loads is a rather complex issue, mainly when considering that, in multidirectional laminates, this process interacts with the damage in the off-axis plies such as transverse cracks and delaminations. Therefore, for the definition of a reliable predictive tool for such a complicated phenomenon, it is first necessary to understand how the different fiber-related damage mechanisms initiate and evolve until reaching the final failure.

The on-axis fatigue behavior of UD laminates under tension-tension loading conditions has been studied over many years [29, 8, 9]. The different damage mechanisms involved in this type of material under these loading conditions have been identified qualitatively through experiments in these studies. Damage in the on-axis UD laminates initiates from the first applied cycle when multiple fiber breaks occur. These breaks can occur in different fibers (isolated) or along individual fibers (i.e., fragmentation) due to the statistical strength distribution of the fibers. When the fiber/matrix interface is relatively weak (e.g., in some glass/epoxy materials), fiber/matrix debondings initiate at the fiber crack tip due to the high shear stress concentration on the fiber in the vicinity of the break. The debonds start growing with the number of cycles redistributing in this way the load in the neighboring fibers. When a weak segment in one of the neighboring fibers is overloaded, it may fail and give rise to new debonds and so on. In some cases, isolated fiber breaks coalesce due to matrix cracks. The coalescent mechanism has led to the belief that the final failure comes from a critical fracture plane within a localized zone caused by coalescence between many isolated fiber breaks [7, 1]. However, there is no experimental evidence so far that proves that this is, in fact, the damage mechanism that leads to the final failure in on-axis UD composites under fatigue loading conditions.

Nevertheless, based on the previous damage description of the UD composites, it is clear that the progressive fiber breaking is an important phenomenon in the failure process. This is why this topic received quite a lot of attention and was studied by

several researchers since the 1970s, considering the behavior of single and multiple fibers embedded in a matrix. The breaking progression of single fibers under static loadings has been analyzed experimentally [23, 21, 32, 18] and analytically [15, 6, 16] in different studies. An important analytical study was that developed by Hui et al. [16], in which exact equations for the evolution of fiber fragments in single fibers loaded under increasing strain, whose strength follows a Weibull distribution, were developed.

However, as fibers are not used as single fibers in real composites but as multiple fibers embedded in a matrix, different experimental [14, 19, 30, 3, 1, 28] and analytical [27, 2, 14, 22] studies have been carried out in order to understand how the fiber breaking initiates and evolves in a group of fibers until reaching the final failure by considering the effect of the fiber interaction. Smith [27] proposed, for example, a probabilistic model that relates the Weibull probability strength distribution function of single fibers with the probability of failure of a composite material made of multiple parallel fibers subjected to quasi-static tension loading conditions. However, Aroush et al. [1] showed by experimental observations with specimens made of 125 single fibers that the model proposed by Smith [27] overestimates the critical number of broken fibers needed to lead the final failure of the material. Moreover, the maximum number of fiber breaks in a cluster of broken fibers observed by Aroush et al. in [1] agreed well with the ones observed by Swolfs et al. in [28], where a total of about 5500 UD fibers in the cross-section of $[90/0]_s$ laminates were analyzed.

All previous studies focused on the fiber-breaking progression of the on-axis UD composites under quasi-static loading conditions; fewer studies have considered the fiber-related damage progression under fatigue loading conditions [24, 10, 11, 12, 13, 17, 33]. In recent years, for example, Garcea et al. [10, 11, 12, 13] have worked on the evaluation of the fiber-related damage evolution in notched $[90/0]_s$ carbon/epoxy laminates by using synchrotron X-ray computed tomography. From this evaluation, it was found that only few fibers failed in the bulk composite within the 0° plies, which normally occurred as isolated events rather than as clusters of broken fibers. It was showed, indeed, that most fibers failed along 0° ply splits originated at the notch tips, due mainly to the presence and failure of bridging fibers.

Moreover, Zangenberg et al. [33] established a damage progression scheme for UD non-crimp fabric (NCF) under fatigue tensile loading conditions. The NCF materials consisted of UD fiber bundles reinforced with off-axis backing fiber bundles to provide a higher strength, ease of handling, and lower manufacturing costs compared to pure UD fibers. Recently, the damage progression scheme established by Zangenberg et al. [33] was expanded by Jespersen et al. [17] based on observations made through a 3D x-ray computed tomography analysis. These observations showed that the fiber breaking phenomena were located mainly in regions where the 0° fibers intersect the backing bundles.

Although these studies provide valuable information for further improvements in the ability to predict the fiber-related damage in multidirectional laminates, it is still not clear how this type of damage evolves from the first cycle through the fatigue lifetime and leads, possibly, to the final failure. In addition, it is worth mentioning that the works cited above deal with non-purely UD configurations, also in the presence of a notch [10, 11, 12, 13], for which it was shown that the fiber-related damage in the bulk material was negligible. As a consequence, "the mechanism for fatigue fiber failure in the bulk composite, and its effect on residual strength is not understood" [12] at present, as well as its evolution from the first cycle to the final failure.

In this frame, the purpose of this work is to investigate the microscale fiber-related damage initiation and progression throughout the lifetime of plain on-axis UD glass/epoxy laminates under tension-tension fatigue loading conditions. For that, uniaxial fatigue tests under different load levels were carried out, monitoring with optical microscopy the microscale damage evolution throughout the fatigue life. The damage evolution was evaluated, both qualitatively and quantitatively, in terms of initial fiber breaks, evolution of the density of fiber breaks and fragmentation progression. As previously mentioned, gaining a clear understanding of these phenomena is fundamental for the development of reliable design tools. Accordingly, this work is meant as the first step toward the definition of a procedure for the prediction of fiber-related damage evolution and failure in UD and multidirectional laminates under cyclic loading.

2 Material and Methods

In the present study, unidirectional (UD) laminates made of glass UT-E500 fibers by Gurit and epoxy RIM-235 resin by Momentive, with lay-up $[0]_6$, were infused and tested. 17 mm wide, 195 mm long, and 1.8 mm thick specimens were obtained from panels of 200 x 300 mm fabricated by vacuum resin infusion, cured for three days at room temperature and then post-cured at $60°C$ for 12 hours. On both ends of the specimens, rectangular-shaped carbon-epoxy tabs with 30 mm length and thickness of 3 mm were bonded using epoxy adhesive.

The UD glass/epoxy specimens were tested under uniaxial tension-tension fatigue loading conditions using a MTS 858 hydraulic machine. The tests were performed in load control with maximum cyclic tensile stresses $\sigma_{x,max}$ of 200, 300, 320, and 340 MPa with an R-ratio (i.e., ratio between the minimum and maximum cyclic stress, $R = \sigma_{min}/\sigma_{min}$) of 0.05. The tests were repeated twice for each load level, except for $\sigma_{x,max} = 200MPa$ case, for which only one test was carried out.

The damage evolution of the material was monitored in terms of stiffness degradation and fiber breaks. The stiffness of the specimens was monitored using an

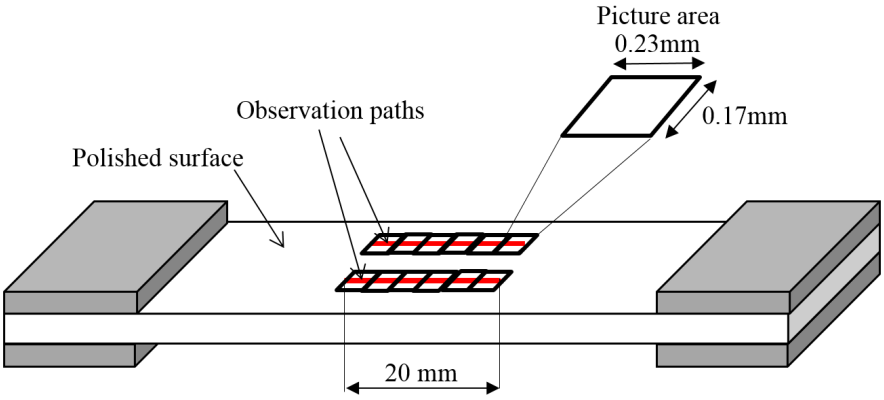

Figure 1: Schematic of the observation paths.

MTS632.29F-30 extensometer with a 25 mm initial length. In order to monitor the damage evolution in terms of fiber breaks, the top surface of the specimens was carefully polished. The polishing process started with P180 sandpaper and ended with a 0.1μm SiO_2 suspension. The choice of observing the damage development by means of surface microscopic analyses is due the fact that, only with an optical microscope, micro- and sub-microscale details, such as debonds and matrix micro-cracks and shear bands, can be revealed (see, for example, [26, 20]). On the other hand, this limits the observation to a surface and not a volume of the material, thus losing the 3D evolution of damage. This could be overcome by combining optical microscopy with computed tomography (CT) analyses, which were not carried out in the present work.

During the test, the load was regularly interrupted (i.e., 1, 10, 100, 1000, etc. cycles), and the specimen was removed from the hydraulic machine to be observed with an optical microscope. Around 150 pictures were taken on the polished surface at each interruption, each corresponding to small areas of 0.23 x 0.17 mm^2. The small areas were located along two 20 mm long observation paths, located far from the tabs, across the mid-length of the specimens (see Fig. 1). From the pictures, around 1000 fibers per specimen were analyzed and the number of initial fiber breaks, the evolution of the density of broken fibers, and the fragmentation evolution were quantified throughout the fatigue life.

3 Results and Discussions

In this section, the results obtained from the fatigue tests are analyzed from qualitative and quantitative points of view. In the qualitative analysis, different damage scenarios observed in terms of fiber breaks, fragmentation, increasing opening, matrix yielding, and debonding are described; whereas, in the quantitative analysis, a discussion about the stiffness and the evolution of the density of broken fibers during the fatigue life is presented.

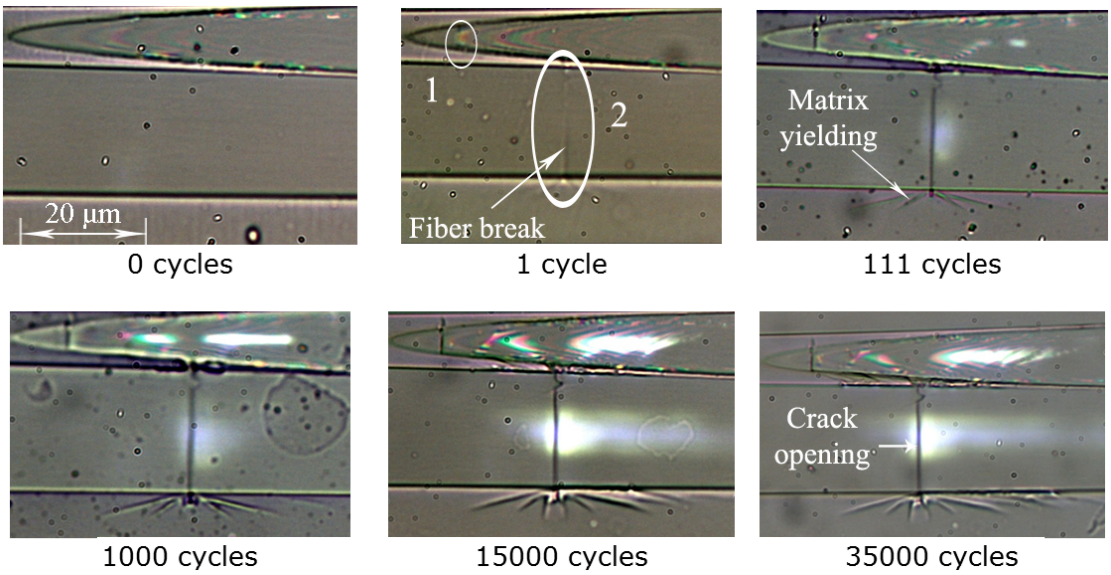

Figure 2: Material damage evolution under $\sigma_{x,max} = 300MPa$, specimen No 1.

3.1 Qualitative description of damage scenarios

The damage scenarios observed from the different specimens were in agreement with those described in [29, 8, 9]. For all specimens, the fatigue damage initiated during the first cycle when some fibers failed at the weakest locations (see Fig. 2-4). This fiber breaking occurred at applied maximum stresses lower than the static stress to failure of the fiber due to the statistical strength distribution.

Close to the fiber breaks, shear yielding or fiber/matrix debonding developed due to high shear stresses in the interface region. These progressive mechanisms result in a redistribution of stresses in the area close to the fiber break causing either arrest or continuation of the damage process depending on the applied load level.

For the lower load levels (i.e., $\sigma_{x,max} = 200MPa$ and $300MPa$)), matrix yielding was observed at the fiber crack tip (see Fig. 2). As shown in Fig. 2, the extension of the yielded zone, characterized by the presence of shear bands in the matrix, propagated along the fatigue life as a result of the energy dissipation, which also contributed to the increase of crack opening. In fact, as shown in Fig. 2, the fiber crack, initiated at the first cycle, became increasingly visible as the number of cycles increased. However, for lower load levels, no fiber/matrix debonding was observed throughout the fatigue life. This could indicate that the debonds stopped growing at a short distance from the fiber breaks because the threshold needed to continue propagating was not reached. As no debonds growing occurred, the local stresses in the neighboring fibers did not sensibly change and no, or few, new fiber breaks occurred (see Figs. 2 and 3).

In contrast, for higher load levels (i.e., $\sigma_{x,max} = 320MPa$ and $340MPa$), it was possible to observe fiber/matrix debonds growing from some fiber breaks right after the

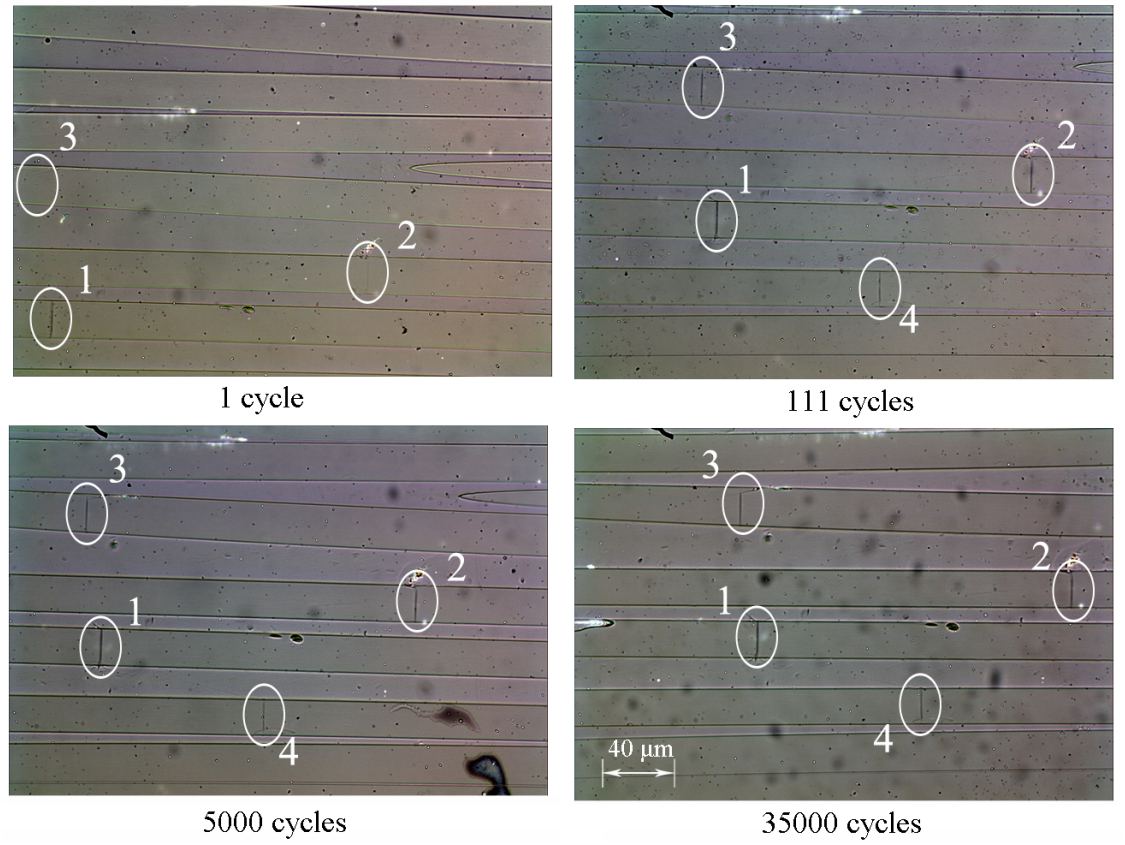

Figure 3: Material damage evolution under $\sigma_{x,max} = 300MPa$, specimen No 1.

first cycle, in addition to the matrix yielding at the tip of the fiber break (see Fig. 4). As the debonds grew, a redistribution of the stresses in the neighbor fibers took place, and some of them failed when the local strength of their weak segments was exceeded (see Fig. 4). Moreover, it was observed that weak segments along the fibers were sometimes related to the presence of local defects (see examples in Fig. 5).

Furthermore, even though the propagation rate of the debonding was not quantified in this study, it was observed that the debond propagation rate was not uniform. For example, different debond lengths between the two crack tips of the same broken fiber were observed in some cases as well as a non-axisymmetric debond growing in individual fibers (see Fig. 6). This can be because the debond growth depends on the local interfacial properties between the fibers and the matrix, which can vary statistically from one location to another, as well as on the position of the neighboring fibers. In fact, as discussed in [34], the shorter the distance between the broken fiber and the neighboring fiber, the higher the energy release rate (ERR), and, as a consequence, the debond lengths can reach higher values. This can be seen in the fiber fragmented twice in Fig. 6 and the one also fragmented twice in Fig. 7, in which the

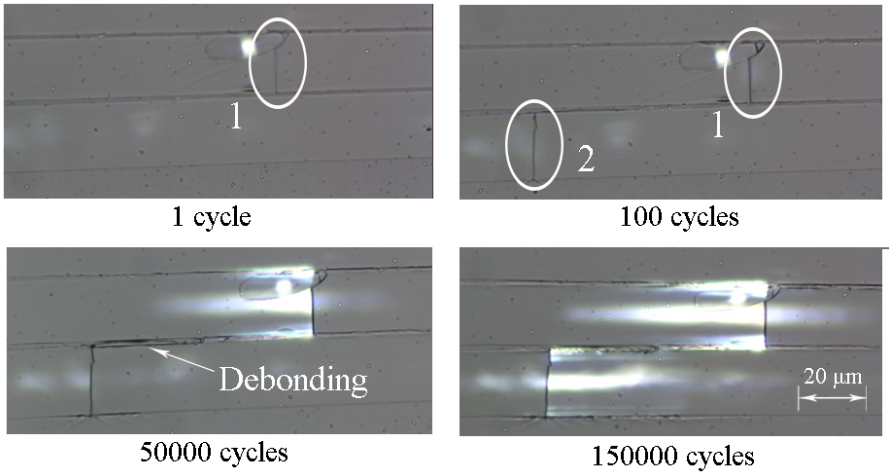

Figure 4: Material damage evolution under $\sigma_{x,max} = 320MPa$, specimen No 2.

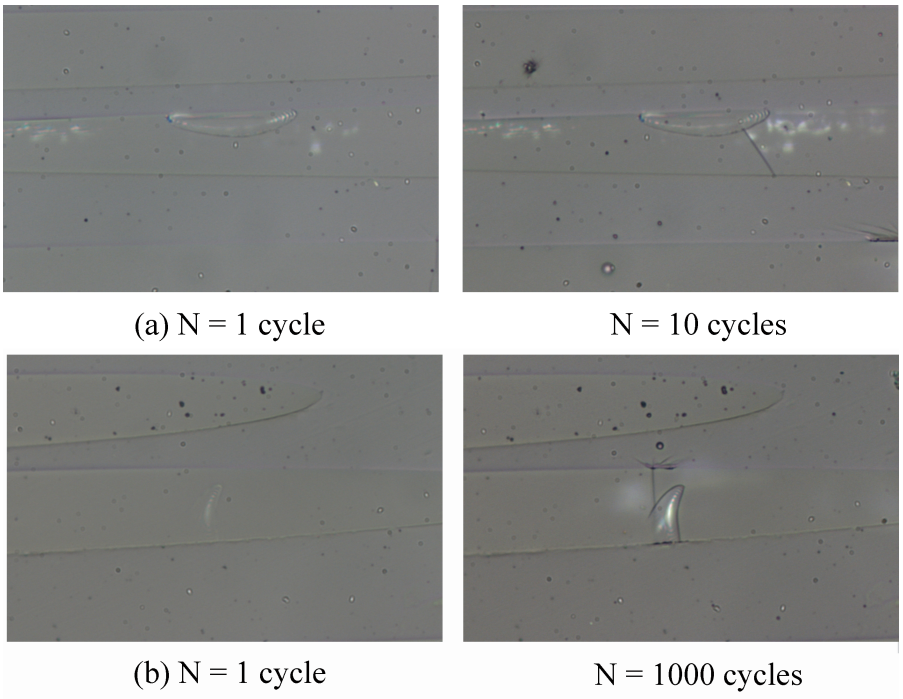

Figure 5: Effect of fiber defects on the probability of fiber breaks.

debonds extended from the two breaks are longer on the side near the neighboring fibers than on the opposite side where there is a high matrix content.

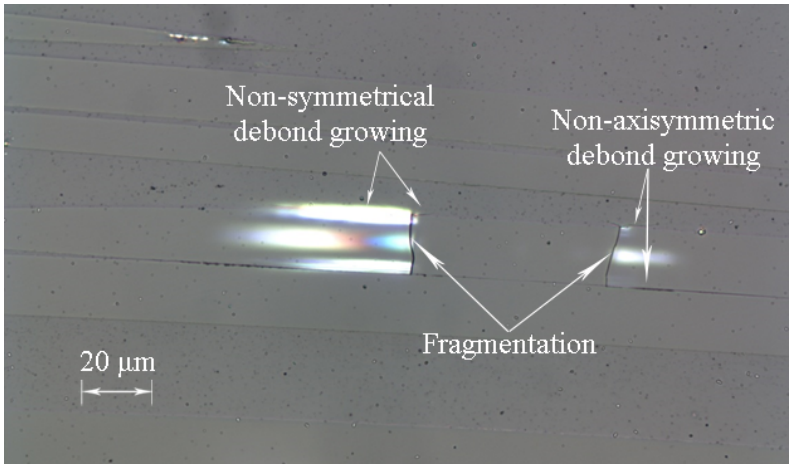

Figure 6: Fiber fragmentation and irregular debond growing.

As shown in figures 6 and 7, another observed damage mechanism was the fragmentation of single fibers. However, this phenomenon was not so common, and the damage was seen to progress mainly by the failure of new fibers, as quantified in the next section.

Moreover, in some cases, a tendency of crack coalescence was also observed in correspondence of neighboring fiber breaks, and a short debond grew from the fiber crack tip (see Fig. 7). This agrees with what was discussed in [35], where it was found that short debond cracks tend to kink out into the matrix and grow toward the neighboring fibers, thus enhancing the local stress and causing possible breakages in the neighboring fibers (as shown in Fig. 7).

The coalescence of isolated fiber breaks has been considered in previous studies [1, 28] as one of the main damage mechanisms that lead to the final failure of the material. Aroush et al. in [1] showed, for example, that a critical fracture plane is created in specimens made of 125 single fibers when a critical cluster of broken fiber coalesce, which triggers the catastrophic failure of the composite. However, it is still not clear how many coalescence fiber breaks are needed to create the critical fracture plane. In fact, it is not clear either if this critical fracture plane is the final failure mechanism or if it leads to another more critical mechanism (e.g., instable splitting) that does lead to the final failure. Unfortunately, in this work, it was not possible to identify the final failure mechanism because the evaluated coupon specimens failed with parallel splitting in the fiber direction initiated from the tabs as a result of the high-stress concentrations in these regions.

In addition to all these observations, it was also found that the propagation of the

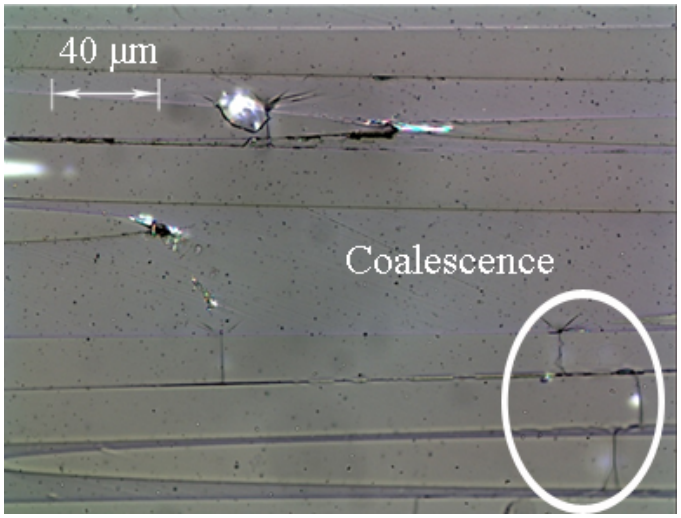

Figure 7: Coalescence of fiber breaks.

damage was not uniform along the observation region. In fact, the damage propagated easier in regions with high concentration of matrix, especially in those regions near the scrim fiber used to hold the primary longitudinal fibers in place during fabrication and handling. This can be seen in Fig. 8, which shows a comparison between the damage progression in regions close and far to the scrim fiber for different load levels. As shown in Fig. 8, under the same load level, the number of fiber breaks, fragmented fibers, coalescence of fiber breaks, and debond lengths is always higher in those regions near the scrim fiber. These observations agree well with those presented in [17] regarding UD non-crimp fabric reinforced polyester composites, in which it was also found that the fiber breaks typically emanate from the matrix-rich regions close to the backing fibers.

As shown in Fig. 8(a) and 8(c), in the regions close to the scrim fibers, the debonds tend to grow faster toward the matrix-rich areas where the scrim fibers are located. The increase of the local stresses due to this fast debond growing, along with stress perturbation due to the out-of-plane fiber waviness in these regions, is reasonably the main reasons for the greater number of fiber breaks, fragmented fibers, and coalescence of fiber breaks.

3.2 Quantitative analysis of damage progression

From the qualitative analysis reported in the previous section, it is clear that the number of fiber breaks during the first cycle and its evolution during the fatigue lifetime are significant parameters to be considered in predictive models for UD glass/epoxy composites under fatigue loading. In this section, a quantification of the initial fiber breaks and the progressive appearance of new breakages both in different fibers (isolated) and along individual fibers (i.e., fragmentation) during the fatigue life

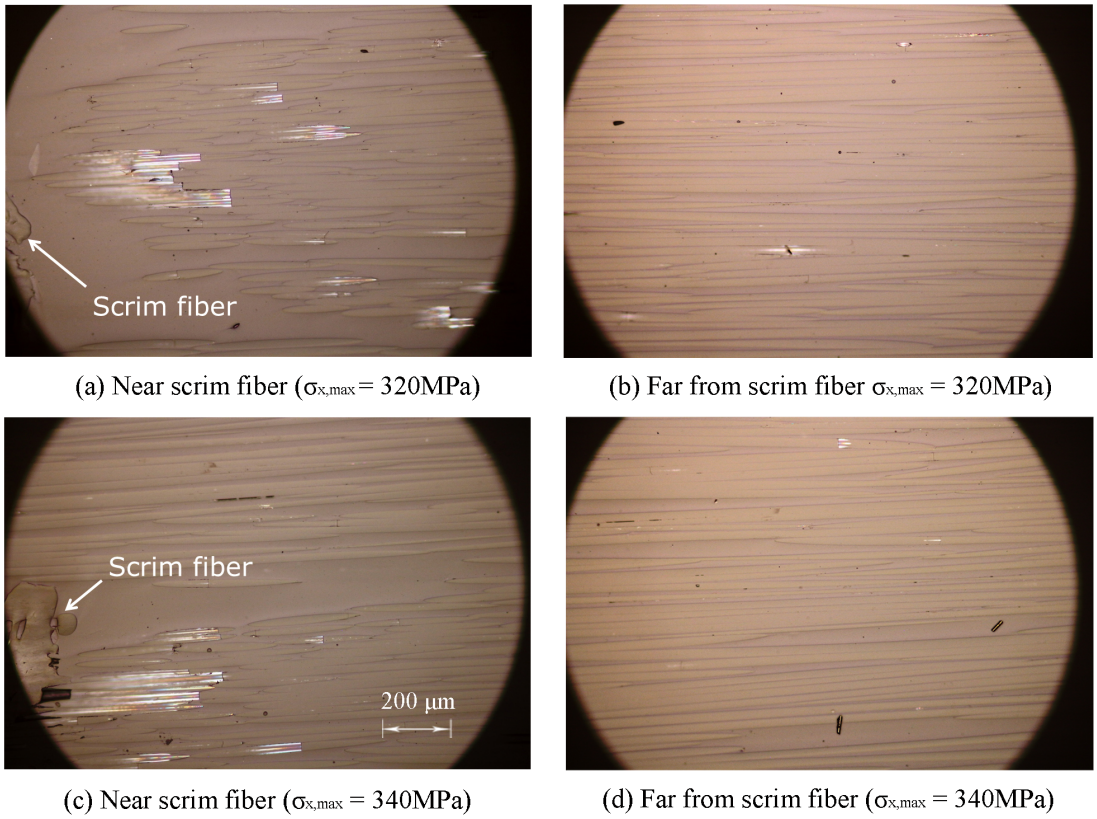

(a) Near scrim fiber ($\sigma_{x,max}$ = 320MPa)

(b) Far from scrim fiber $\sigma_{x,max}$ = 320MPa)

(c) Near scrim fiber ($\sigma_{x,max}$ = 340MPa)

(d) Far from scrim fiber ($\sigma_{x,max}$ = 340MPa)

Figure 8: Comparison between the damage progression in regions close and far to the scrim fiber for different load levels: (a) and (b) $\sigma_{x,max} = 320MPa$; (c) and (d) $\sigma_{x,max} = 340MPa$.

is presented. In addition, the effect of the progressive damage on the material stiffness is also analyzed.

To quantify the damage state, the specimens were removed from the testing machine and observed under the microscope, scanning the polished front surface along two lines with a length of 20 mm (see Fig. 1). Along these lines, consecutive pictures were taken, the longitudinal dimension of which is referred to as L_f.

The first important result that can be drawn from this analysis is the probability of survival (P_{sf}) of a fiber segment with length L_f. This was calculated as the sum of the fiber segments without any break, divided by the total number of fiber segments, for each specimen. The resulting probability of survival is plotted in Fig. 9, as a function of the number of cycles. For the specimen tested at 200 MPa, the curve is flat, meaning that all the breaks occur at the application of the first cycle, and no new breaks form in the remaining part of the life. In fact, as mentioned in the previous section, this load level is too low for promoting debond propagation, as well as to initiate new independent fiber breaks. For the other stress levels, a decreasing trend can be observed, even if, again, most of the damage is created by the first load cycle. However, in these cases, damage

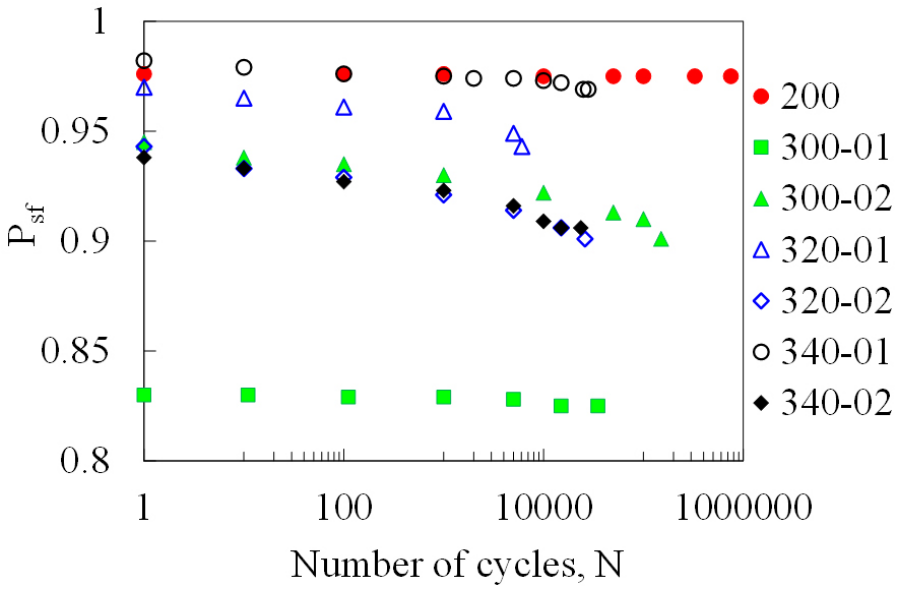

Figure 9: Evolution of the survival probability along the fatigue lifetime.

evolves during the fatigue lifetime, and this leads to the possible failure after a certain amount of cycles, when a critical state is reached.

Furthermore, the broken fibers may show only one break (within the length L_f), or more. In this sense, according to [31], the fragmentation phenomenon in UD composites can be analyzed in terms of a normalized density of breaks in the same fiber, defined as

$$\rho_{fb} = n_{fb} \cdot r_f / L_f \tag{1}$$

where n_{fb} is the number of breaks in a single fiber, r_f is the fiber radius, and L_f is the length of the observation area. In the present work, r_f is equal to $8.66\mu m$, and L_f can vary depending on the length of the selected observation area.

Based on the experimental observations, the evolution of the number of fibers with a given ρ_{fb} normalized with the total number of observed fibers, $n_{f,\rho_{fb}}/n_{f,total}$, along the fatigue life is shown in Figs. 10 and 11. In these figures, $n_{f,\rho_{fb}}/n_{f,total}$ is plotted as a function of ρ_{fb} for different applied load levels. It should be noted that the total number of fibers, $n_{f,total}$, taken into account for each analyzed case was around 1000 fibers, which is a representative sample size if assuming a confidence level of 95% and a margin of error of 3%.

As shown in Figs. 10 and 11, the lower is the density of fiber breaks, the higher is $n_{f,\rho_{fb}}/n_{f,total}$ ratio for all applied number of cycles, N. This means that, over fatigue life, one break is the most likely number of breaks in damaged fibers and that the fragmentation of single fibers (i.e., two or more breaks in a single fiber) occurs less frequently. This is in agreement with the observations described in section 3.1.

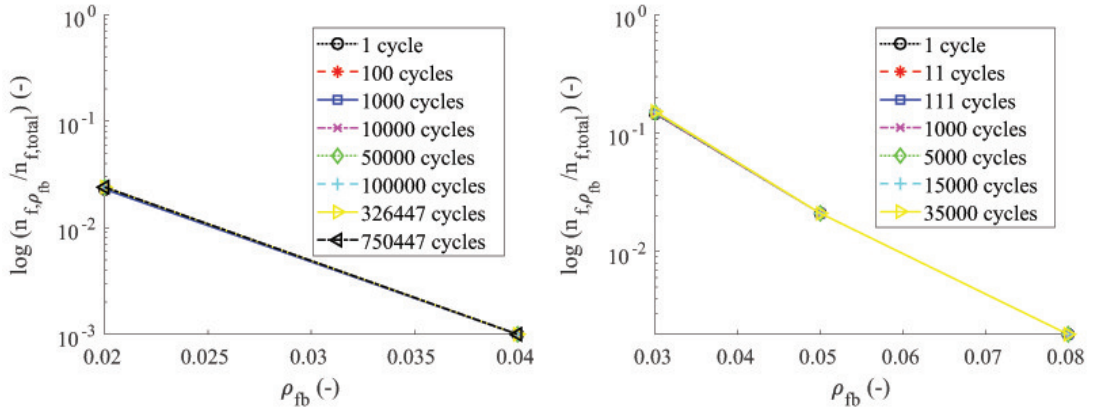

(a) σx,max = 200MPa (b) σx,max = 300MPa

Figure 10: Normalized number of fibers with a given ρ_{fb}, $n_{f,\rho_{fb}}/n_{f,total}$, versus normalized density of fiber breaks, ρ_{fb}, along the fatigue life for: (a) $\sigma_{x,max} = 200MPa$ and $r_f/L_f = 0.02$; (a) $\sigma_{x,max} = 300MPa$ and $r_f/L_f = 0.03$.

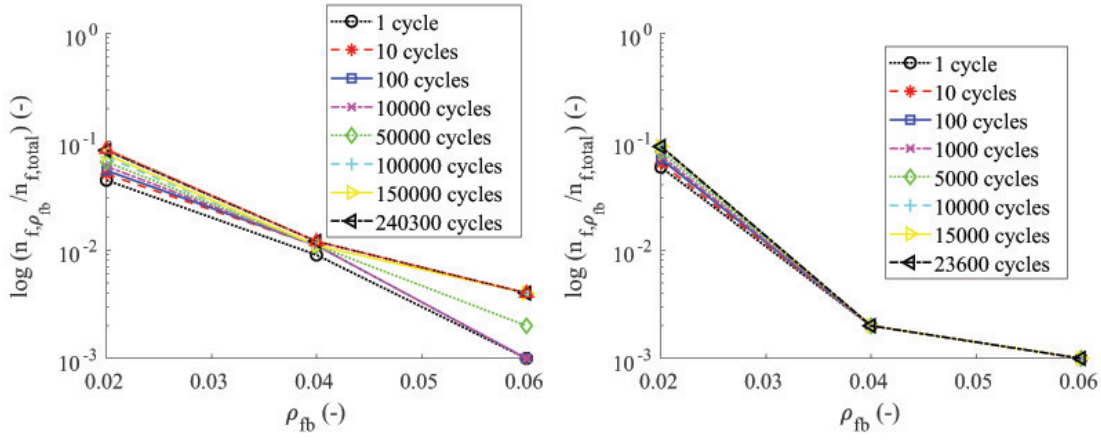

(a) σx,max = 320MPa (b) σx,max = 340MPa

Figure 11: Normalized number of fibers with a given ρ_{fb}, $n_{f,\rho_{fb}}/n_{f,total}$, versus normalized density of fiber breaks, ρ_{fb}, along the fatigue life for: (a) $\sigma_{x,max} = 320MPa$ and $r_f/L_f = 0.02$; (a) $\sigma_{x,max} = 340MPa$ and $r_f/L_f = 0.02$.

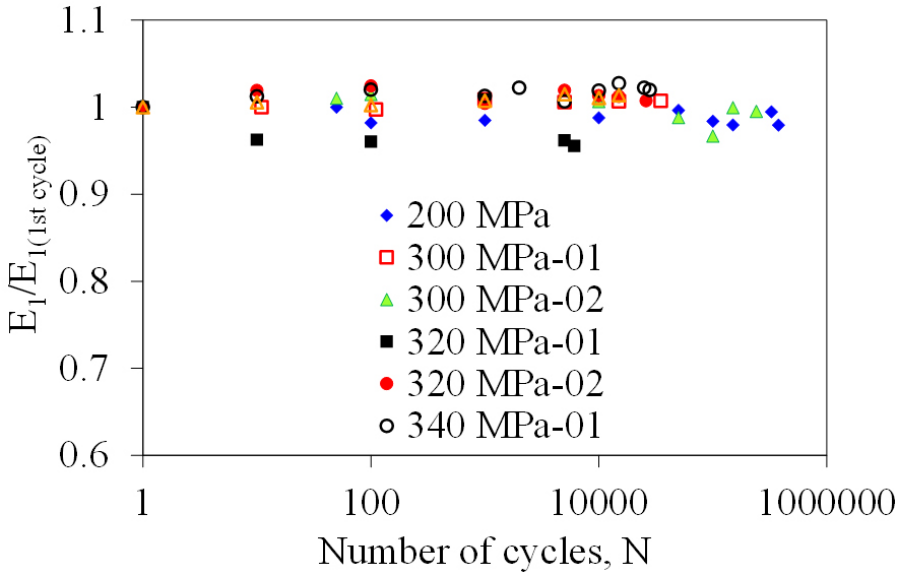

Figure 12: Stiffness versus number of cycles for different load levels and specimens.

Concerning the laminate stiffness, Fig. 12 shows the stiffness curve normalized with the stiffness at the first cycle, $E_1/E_{1(1st-cycle)}$, as a function of the number of cycles for all cases analyzed in this study.

As shown in Fig. 12, regardless of the load level, the stiffness does not seem to decrease substantially. This is reasonably due to the fact that most of the broken fibers have only one break (see Figs. 10 and 11). Thus, few fibers are fragmented and that the fragmentation length is long. As a consequence, a part from a small region close to the fiber break, the fibers recover their nominal load-bearing capacity and their damage affects only marginally the laminate stiffness. This indicates that, in terms of modelling, it may not be necessary to precisely estimate the fiber breaks to predict the stiffness of composite laminates, at least for low densities of fiber breaks.

4 Conclusions

In this study, experimental-based qualitative and quantitative analyses of the damage initiation and progression in UD glass/epoxy materials under tension-tension fatigue longitudinal loading conditions were presented.

In the qualitative analysis, it was shown that the fatigue damage initiates during the first cycle when some fibers fail as a result of the statistical distribution of the fiber strength. Then, from these fiber breaks, either yielding of matrix or fiber/matrix debonding develop depending, among others, on the applied load level. For lower load levels, shear bands in the matrix take place at the fiber crack tip and fiber/matrix debonds stop growing at a short distance from it. This causes that no, or few, new fiber breaks

in the neighboring fibers occur as the number of cycles increases. For higher load levels, in addition to the matrix yielding, fiber/matrix debonds sometimes grow from the fiber crack tip, often reaching neighboring fibers. This results in a redistribution of stresses causing further fiber breaks and, therefore, new matrix yielding or new fiber/matrix debonding throughout the fatigue lifetime. Additionally, it was shown that the damage does not propagate uniformly along the materials. In fact, in regions near the scrim fiber bundles the damage was seen to develop with a higher rate.

From the quantitative point of view, it was possible to obtain the trend of the probability of survival of the fibers, it being decreasing for stress levels higher than 200 MPa, even if most of the damage seemed to be due to the first load application (i.e., first cycle). It was also shown that fiber fragmentation occurs, even if most fibers have only one break. As a consequence, the stiffness did not change throughout the fatigue lifetime, as most of the fibers maintain, or recover, their nominal load-bearing capacity, a part from a small ineffective length.

As these conclusions are based on observations obtained on a laminate surface, further experimental studies may be needed involving the 3D analysis of the bulk material under the same loading conditions to confirm the findings of the current study.

Acknowledgements

This work was part of a Ph.D. external stay at the University of Padova, which provided all materials and facilities to develop this research. The Ph.D. project is supported by the Danish Centre for Composite Structures and Materials for Wind Turbines (DCCSM), grant no. 09-067212 from the Danish Strategic Research Council. Financial support from Otto Mϕnsteds Fond is also gratefully acknowledged.

References

[1] D.R.-B. Aroush, E. Maire, C. Gauthier, S. Youssef, P. Cloetens, and H.D. Wagner. A study of fracture of unidirectional composites using in situ high-resolution synchrotron x-ray microtomography. *Composites Science and Technology*, 66(10):1348 – 1353, 2006.

[2] M.G. Bader. Tensile strength of uniaxial composites. *Science and Engineering of Composite Materials*, 1(1):1–12, 1988.

[3] I.J. Beyerlein and S.L. Phoenix. Statistics for the strength and size effects of microcomposites with four carbon fibers in epoxy resin. *Composites Science and Technology*, 56(1):75–92, 1996.

[4] P.A. Carraro, L. Maragoni, and M. Quaresimin. Prediction of the crack density evolution in multidirectional laminates under fatigue loadings. *Composites Science and Technology*, 145:24–39, 2017.

[5] P.A. Carraro, E. Novello, M. Quaresimin, and M. Zappalorto. Delamination onset in symmetric cross-ply laminates under static loads: Theory, numerics and experiments. *Composite Structures*, 176:420–432, 2017.

[6] W.A. Curtin. Exact theory of fibre fragmentation in a single-filament composite. *Journal of Materials Science*, 26(19):5239–5253, Oct 1991.

[7] E.K. Gamstedt. Effects of debonding and fiber strength distribution on fatigue-damage propagation in carbon fiber-reinforced epoxy. *Journal of Applied Polymer Science*, 76(4):457–474, 2000.

[8] E.K. Gamstedt, L.A. Berglund, and T. Peijs. Fatigue mechanisms in unidirectional glass-fibre-reinforced polypropylene. *Composites Science and Technology*, 59(5):759–768, 1999.

[9] E.K. Gamstedt and R. Talreja. Fatigue damage mechanisms in unidirectional carbon-fibre-reinforced plastics. *Journal of Materials Science*, 34(11):2535–2546, 1999.

[10] S.C. Garcea, M.N. Mavrogordato, A.E. Scott, I. Sinclair, and S.M. Spearing. Fatigue micromechanism characterisation in carbon fibre reinforced polymers using synchrotron radiation computed tomography. *Composites Science and Technology*, 99:23–30, 2014.

[11] S.C. Garcea, I. Sinclair, and S.M. Spearing. In situ synchrotron tomographic evaluation of the effect of toughening strategies on fatigue micromechanisms in carbon fibre reinforced polymers. *Composites Science and Technology*, 109:32–39, 2015.

[12] S.C. Garcea, I. Sinclair, and S.M. Spearing. Fibre failure assessment in carbon fibre reinforced polymers under fatigue loading by synchrotron x-ray computed tomography. *Composites Science and Technology*, 133:157–164, 2016.

[13] S.C. Garcea, I. Sinclair, S.M. Spearing, and P.J. Withers. Mapping fibre failure in situ in carbon fibre reinforced polymers by fast synchrotron x-ray computed tomography. *Composites Science and Technology*, 149:81–89, 2017.

[14] R. Gulino and S.L. Phoenix. Weibull strength statistics for graphite fibres measured from the break progression in a model graphite/glass/epoxy microcomposite. *Journal of Materials Science*, 26(11):3107–3118, Jun 1991.

[15] R.B. Henstenburg and S.L. Phoenix. Interfacial shear strength studies using the single-filament-composite test. ii. a probability model and monte carlo simulation. *Polymer Composites*, 10(6):389–408, 389–408, 1989.

[16] C.-Y. Hui, S.L. Phoenix, M. Ibnabdeljalil, and R.L. Smith. An exact closed form solution for fragmentation of weibull fibers in a single filament composite with applications to fiber-reinforced ceramics. *Journal of the Mechanics and Physics of Solids*, 43(10):1551 – 1585, 1995.

[17] K.M. Jespersen, J. Zangenberg, T. Lowe, P.J. Withers, and L.P. Mikkelsen. Fatigue damage assessment of uni-directional non-crimp fabric reinforced polyester composite using x-ray computed tomography. *Composites Science and Technology*, 136:94–103, 2016. CC BY-NC-ND 3.0.

[18] B.W. Kim and J.A. Nairn. Observations of fiber fracture and interfacial debonding phenomena using the fragmentation test in single fiber composites. *Journal of Composite Materials*, 36(15):1825–1858, 2002.

[19] Z.-F. Li, D.T. Grubb, and S.L. Phoenix. Fiber interactions in the multi-fiber composite fragmentation test. *Composites Science and Technology*, 54(3):251 – 266, 1995.

[20] L. Maragoni, P.A. Carraro, and M. Quaresimin. Effect of voids on the crack formation in a [45/-45/0](s) laminate under cyclic axial tension. *Composites Part A-applied Science and Manufacturing*, 91:493–500, 2016.

[21] A.N. Netravali, R.B. Henstenburg, S.L. Phoenix, and P. Schwartz. Interfacial shear strength studies using the single-filament-composite test. i: Experiments on graphite fibers in epoxy. *Polymer Composites*, 10(4):226–241, 1989.

[22] J.M. Neumeister. A constitutive law for continuous fiber-reinforced brittle-matrix composites with fiber fragmentation and stress recovery. *Journal of the Mechanics and Physics of Solids*, 41(8):1383–1404, 1993.

[23] T. Ohsawa, A. Nakayama, M. Miwa, and A. Hasegawa. Temperature dependence of critical fiber length for glass fiber-reinforced thermosetting resins. *Journal of Applied Polymer Science*, 22(11):3203–3212, 1978.

[24] A. Pupurs and J. Varna. Energy release rate based fiber/matrix debond growth in fatigue. part i: Self-similar crack growth. *Mechanics of Advanced Materials and Structures*, 20(4):276–287, 2013.

[25] M. Quaresimin. A damage-based approach for the fatigue design of composite structures. *Iop Conference Series: Materials Science and Engineering*, 139(1):012006, 2016.

[26] M. Quaresimin, P.A. Carraro, and L. Maragoni. Early stage damage in off-axis plies under fatigue loading. *Composites Science and Technology*, 128:147–154, 2016.

[27] R.L. Smith. A probability model for fibrous composites with local load sharing. *Proceedings of the Royal Society of London Series A-mathematical Physical and Engineering Sciences*, 372(1751):539–553, 1980.

[28] Y. Swolfs, H. Morton, A.E. Scott, L. Gorbatikh, P.A.S. Reed, I. Sinclair, S.M. Spearing, and I. Verpoest. Synchrotron radiation computed tomography for experimental validation of a tensile strength model for unidirectional fibre-reinforced composites. *Composites Part A-applied Science and Manufacturing*, 77:106–113, 2015.

[29] R. Talreja. Fatigue of composite materials: Damage mechanisms and fatigue-life diagrams. *Proceedings of the Royal Society of London A: Mathematical, Physical and Engineering Sciences*, 378(1775):461–475, 1981.

[30] P.W.J. van den Heuvel, Y.J.W. van der Bruggen, and T. Peijs. Failure phenomena in multi-fibre model composites: Part 1. an experimental investigation into the influence of fibre spacing and fibreâĂŤmatrix adhesion. *Composites Part A: Applied Science and Manufacturing*, 27(9):855 – 859, 1996.

[31] J. Varna and J. Eitzenberger. Modeling ud composite stiffness reduction due to multiple fiber breaks and interface debonding. In *Proceedings of COMP07 : 6th International Symposium on Advanced Composites 16-18 May, 2007, Corfu, Greece*, volume Paper COMP07-073, 2007. Godkänd; 2007; 20071128 (ysko).

[32] R.J. Young, C. Thongpin, J.L. Stanford, and P.A. Lovell. Fragmentation analysis of glass fibres in model composites through the use of raman spectroscopy. *Composites Part A: Applied Science and Manufacturing*, 32(2):253–269, 2001.

[33] J. Zangenberg, P. Brøndsted, and J.W. Jr Gillespie. Fatigue damage propagation in unidirectional glass fibre reinforced composites made of a non-crimp fabric. *Journal of Composite Materials*, 48(22):2711–2727, 2014.

[34] L. Zhuang, A. Pupurs, J. Varna, and Z. Ayadi. Effect of fiber clustering on debond growth energy release rate in ud composites with hexagonal packing. *Engineering Fracture Mechanics*, 161:76–88, 2016.

[35] L. Zhuang, R. Talreja, and J. Varna. Tensile failure of unidirectional composites from a local fracture plane. *Composites Science and Technology*, 133:119–127, 2016.

{2.7182818284}ϑφερτυθιοπσδφγηξκλ